Modeling and Analysis of the Formation of Oxides of Nitrogen and Formaldehyde in Large-Bore, Lean-Burn, Natural Gas Engines

Anamol Pundle

A thesis
submitted in partial fulfillment of the
requirements for the degree of

Master of Science in Mechanical Engineering

University of Washington
2013

Committee:
John C. Kramlich
Philip C. Malte
David G. Nicol

Program Authorized to Offer Degree:
Mechanical Engineering

TABLE OF CONTENTS

LIST OF FIGURES

LIST OF TABLES

ACKNOWLEDGEMENTS

The author wishes to express immense gratitude to the following:

- Co-advisors Professors John Kramlich and Philip Malte, for their unending support, guidance and encouragement, as well as the opportunity to work on this project.
- Dr. David Nicol, for his help with the UWSI and Mark 3 computer programs, without which this project would have been significantly harder.
- Shazib Vijlee and Megan Karalus, for being a great help to the author whenever he was stuck with something, as well as for their inputs during the combustion meetings.
- Dr. Igor Novosselov, for his valuable inputs during the weekly combustion meetings.
- Mathias Neumayer, for his valuable inputs during the combustion meetings and German-to-English translation.
- The Department of Mechanical Engineering, for financial support in the form of Teaching Assistantships and Tuition Waivers.

Finally, the author would like to thank his brother, parents and friends for their unending love and support.

.

1.0 Introduction

1.1 Background

Large-bore, spark ignition internal combustion engines operating on natural gas are widely used for a variety of industrial applications, such as pumping natural gas, stationary power generation and various mechanical drive applications. Varying in size from 1 MW to 15 MW, these engines generate a significant amount of pollution that can pose a serious environmental problem, especially in non-attainment areas. Both two-stroke and four-stroke engines exist, though four-stroke engines are more widely used. Four-stroke engines tend to be smaller in size and run faster, while two-strokes are larger and run slower. Both homogenous and stratified charge engines are common. Both run on natural gas, with many of the stratified charge engines using diesel fuel for the pilot flame. This study focuses only on large-bore spark ignition engines running on natural gas. Though largely soot and sulfur free, these engines emit substantial amounts of oxides of nitrogen ($NO + NO_2 = NOx$), unburned hydrocarbons (UHCs) and carbon monoxide, often exceeding allowable standards. In the late 70's and early 80's various NOx reduction strategies were implemented in these engines, reducing NOx emissions from typically 20gm/bhp-hr to about 2 gm/bhp-hr, a reduction of 90%.

These engines were formerly run at higher fuel-air equivalence ratios (in the range of 0.8) before environmental regulations forced the reduction of NOx emissions. This was done by operating these engines at leaner conditions, with a fuel-air equivalence ratio in the range of 0.6 to 0.7. Though NOx emissions were reduced, this led to an increase in UHC and CO emissions.

Further improvements made to these engines include a "jet-cell" or stratified-charge combustion, which permitted the engines to run leaner than homogeneous charge engines. The jet-cell consists of a pre-chamber (separate from the main chamber) which houses the spark plug and a separate fuel injector. The fuel-air equivalence ratio is higher in the jet-cell than in the main chamber, which provides improved flame stability. After ignition, the hot combustion gases expand, producing a jet that shoots out of the pre-chamber into the main chamber, igniting the leaner fuel-air mixture present therein. The term "clean burn" is frequently used to describe these engines. Figure 1.1 shows a schematic diagram of an engine with a jet-cell.

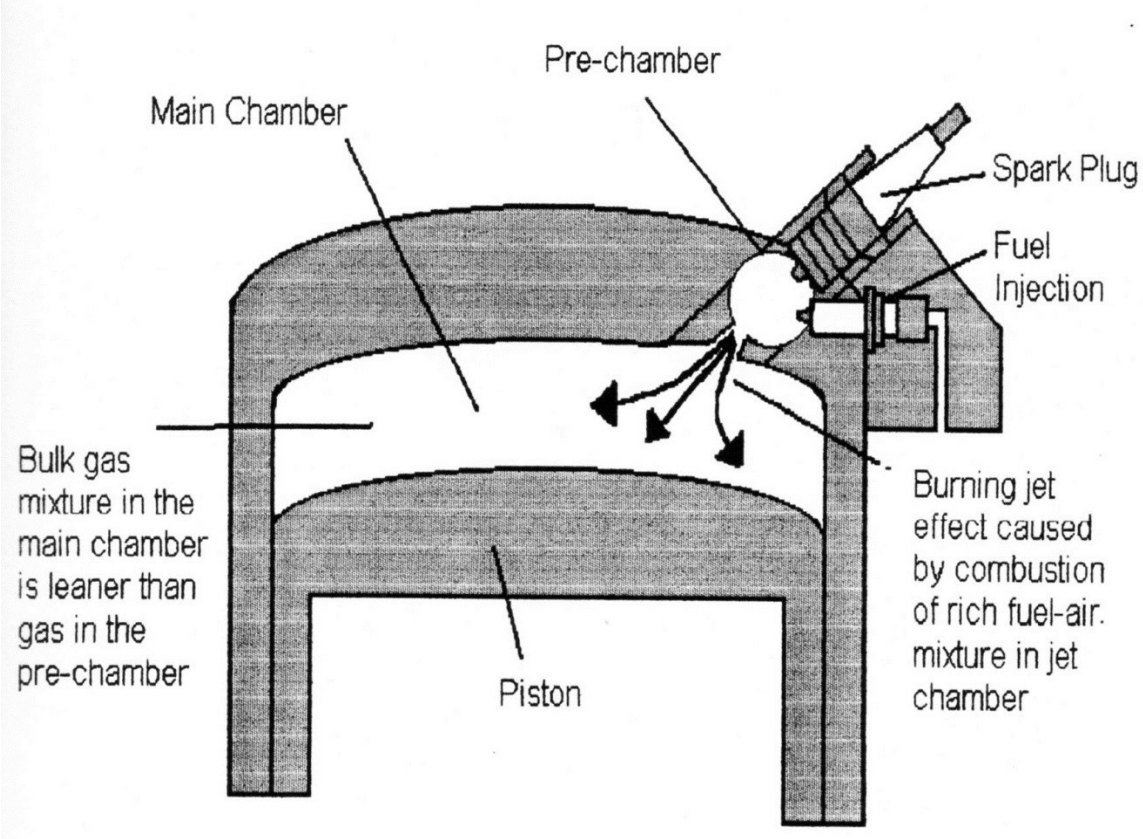

Figure 1.1: Diagram of a Stratified Charge Engine, Denuski (1995)

The formation pathways of NOx have been studied extensively and are well understood. These include the Zeldovich mechanism, the nitrous oxide mechanism, the NNH mechanism and the Fenimore prompt mechanism (Fackler, 2011). However, it is unclear which of these mechanisms contributes to NOx formation in lean-burn natural gas engines and how the distribution changes with changing operating conditions. Heywood (1988) states that the Zeldovich pathway is the most significant contributor to NOx formation in spark-ignition engines. The chemical kinetic modeling and experiments of Wolfrum (1972) indicate that the nitrous oxide pathway could also contribute to NOx formation in spark-ignition engines. It is also indicated that NOx is not primarily formed in the flame front, but in the post-flame region. A computational model of a spark-ignition large-bore natural gas engine has been developed by Clark (1989), who used it to predict NOx emission from these engines. Clark's NOx sub-mechanism included only the Zeldovich pathway, and could predict about 60 percent of the NOx recorded in test data, which indicates that the other NOx pathways could be responsible for significant NOx emission. Denuski (1995) improved upon Clark's model by removing its dependence on an external pressure trace and utilizing full chemical kinetic mechanisms. Several other improvements were also made by Denuski, such as the option of stratified charge combustion. Another model for gas phase combustion in natural gas spark-ignition engines has been developed by Golub and Ghoniem (1999) and used to predict NOx emission in small-bore homogeneous natural gas engines at fuel-air equivalence ratios of 0.91 and 0.66. This NOx sub-mechanism in this model includes only the Zeldovich pathway. The model predicts NOx emissions well at the higher equivalence ratio, but significantly under-predicts NOx at the lower equivalence ratio.

Formaldehyde formation has been studied experimentally, but a significant modeling effort has not been made using updated chemical kinetic mechanisms. Olsen and Mitchell (1999) and Olsen et al. (2000) have explored the mechanisms of formation of formaldehyde through experimental data and have identified certain phenomena as having a possibility of producing formaldehyde. These include end gas reactions, mixing effects (since lean-burn engines may have pockets of lean charge too weak to sustain a propagating flame, which may react to the extent that partial oxidation products such as formaldehyde are formed), reactions leading to pre-ignition, wall quenching and unburned gas released from cracks and crevices in the engine. A trend of increasing HCHO emission with increasing CO emission has also been noted, while NOx emission is indicated to not correlate well with HCHO emission. A modeling study using older chemical kinetic mechanisms has been done by Nicol and Malte (1997), in which some of these phenomena have been explored.

1.2 Objectives

The objectives of this study are as follows:

1. Develop a calibrated quasi-dimensional model, based on full chemical kinetics, of a large-bore, lean-burn gas engine. Calibration data are drawn from a baseline single-cylinder engine test case giving cylinder pressure trace and exhaust emission data. Additional data are from measurement of NOx as a function of fuel-air equivalence ratio.

2. The calibrated model is used to explore HCHO formation and emission, leading to a better understanding of how this pollutant forms in these engines, for which it is significant.
3. Explore the NOx formation in these engines, and develop a simple-to-use predictor for NOx emission.

2.0 Modeling Approach

2.1 Overview

We must understand the processes occurring within the engine in order to accurately model its behavior. As the inlet valve or port opens, compressed air from the inlet manifold enters the main chamber which forces the exhaust gas out of the cylinder, into the exhaust manifold. After this scavenging process, the combustion chamber contains air with a small percentage of unreactive exhaust gas. Once both the inlet and outlet valves or ports close, fuel is injected into the cylinder. The goal is for the fuel to mix with the air prior to spark ignition, resulting in as uniform a fuel-air ratio as possible in the main chamber. The spark plug fires at a user-defined crank angle and ignites the mixture inside the pre-combustion chamber. The pre-combustion chamber is assigned a higher fuel-air ratio than the main chamber, to account for the excess fuel injected into the jet-cell. As combustion gases shoot out of the jet-cell, the charge in the main chamber ignites and the flame front propagates across the cylinder. The flame speed weakens before the flame fully covers the cylinder, resulting in pockets of unburned charge. These unburned pockets may mix into the burned gas and react. After the piston lowers sufficiently, the exhaust valve or port opens and the burned gas (along with any unburned pockets) is forced into the exhaust manifold, where it subsequently runs through a turbocharger, which compresses the air coming into the inlet manifold to the pressure desired..

A quasi-dimensional computational model of a representative engine has been previously developed at the University of Washington by Clark (1989) and was modified to generate its own pressure trace by Denuski (1995). Further changes to the program were made by

Nicol and Malte (1997). The engine modeled was a single cylinder research engine based on the Cooper-Bessemer Z-330, a turbocharged, two-stroke, loop-scavenged engine with a bore and stroke of 20 inches each. For the test cases considered, the power output of the engine was 681 bhp, running at a constant speed of 330 RPM and a brake mean effective pressure of 130 psi. The UWSI code models emissions from this engine and also calculates a pressure trace. It is based on chemical kinetic calculations and utilizes full chemical kinetic mechanisms. It does not assume complete combustion or chemical equilibrium to predict the concentration of species.

The modeling approach taken can be understood better if it is split into three processes: energy modeling, chemical modeling and calibration with experimental data.

2.2 Energy Modeling

The Cooper-Bessemer Z-330 is cylinder-injected, i.e., fuel is injected directly into the combustion chamber after the intake and exhaust ports are closed. Hence, the scavenging process consists of compressed air forcing exhaust gases out of the combustion chamber, leaving behind some residual burned gas. The mass of the initial unburned gas is the mass of the inducted air plus the residual fraction left over from the previous cycle. UWSI determines the initial state of the unburned gas by the pressure and temperature of air in the intake manifold, the pressure and temperature of gas in the exhaust manifold, the delivery ratio and charging efficiency of the engine, and the crank angle at intake port closure. Scavenging parameters and models from Heywood (1988) are followed for calculating the mass of air retained after the scavenging process. The delivery ratio, Λ is defined as

$$\Lambda = \frac{mass\ of\ air\ delivered\ per\ cycle}{reference\ mass\ of\ cylinder}$$

A complete mixing model is assumed for the scavenging process, in which incoming charge is assumed to mix instantaneously and uniformly with residual gas. Using this model, the charging efficiency is defined as:

$$\eta_{ch} = 1 - e^{-\Lambda}$$

The trapping efficiency is calculated by dividing the charging efficiency by the delivery ratio. The trapping efficiency is defined as the mass of delivered air (or mixture) retained divided by the mass of air (or mixture) delivered. The mass of air trapped can easily be determined with knowledge of the air flow rate through the engine and the trapping efficiency. The temperature of the mixture hence obtained is based on mixed-mean enthalpies of the trapped fresh air and unexhausted products, while the temperature of the exhaust gas is based on mixed-mean enthalpies of the untrapped fresh air and exhausted products. The pressure of the contents of the cylinder prior to compression by the piston is taken to be the mean of the pressures in the exhaust and intake manifold. Following port closure, fuel is injected separately into the jet-cell and the main chamber. Mixing with air (and residual gas) in each chamber is assumed to be uniform (though of course, non-uniformities are likely to occur in the real engine). The state of the gas prior to spark firing is calculated by compressing the fuel+air+residual gas mixture by a polytropic process.

Though the flame speed is not directly modeled, the treatment of flame speed is effectively accounted for by an empirical relation known as the Wiebe function. Burned

mass fraction profiles are dimensionless and follow an S-shaped curve. The Wiebe function relates the mass fraction of charge burned to the rapid burn angle and spark ignition timing. This function is:

$$x_b = 1 - \exp[-a\left(\frac{\theta - \theta_0}{\Delta\theta}\right)^{m+1}]$$

Where x_b is the mass fraction of charge burned, θ is the crank angle, θ_o is the spark timing, $\Delta\theta$ is the rapid burn angle, and a and m are adjustable parameters. The rapid burn angle is defined as the crank angle interval required to burn the bulk of the charge. It is taken to be the interval between the end of the flame development stage and the end of the flame propagation process, usually a mass fraction burned of 90%. For automotive engines, it is typically 40° engine crank angle. However, for the relatively slower large-bore natural gas engines, this value is found to be about 15° engine crank angle.

The Wiebe function used to model the Z-330 engine was modified by Denuski (1995) on the basis of its ability to predict a representative pressure trace (obtained from Cooper-Bessemer) of the engine operating at 330 rpm with a power output of 681 bhp at 315% delivered theoretical air. It is given by:

$$x_u = 0.71 \exp\left[-0.7422\left(\frac{\theta - \theta_o}{\Delta\theta}\right)^{3.6}\right] + 0.29$$

Where x_u is the mass fraction of unburned charge and all other parameters are defined above. This function is used to predict both the combustion in the jet-cell as well as combustion in the main chamber. The rapid burn angle for both processes was found to be 15° crank angle for this case. The amount of time (in crank angles) taken by the flame

to propagate through the stratified charge is calculated by equating x_u to the mass fraction of the jet-cell. For this case, combustion in the jet-cell occurs from spark ignition until about 4^o ATDC. The unburned mass fraction as a function of crank angle is shown in Figure 2.1. The figure shows rapid flame propagation predicted by the Wiebe function until 18^o crank angle, after which no flame propagation is observed. The flame speed is indicated to become very weak, leading to incomplete propagation of the flame across the cylinder. This is consistent with the partial-burn concept discussed in Heywood (1988). However, slow mixing of gas left unburned by the flame into the burned gas can result in continued oxidation of the fuel. This is shown by the UWSI prediction in Figure 2.1. As an engine is leaned out, a lengthening of combustion phenomena in the cylinder (flame development and rapid burn) occurs. This causes the flame to complete propagation just before the opening of the exhaust valve. As the burning length increases, the flame reaches extinction before the exhaust valve opens. When this phenomenon occurs for a significant number of cycles, the engine is said to be operating in the partial burn regime. For a given fuel, the partial burn regime is governed by the spark timing, fuel-air equivalence ratio and the speed of the engine. Figure 2.2 shows a plot describing the partial burn regime in a methane fueled SI engine operating at 1200 RPM (Heywood 1988).

Combustion after 18^o crank angle is modeled either using the prescribed mixing model (PMM), which mixes a prescribed percentage (by mass) of unburned charge into burned gas per crank angle, or a second Wiebe function. The rapid burn angle of the second Wiebe function and the prescribed mixing rate in the PMM are selected such that they give good agreement with the experimental pressure trace.

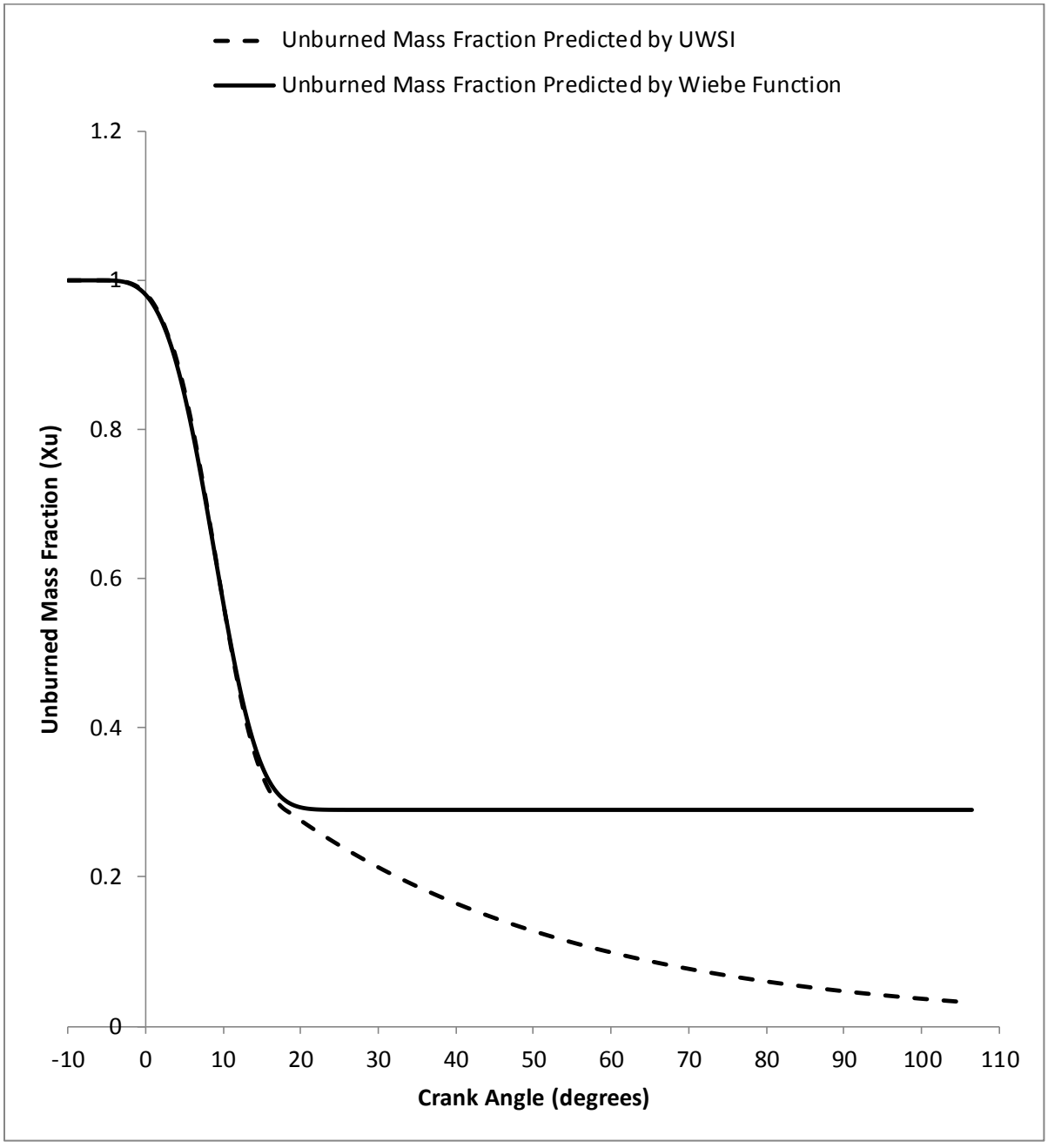

Figure 2.1: Unburned Mass Fraction as a function of Crank Angle predicted by UWSI and the Wiebe function

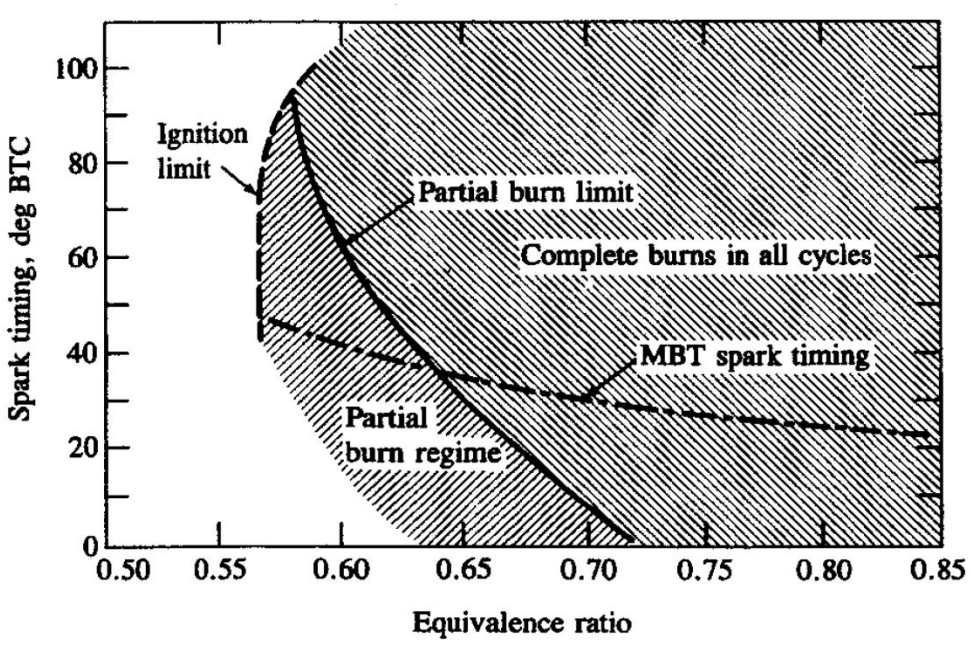

Figure 2.2: Limiting Combustion Regimes for a Lean-operating Engine, Heywood (1988)

2.3 Chemical Modeling

The UWSI code is based entirely on chemical kinetic calculations and does not rely on assumptions of complete combustion or chemical equilibrium to model concentrations of major species. It utilizes full chemical kinetic mechanisms, consisting of a large number of species and reaction steps.

The gas inside the cylinder is divided at any time into distinct regions (referred to as gas elements), representing burned gas, unburned gas and newly burned gas (the flame front), as shown in Figure 2.3. The unburned gas element is further sub-divided into a fuel-rich gas element (the jet-cell) and a leaner region (the main chamber), both occupying a different volume. The flame front is modeled as a perfectly stirred reactor sized to blowout conditions for the first part of the time step followed by a plug flow reactor for the rest of the time step. The burned gas is modeled as an adiabatic batch reactor. The properties of these gas elements are updated at the end of every crank angle increment.

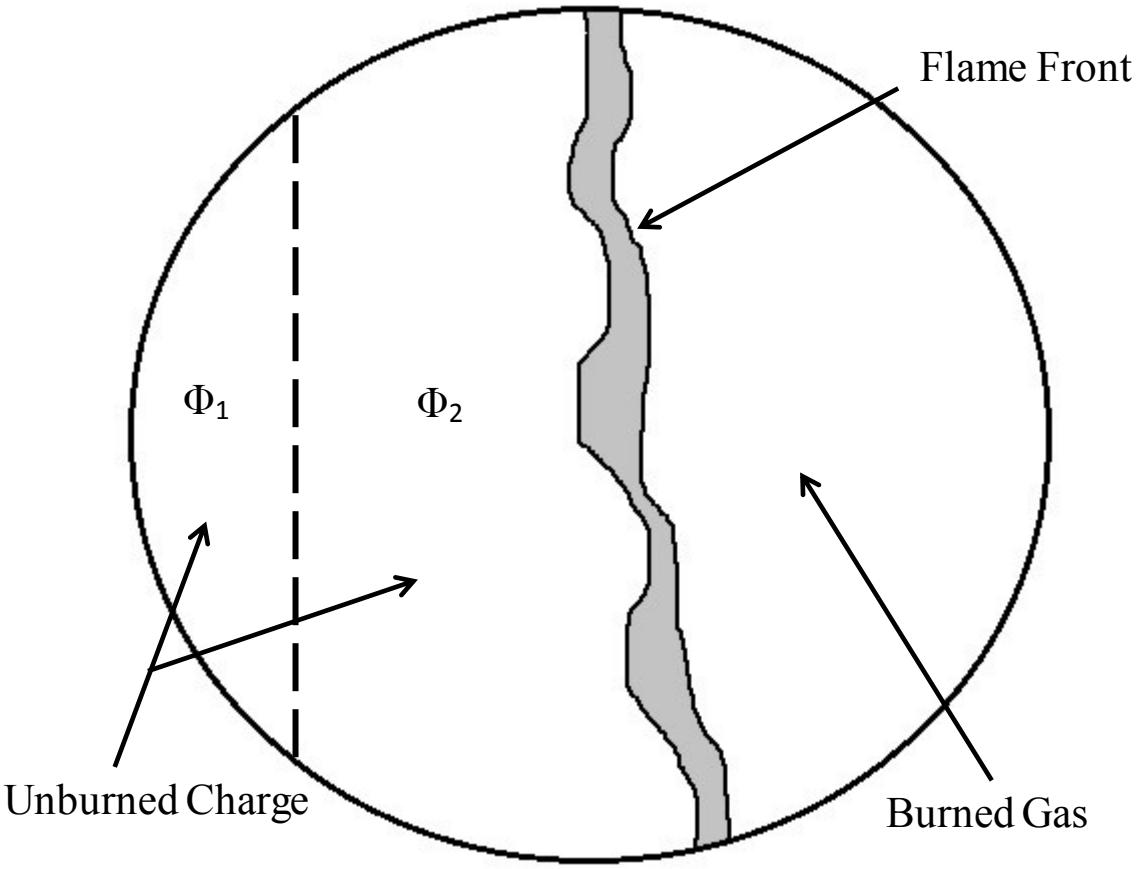

Figure 2.3: Simplified Schematic of Gas Element Structure in UWSI

UWSI has two distinct procedures for modeling burned gas elements; the "quiescent" model and the "turbulent" model. The quiescent model treats the gas burned at each crank angle increment as a separate gas element, with no interaction between any two burned gas elements. Therefore, this element contains many computational elements, one for the unburned gas, one for the flame front and one for each parcel of gas burned in a crank angle increment. This is representative of an engine with low turbulence levels. The turbulent model assumes perfect mixing and treats all of the burned gas as one gas element. Hence, it has only three gas elements; one for the burned gas, another one for the unburned gas and one for the flame front. This is representative of an engine with

high turbulence levels and mixing. Both models are shown in Figure 2.4. The turbulent model was used in this study, since the turbulent model required less computational time.

The residual gas composition can be estimated using one of two options. This residual gas may be assumed to consist of either the products of complete combustion for the specified fuel-air ratio or a "realistic" residual fraction, corresponding to the exhaust gas composition at exhaust port opening. Emissions predicted using the realistic residual fraction model are approximately 10% higher than emissions predicted with the assumption of complete combustion products. The realistic residual fraction is used in this study.

2.4 Calibration with Experimental Data

UWSI needs to be calibrated to match experimental operating conditions and data before it can be used for detailed modeling. The model is calibrated using data from the thesis of Clark (1989). The data set from a single experiment of the research engine is used for calibration. The information used for calibration includes the pressure trace, stack emissions of NOx, CO and UHC, the overall air and fuel flow rates, the intake manifold pressure and temperature, the exhaust manifold pressure and temperature, engine rpm, bhp, engine geometry and spark timing. These are shown in Table 2.1. This is called the baseline case.

UWSI is set up to model this test case. All parameters are matched and the rapid burn angle is adjusted in order to keep the brake power output at 681 hp, corresponding to a brake mean effective pressure of 130 psia at 330 rpm. This is found to be 15^{o} for both the

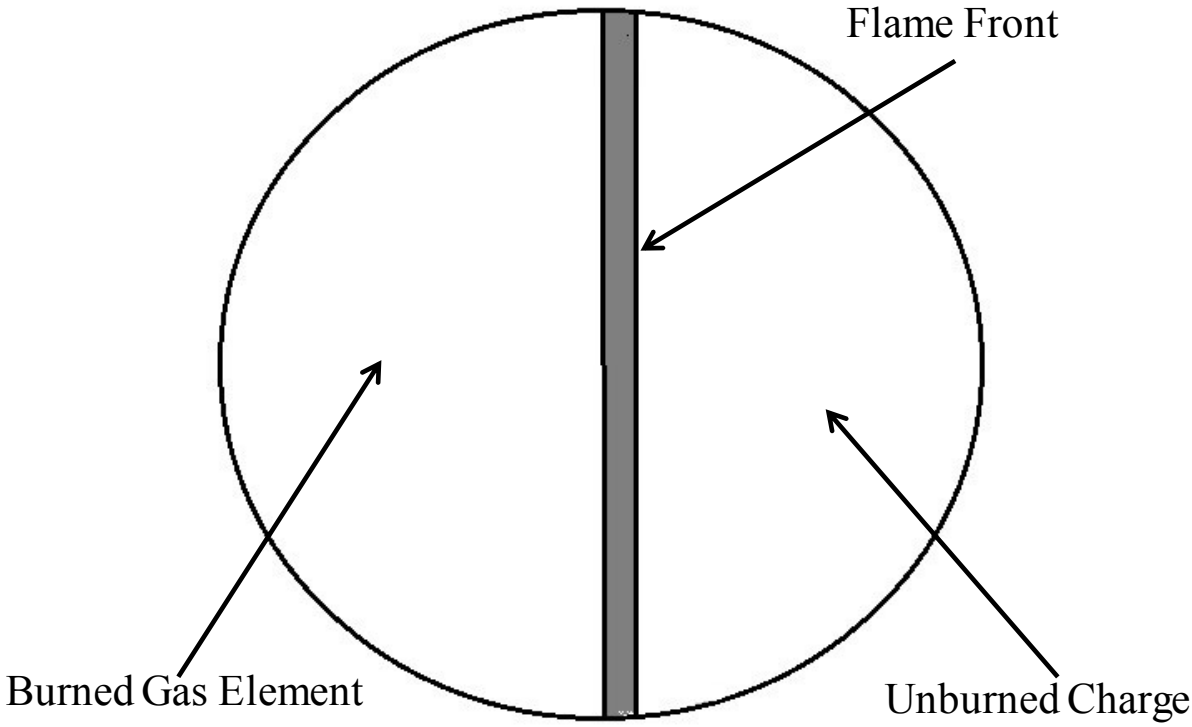

Figure 2.4a: UWSI "Turbulent" Model

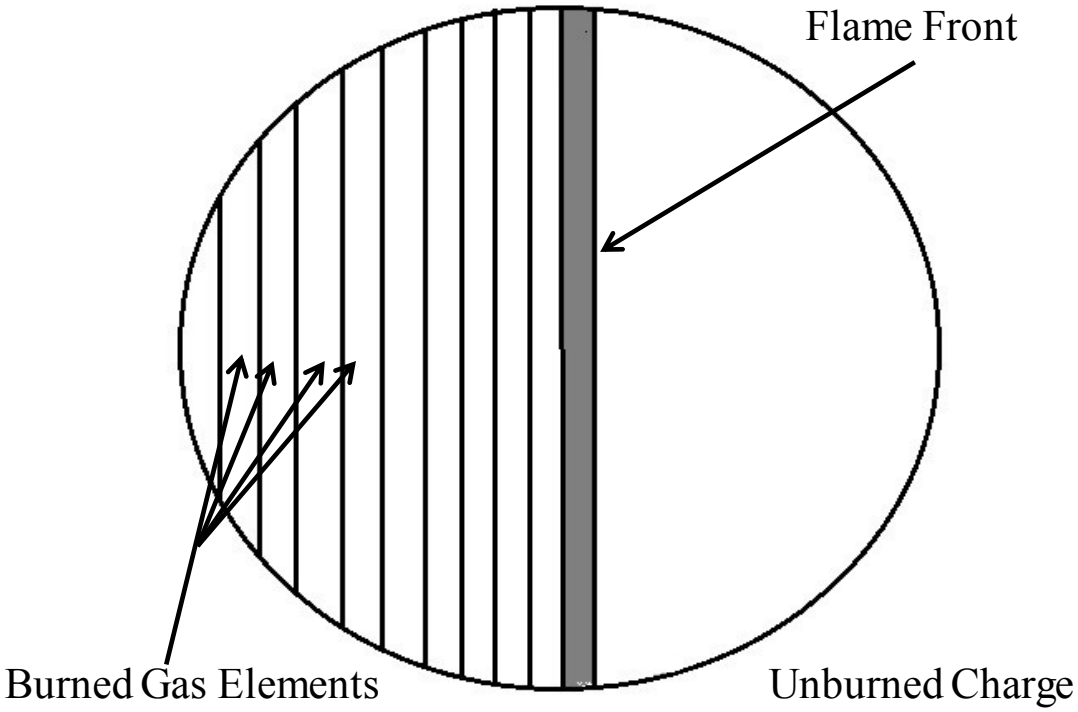

Figure 2.4b: UWSI "Quiescent" Model

NOx	6.7 gm/(bhp-hr)
CO	1.5 gm/(bhp-hr)
UHC	5.3 gm/bhp-hr)
Pressure Trace	
Air flow rate	1.551 kg/s
Fuel low rate	0.0287 kg/s
Intake Manifold Pressure	217 kPa
Exhaust Manifold Pressure	198 kPa
Intake Manifold Temp.	317 K
Exhaust Manifold Temp.	597 K
BHP	681
Engine Speed	330 RPM
Spark Timing	-6^{o} ATDC
Engine Geometry	

Table 2.1: Data Set used for calibration of UWSI, Clark (1989)

main chamber as well as the pre-combustion chamber. The modified Wiebe function accounts for the combustion of 71% of the charge; the Prescribed Mixing Model is selected to model the combustion of the remaining 29%. The "realistic" residual fraction option is selected to model the residual gases in the cylinder.

The simulation was run once and the predicted NOx values were compared to the experimental NOx values. The predicted values were less than the experimental values, which suggests that the temperature of the burned gas predicted by UWSI was low. In order to raise the temperature of the burned gas and correctly predict NOx emission, the fuel-air equivalence of the stratified charge is increased. Predicted NOx emissions matched the experimental NOx emissions at a stratified charge fuel-air equivalence ratio of 0.983. The UHC and CO emissions are matched by increasing the mixing rate in the PMM to 1.3% of the unburned charge per half-degree crank angle. Since the mixing rate has very little effect on NOx emissions (Denuski 1995) this parameter could essentially

be varied independently of the stratified charge fuel-air equivalence ratio. After calibration, the model was used to predict emissions for test cases taken from the paper by Danyluk and Schaub (1981).

3.0 NOx Measurements

NOx measurements from the Z-330 research engine are examined in this chapter. These measurements are also compared to predicted NOx values by the UWSI model.

The early 1980's were a period of intense research and development for NOx reduction techniques from two-stroke and four- stroke large bore natural gas IC engines. NOx measurements from a paper published by Danyluk and Schaub (1981) are used in this study. In addition, modeling techniques and data are also taken from a report by Nicol and Malte (1997). These documents deal with two-stroke large bore natural gas engines. All NOx measurements taken from these sources pertain to the research version of the Cooper-Bessemer Z-330, a single cylinder 20 inch stroke and 20 inch bore two-stroke IC engine fired on natural gas and equipped with a pre-combustion chamber. The data in the paper mentioned above is in the form of % air and heat rate. The former term is the ratio of the total mass flow rate of air through the engine divided by the product of the standard air density, displacement volume of the engine and engine RPM, while the latter is the energy input into the engine per hour divided by the brake horsepower.

The engine is maintained at a constant speed of 330 rpm and brake mean effective pressure of 130 psia, resulting in a constant brake horsepower of 681 bhp. The inlet air manifold temperature is held constant at 110^{o}F with an air pressure of 217kPa maintained by a turbocharger. The spark timing is 5^{o} BTDC.

The heat rate (in BTU/hp-hr) for each test case is converted to the energy rate (BTU/hr) by multiplying it with the given bhp. This value is divided by the nominal lower heating value of natural gas (44,680 BTU/kg) to obtain the fuel flow rate. The overall air flow

rate is calculated from the given % air, engine displacement and rpm. The % theoretical air is calculated using the fuel and air flow rates.

The matching of NOx measurements is carried out using the UWSI model. The chemical kinetic mechanism used is GRI 3.0. The model is run first with one Wiebe function and the Prescribed Mixing Model (PMM) with a mixing rate of 1.3% unburned charge per half degree crank angle and then with a second Wiebe function instead of the PMM.

A comparison of the measured emissions and predicted emissions in shown in Table 3.1. In Table 3.1, Version 1 refers to the prediction made in this study using GRI 3.0 with a single Wiebe function and the PMM, while Version 2 refers to the prediction made using the second Wiebe function instead of the PMM. In Version 3, GRI 3.0 is replaced with the older GRI 2.11 mechanism

The main features of the models are summarized below:

- In Version 1, the GRI 3.0 mechanism is used, with a phi of 0.983 in the combustion chamber. The single Wiebe function model with the PMM is used. This configuration gives the best NOx, UHC and CO prediction out of all models.
- In Version 2, the PMM has been replaced by the second Wiebe function. The NOx and UHC emissions are elevated, while CO emission drops dramatically.
- In Version 3, the GRI 2.11 mechanism is used instead of the GRI 3.0 mechanism with the Prescribed Mixing Model. All other conditions are the same as Version 1.

- In Version 4, the chemical kinetic mechanism of Hunter et al. (1994) is used in place of the GRI mechanism. All other conditions are the same as Version 1. This mechanism does not contain a NOx sub-mechanism.

The NOx is well predicted in general, except for the over prediction by 2-Wiebe function models. The 2-Wiebe function model under-predicts CO emission. The CO predicted by the Hunter et al. mechanism is about a factor of 2.5 greater than the measured emission. Though HCHO emission was not measured, it is observed that the 2-Wiebe function model predicts negligible amounts of HCHO. The HCHO prediction with the PMM by the Hunter et al. mechanism is about twice the prediction of the GRI 3.0 mechanism.

Figure 3.1 shows NOx emissions obtained from UWSI for test cases of 5^{o} BTDC spark timing, along with measured NOx emission from the paper by Danyluk and Schaub (1981). The rapid burn angle is adjusted for each test case to match the constant power output (681 bhp) of the engine. As the engine is leaned out, flame speed reduces and the rapid burn angle increases. The rapid burn angle is varied from 13^{o} to 16.7^{o}. The rapid burn angle as a function of equivalence ratio is shown in Figure 3.2. Predictions for the test cases are made by Version 1 and 3 of the UWSI model, using the chemical kinetic mechanisms GRI 3.0 and GRI 2.11, respectively. The model used with the GRI 3.0 mechanism matches the NOx emissions, since the phi of the pre-combustion chamber is adjusted for each test case. Figure 3.3 shows the phi of the main chamber and the pre-chamber as a function of delivered theoretical air. The phi of the pre-chamber and the main chamber decrease as the engine is leaned out. NOx predictions using the GRI 2.11 mechanism for the same conditions as Version 1 for each test case are made. The model

used with GRI 2.11 also predicts NOx emissions quite well, except at the richest case, where the NOx is under-predicted.

Version 1 of the UWSI model is also used to predict NOx emissions at very lean operating condition, extending beyond the range of the test cases, also shown in Figure 3.1. NOx emissions from 0.8 gm/hp-hr to 0.2 gm/hp-hr were predicted. The pre-chamber phi for these cases is kept fixed at 0.68.

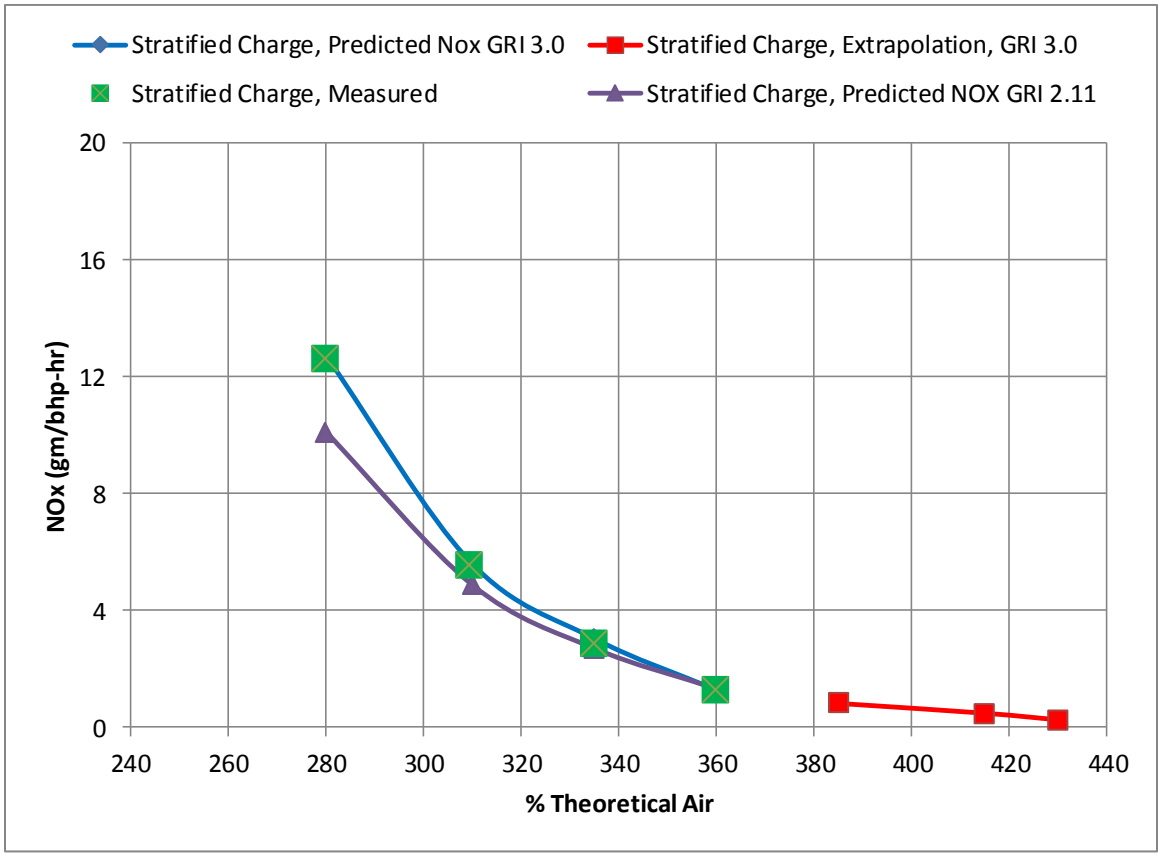

Figure 3.1: Predicted and measured NOx as a function of delivered theoretical air

From Figure 3.1 and Table 3.1, we can conclude that the UWSI model can accurately predict NOx emission. The primary parameter adjusted to provide an acceptable prediction is the rapid burn angle. A very close replication of NOx emission can be obtained if the stratified charge fuel-air equivalence ratio is also adjusted as the engine is

leaned out. CO and UHC emissions are also well matched using the UWSI model. Since all major emitted species are well matched, the UWSI model is used to predict and study formaldehyde emission in the next section.

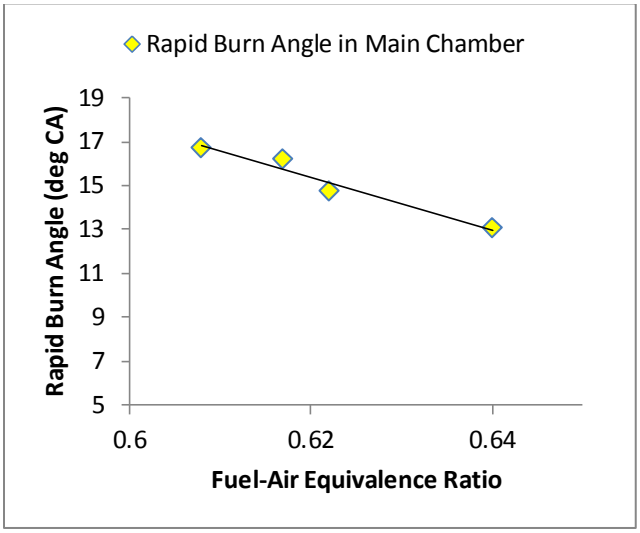

Figure 3.2: RBA as a function of phi

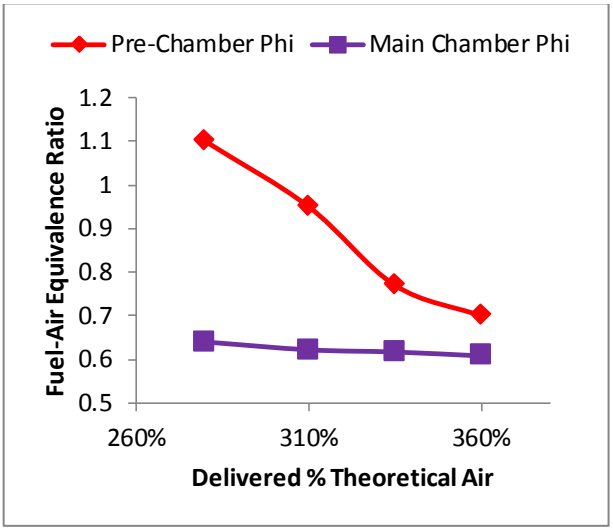

Figure 3.3: Phi as a function of Delivered % Theoretical Air

	Description	NOx (g/hp-hr)	CO (g/hp-hr)	UHC (g/hp-hr)	HCHO (ppmv)
Measured	Baseline Case	6.7	1.53	5.3	NA
Version 1	GRI 3.0 Mechanism, PMM for 2nd stage of combustion, Pre-chamber Phi = 0.983, RBA = 15°	6.69	1.58	5.19	2.86
Version 2	2-Wiebe Function Model, other conditions same as Version 1	7.91	0.21	6.83	0.00
Version 3	Gri 2.11 Mechanism, other conditions same as Version 1	6.73	1.68	5.25	3.12
Version 4	Hunter et al. Mechanism, other conditions same as Version 1	NA	4.17	5.91	7.95

Table 3.1: Measured and Matched Emissions for the Baseline Case

4.0 Formaldehyde Predictions

4.1 Overview

Formaldehyde (HCHO) is a stable intermediate in hydrocarbon combustion that forms in cooler parts of the flame at temperatures below 1000 K. It is relatively stable below 1000 K, but is rapidly combusted at temperatures above 1200 K. Formaldehyde is a recognized carcinogen, capable of causing cancer at prolonged exposures to concentrations as low as 15ppm. It can also cause other health effects at short term exposure to high concentrations (CDC Intelligence Bulletin, 1981).

Equilibrium concentrations do not favor the formation of formaldehyde in flames; for stoichiometric and lean mixtures, the amount of formaldehyde produced is about 0.1 ppb, while measured mole fractions of formaldehyde from large-bore natural gas engines can exceed 50ppm (Olsen et al. 2000). This suggests that super-equilibrium quantities of formaldehyde are formed during the engine combustion process and survive into the exhaust stream. While formaldehyde is formed in the upstream part of self-propagating flames in excess of 1000 ppm, virtually all of it is subsequently oxidized in the flame well before the final flame temperature is reached. Therefore, the formaldehyde formed in the pre-flame region is indicated to have very little effect on the amount of formaldehyde emitted from the engine. Partial oxidation and incomplete combustion are thought to be instrumental in the formation of formaldehyde in large bore engines. Since large bore natural gas engines operate in the partial burn regime, it is possible that large amounts of formaldehyde are formed due to partial oxidation resulting from flame extinction before all the charge is burned.

Figure 4.1 shows a diagram of the major reaction steps in methane combustion, taken from a paper by Bauer and Wachtmeister (2009). The importance of formaldehyde as an intermediate species in the path leading to CO formation is apparent. As inferred from the figure, formaldehyde is formed mostly by the partial oxidation of CH_3 and some higher hydrocarbon radicals.

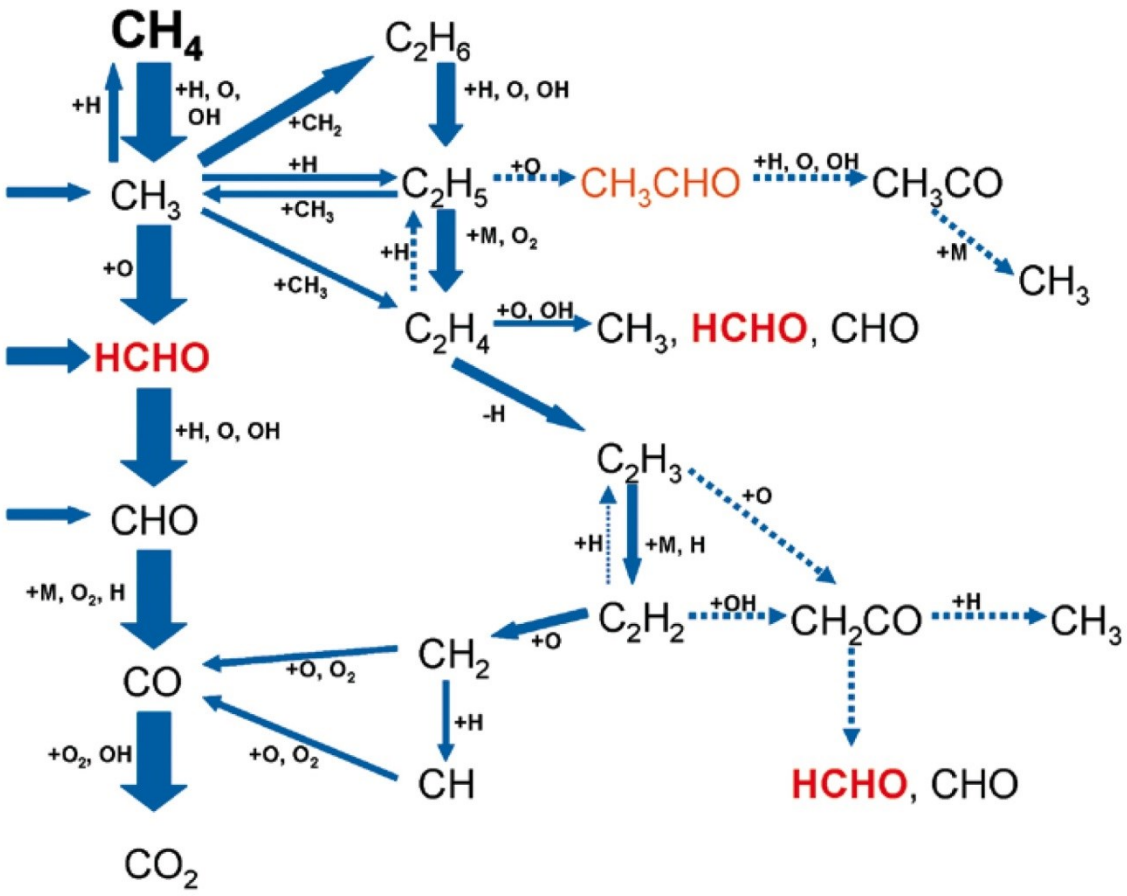

Figure 4.1: Reaction Scheme for Combustion of Methane, Bauer, et al. (2009)

The formaldehyde produced by the flame front and the mixing of unburned charge into burned charge late in the cycle, as well as by other phenomena such as gas escaping from cracks and crevices and auto-reaction of lean pockets is examined in this chapter.

4.2 Mechanism of Formaldehyde Formation

The models set up to match oxides of nitrogen in the previous chapter are applied to provide predictions for the amount of formaldehyde formed during the combustion process. These results are plotted in Figure 4.2, along with formaldehyde measurements from a multi-cylinder, large bore, two-stroke engine equipped with a pre-combustion chamber taken from a paper by De Wit at al. (1998).

Version 4 of the UWSI model, which is based on the chemical kinetic mechanism of Hunter, et al., predicts larger amounts of formaldehyde than the predictions of Version 1. The difference is about 3 ppmv at 280% theoretical air and reaches 9 ppmv at 360% theoretical air. Increasing air flow in the engine also results in an increase in formaldehyde emissions. Version 5 predicts 1 ppmv of formaldehyde at 280% theoretical air, which increases to 10 ppmv at 360% theoretical air. Version 5 is extrapolated to 430% theoretical air, resulting in an increase in formaldehyde emission to 33 ppmv. The UWSI model based on the two Wiebe function model predicts very little formaldehyde. This indicates that significant amounts of formaldehyde are not emitted from flame fronts. Therefore, we can conclude that the formaldehyde predicted by all other versions of the UWSI model is primarily formed due to the mixing of unburned gas into burned gas after the flame has ceased moving across the cylinder.

A correlation between CO and formaldehyde is suggested by the data in Table 3.1. Versions of the UWSI model which predict low formaldehyde emission also predict low CO emission. Version 4, which predicts higher CO emission, also predicts higher formaldehyde emission. Experimental results from a paper by Olsen, et al. (2001) show

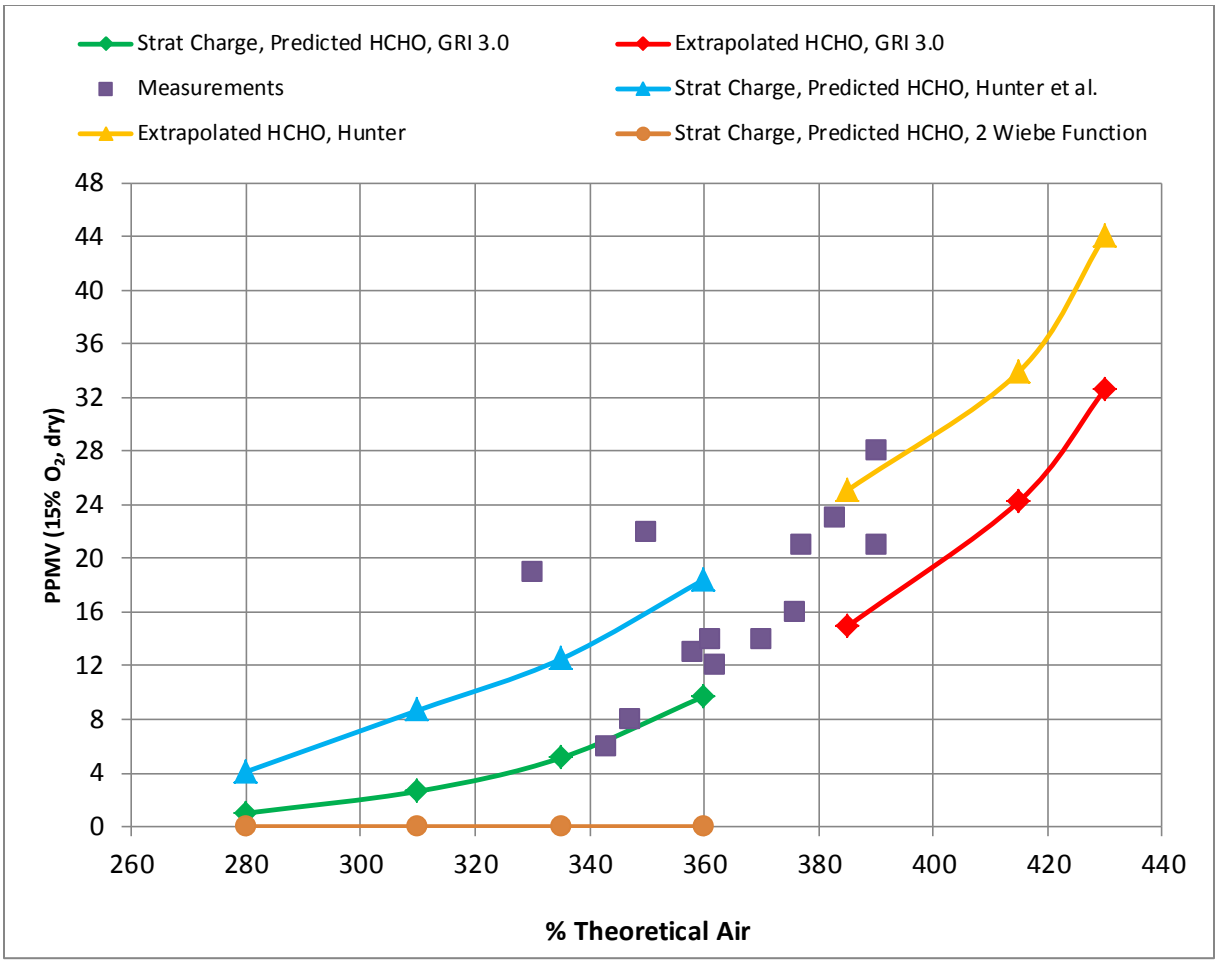

Figure 4.2: Predicted Formaldehyde vs Overall Theoretical Air

some correlation between CO and formaldehyde emission for lean-burn large-bore natural gas engines. This is thought to be due to the generation of CO by the same low temperature reactions responsible for the generation of formaldehyde. Since Version 3 of the UWSI model (the version in which the PMM is replaced with the 2nd Wiebe function) predicts very little CO and formaldehyde, it is clear that a significant portion of both are produced away from the flame and therefore correlate well with each other. From these results, we can conclude that an engine tuned for NOx emissions of 2gm/bhp-hr should exhibit formaldehyde emissions of 10-20 ppmv. If the engine is leaned out to a NOx

emission of 0.2 gm/bhp-hr, the formaldehyde emission would increase to about 30 - 40 ppmv.

The formaldehyde measurements mostly fall between the predictions of the GRI 3.0 mechanism and the mechanism of Hunter et al. Although the measurements show scatter, there is a clear trend of increasing formaldehyde emission with increasing air flow through the engine.

The mechanism of formation of formaldehyde can be explained as follows. Since the engine operates in the partial burn regime, flame propagation through the cylinder is incomplete. Once the flame propagation has weakened, unburned gas is mixed into the burned gas, leading to partial oxidation resulting in the formation of species like formaldehyde. The modeling done in this study also suggests that CO is formed in large bore lean burn engines in the same manner. As the engine is leaned out, this partial oxidation process leads to greater formaldehyde production. Therefore, pockets of lean charge are more likely to be major sources of formaldehyde. Unmixed pockets of charge or pockets of charge too lean to react are emitted as unburned fuel. UWSI accounts for this by leaving some fuel unburned in the Prescribed Mixing Model (PMM). Small amounts of higher hydrocarbon species, such as ethane are also formed during the mixing of burned and unburned charge.

4.3 Formaldehyde as a Function of Engine Crank Angle

Examining the conditions in the cylinder and the pollutant levels as a function of crank angle can give provide valuable insight into formaldehyde formation. The results in this

section pertain to the baseline engine case, running at 315% theoretical air with a spark timing of 6^{o} BTDC, modeled using the GRI 3.0 mechanism.

Figure 4.3 shows the pollutant emissions and the average and burned gas temperatures as a function of crank angle. This plot is for the baseline case, from which the UWSI model was calibrated in Chapter 2. The main chamber phi is 0.617 and the pre-chamber phi is 0.983. The following points are noted:

- The peak value of the burned gas temperature, T_b is about 2500 K and occurs as the flame is leaving the pre-combustion chamber. As the flame propagates through the main chamber, the temperature drops significantly.
- The average of the burned and unburned gas temperatures, T_{avg}, reaches a peak value of 1780 K at about 17^{o} ATDC. T_{avg} drops to 1278 K at exhaust port opening.
- NOx is formed in the engine when the temperature is high and peaks at around 25^{o} ATDC. No NOx is formed after 30^{o} ATDC, and during the latter part of the cycle NOx destruction is observed. This is found to be due to the attack of hydrocarbon radicals on the NO molecule and is addressed in Chapter 5.
- The CO trace shows a spike in the pre-combustion chamber. The CO formed therein is rapidly oxidized as the leaner mixture in the main chamber undergoes combustion. CO formation starts again at 50^{o} ATDC, when the burned gas temperature is about 1650 K. The spike is caused by the near-stoichiometric operating conditions in the pre-chamber; once the flame encounters a lean mixture, the CO quickly oxidizes, but then forms again as gas left unburned by the main flame propagation mixes into the burned gas.

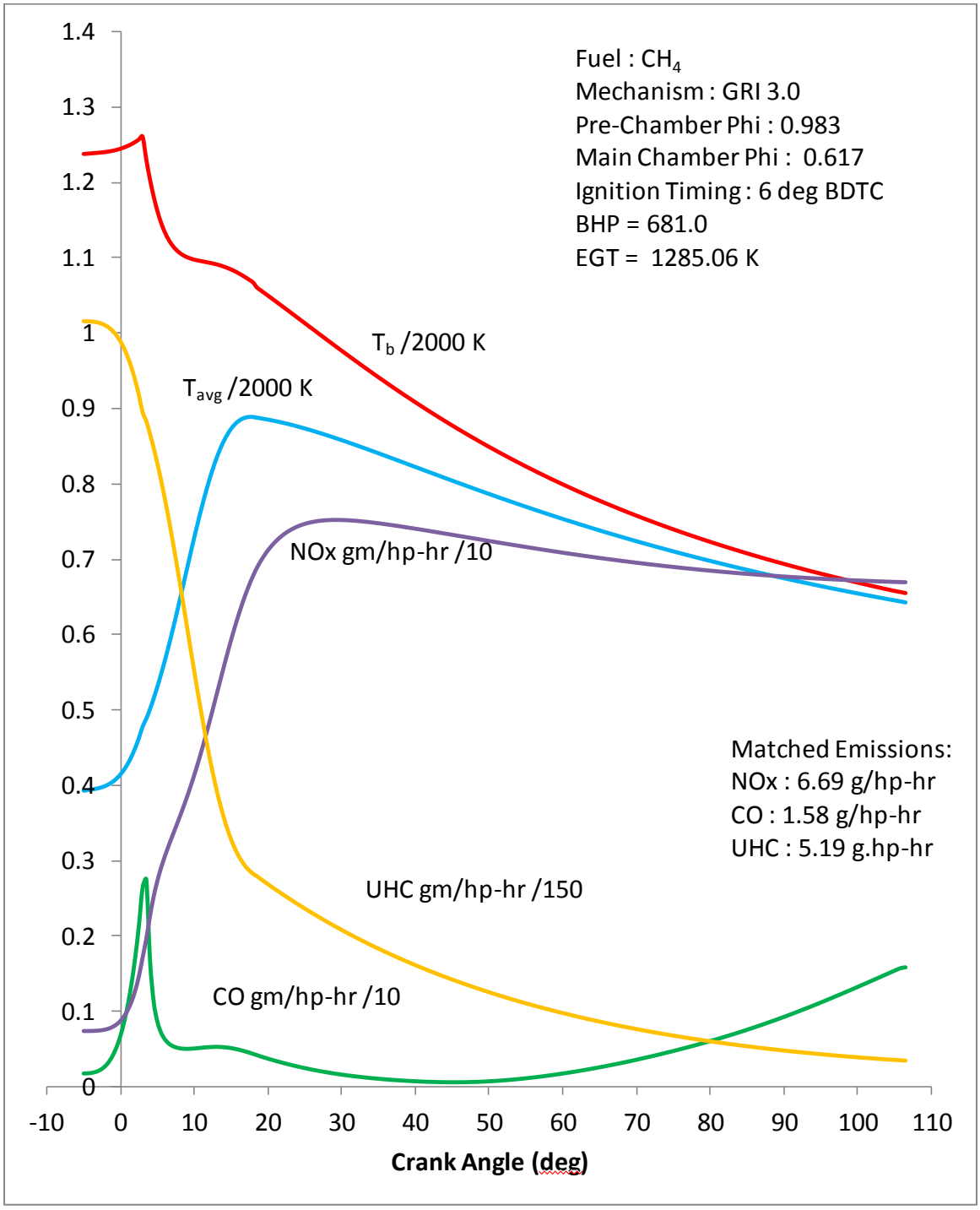

Figure 4.3: Prediction of Pollutant Species and Temperatures for a Single Cylinder, Large Bore, Stratified Charge Natural Gas Engine with Spark Timing 6° BTDC

- The UHC trace is proportional to the unburned mass fraction profile. At the switchover from the Wiebe function to the PMM, the plot of UHC indicates a mass fraction unburned of about 0.3, and at exhaust port opening, the UHC emission of 5.19 gm/bhp-hr corresponds to an unburned mass fraction of 0.034.

Figures 4.4 and 4.5 pertain to the current modeling. Version 4 is set up with a main chamber phi of 0.617 and a residual fraction of 0.11. Figure 4.4 shows a comparison of the experimental pressure trace with the pressure trace generated by version 5 of the model. Good agreement is observed between the two.

Figure 4.5 shows the average and burned gas temperatures and HCHO concentration as a function of crank angle for version 5. HCHO formation starts at about 64^{o} ATDC, when the burned gas temperature has been lowered to 1500 K. HCHO concentration increases as the expansion stroke proceeds and at exhaust port opening, its concentration is 3.3 ppm. No HCHO is seen before 64^{o} ATDC; the high temperatures rapidly oxidize any HCHO formed.

In Figures 4.6 and 4.7, the prescribed mixing model is replaced with the 2-wiebe function model. Figure 4.6 shows the pressure trace generated by this model; good agreement with the experimental pressure trace is observed. Figure 4.7 shows the HCHO trace. It is observed that a negligible amount of HCHO is formed in the cylinder. This further leads to the conclusion that HCHO is not caused by a fully propagating flame. Mixing of unburned charge into burned charge is required for significant HCHO emission.

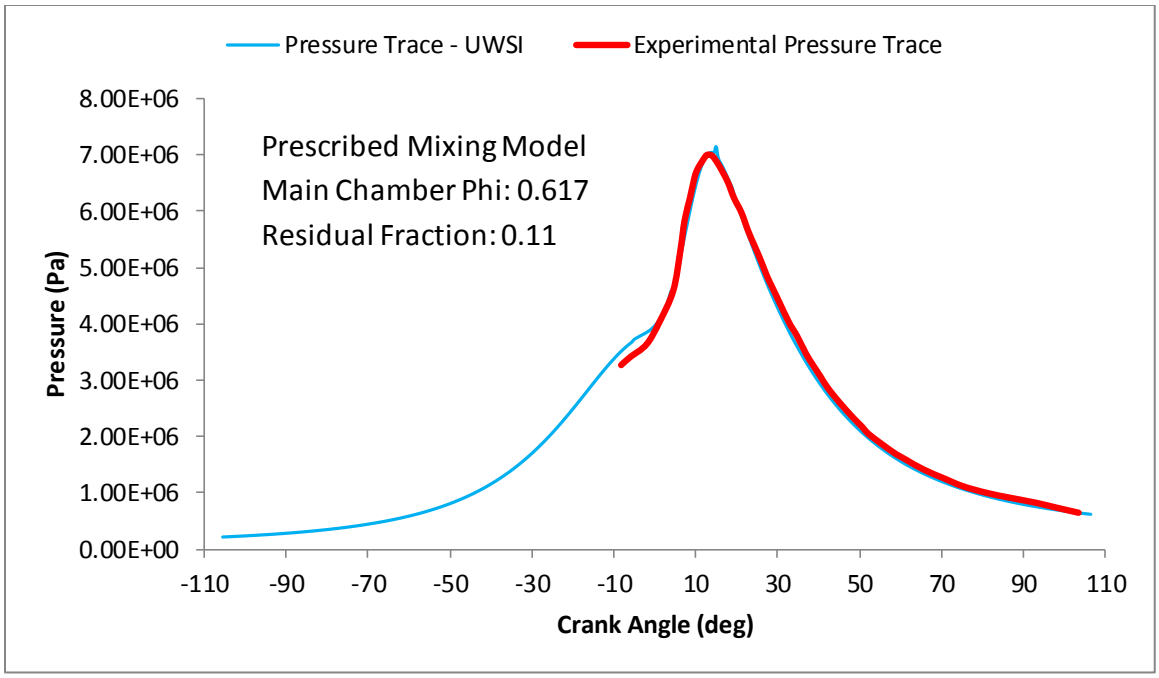

Figure 4.4: Comparison of Experimental Pressure Trace with Pressure Trace Generated by UWSI

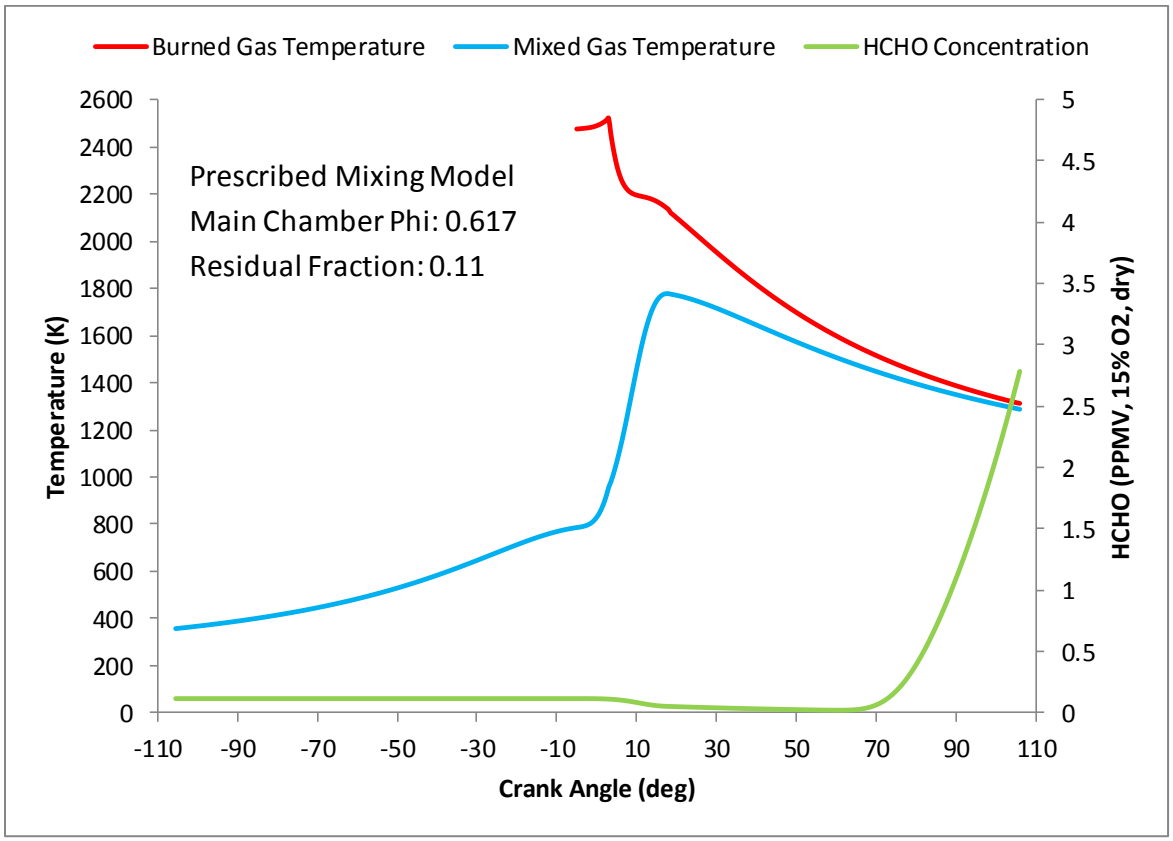

Figure 4.5: Predicted HCHO as a function of Crank Angle using Prescribed Mixing Model

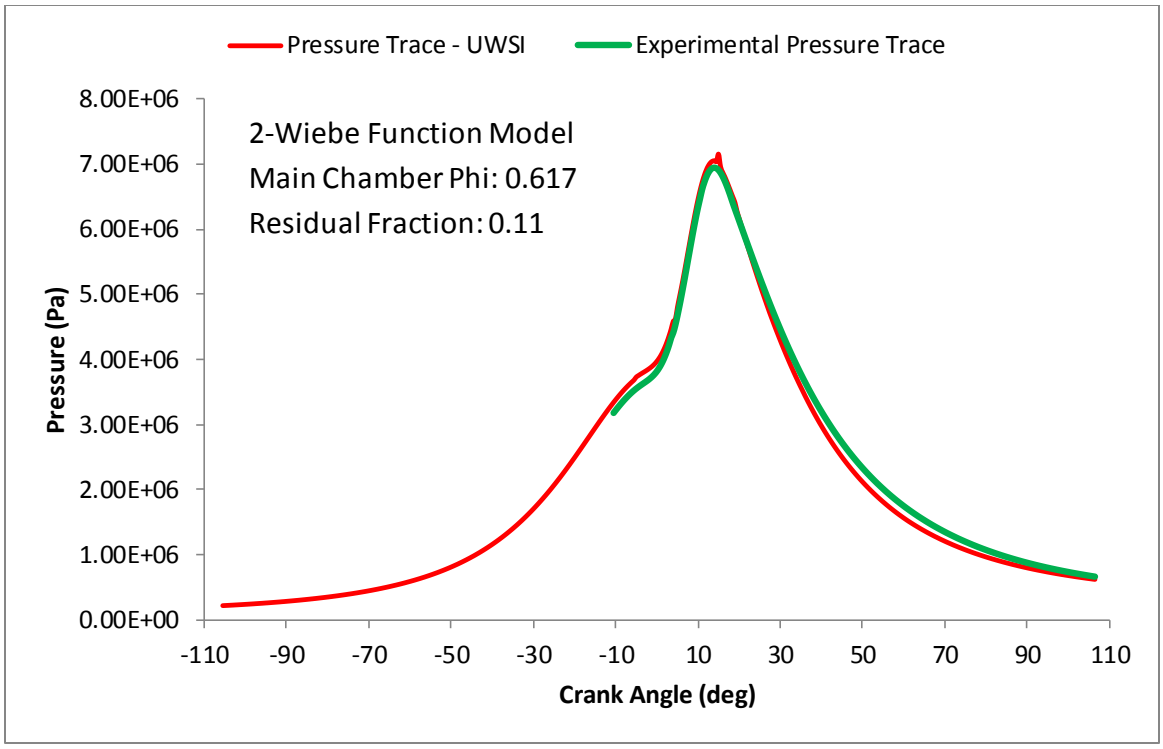

Figure 4.6: Comparison of Experimental Pressure Trace with Pressure Trace Generated by UWSI

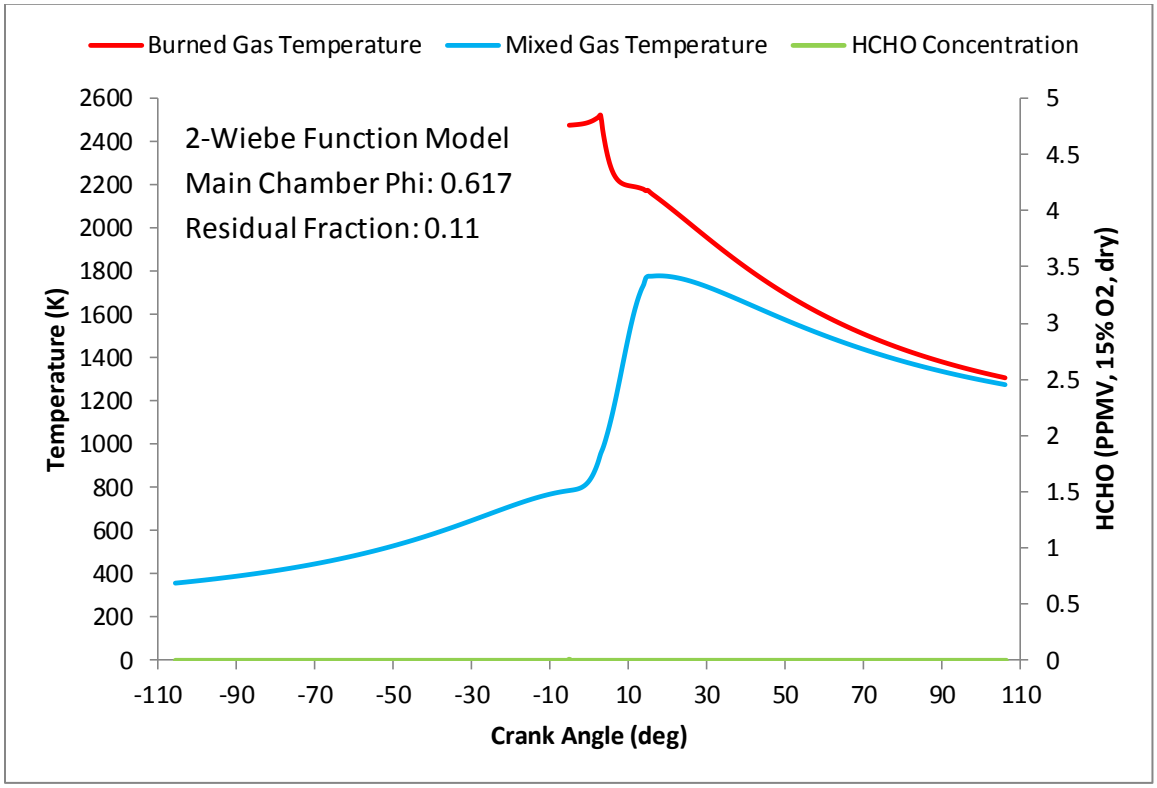

Figure 4.7: Predicted HCHO as a function of Crank Angle using 2-Wiebe Function Model

4.4 Crack and Crevice Modeling

As described in Sections 4.1 and 4.2, the mixing of unburned charge avoided by the flame front with burned gas leads to significant formaldehyde formation. Another potential source of formaldehyde is the unburned charge trapped in cracks and crevices of the engine. A crack and crevice sub-model based on a paper by De Petris, et al. (1995) was added to UWSI by Nicol and Malte (1997). This model is used to simulate the trapping of unburned charge in the spaces around the compression rings of the piston and between the cylinder wall and piston. As the piston compresses the charge during the compression stroke, some charge enters these crevices and is effectively protected from the flame front if the wall separation distance is less than the quenching distance. This unburned charge is released into the main chamber during expansion and reacts with the burned gas present therein. In this sub-model the crevices are modeled with volumes connecting the combustion chamber to the crankcase: immediately below the piston head there is the top landing, then there is the first ring, followed by the second crevice. Further on there is a second ring and then, finally, the crankcase. A diagram of this arrangement is shown in Figure 4.8. The features of this model relevant to the present study are described in greater detail in Appendix A.

The two-Wiebe function model is used in this section in order to eliminate all other sources of unburned charge being mixed into burned gas, other than that released from cracks and crevices in the engine. The study is conducted with both the GRI 3.0 mechanism as well as the mechanism of Hunter, et al. The baseline stratified charge setup from Chapter 4 is used, with a spark timing of 6^{o} BTDC, trapped phi of 0.64 and

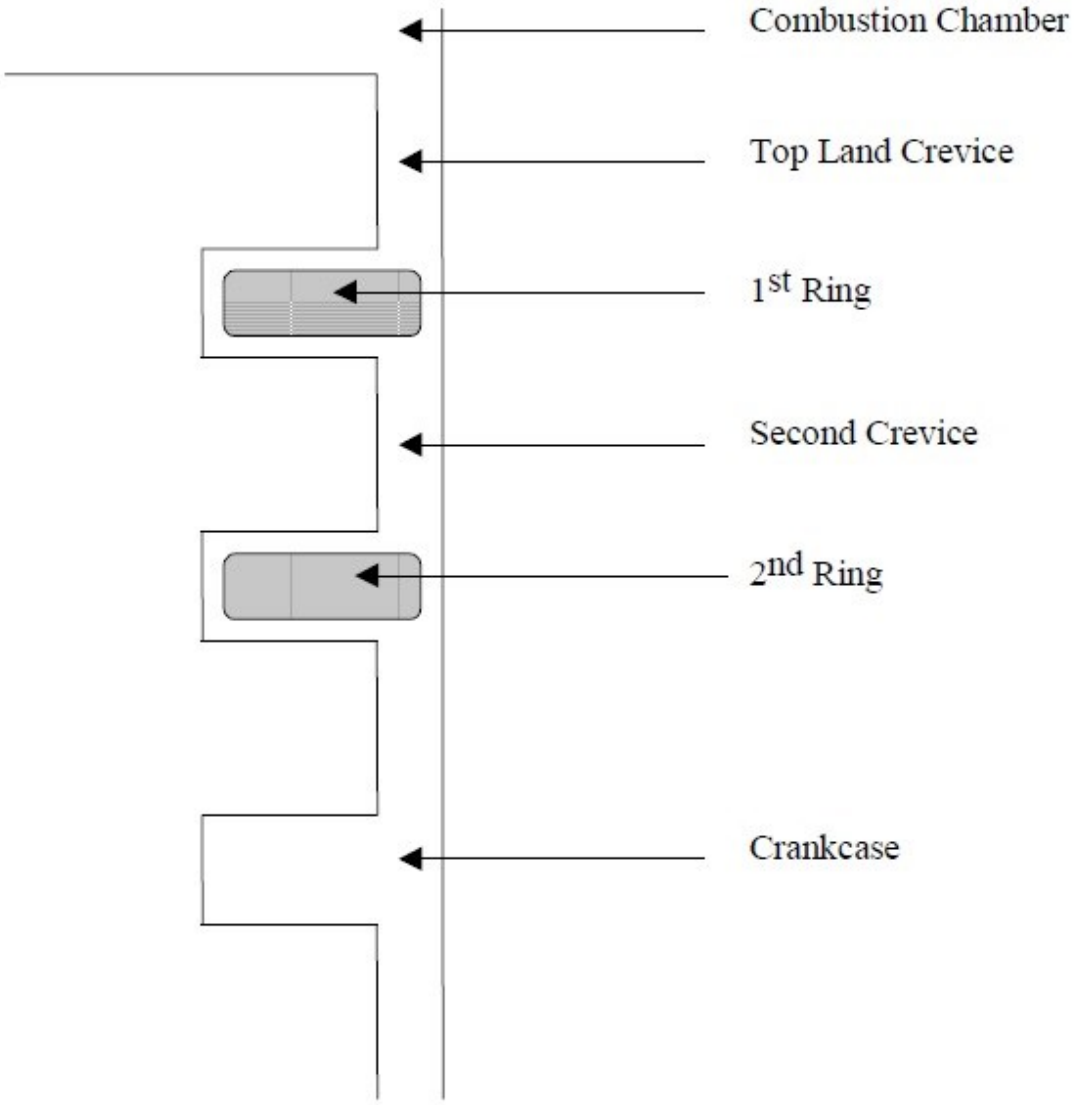

Figure 4.8: Simplified Schematic of Crack and Crevice Model in UWSI

residual fraction of 0.11. The maximum mass of the crevices was varied from 1.9% of the total cylinder mass to 8% of the cylinder mass.

Figures 4.9 through 4.11 pertain to the modeling done with a crevice volume of 1.9% of the total cylinder mass. Figure 4.9 shows the mass flow rate into the crevice volume as a function of crank angle. Gas flows into the crevice during the compression stroke and the

initial part of flame propagation. Flow out of the crevice begins shortly after peak pressure in the main cylinder, at about 16° ATDC, reaches its maximum value at 25° ATDC and falls off to a low level for crank angle exceeding 70° ATDC. Therefore, most of the unburned charge from the crevice is released between 25° and 70° ATDC. Figure 4.10 shows the pressure in the second landing, with the pressure in the main chamber shown for reference.

Figure 4.11 shows the predicted formaldehyde in the main chamber as a function of the crank angle using the GRI 3.0 mechanism, along with the burned gas temperature and the average temperature of the burned and unburned gas in the cylinder. The amount of formaldehyde produced is extremely low. Also, it is noted that most of the formaldehyde is formed after a significant amount of gas has been released from the crevice, i.e., after 70° ATDC. Therefore, gas escaping from the crevice does not contribute significantly to formaldehyde formed in the cylinder, since it is oxidized due to high temperature behind the flame front.

The crevice mass is now increased to 5% of the total mass of the total cylinder mass. Figure 4.12 shows the mass flow rate into the crevice as a function of crank angle, and follows the same trends as fig 4.9. Figure 4.13 shows the formaldehyde concentration as a function of crank angle. The amount of formaldehyde formed is greater than that for a crevice mass of 1.9%, but still very small.

The largest crevice mass considered is 8.0% of the total cylinder mass. The trend of the flow into the crevice, shown in Figure 4.14, is similar to the earlier considered crevice

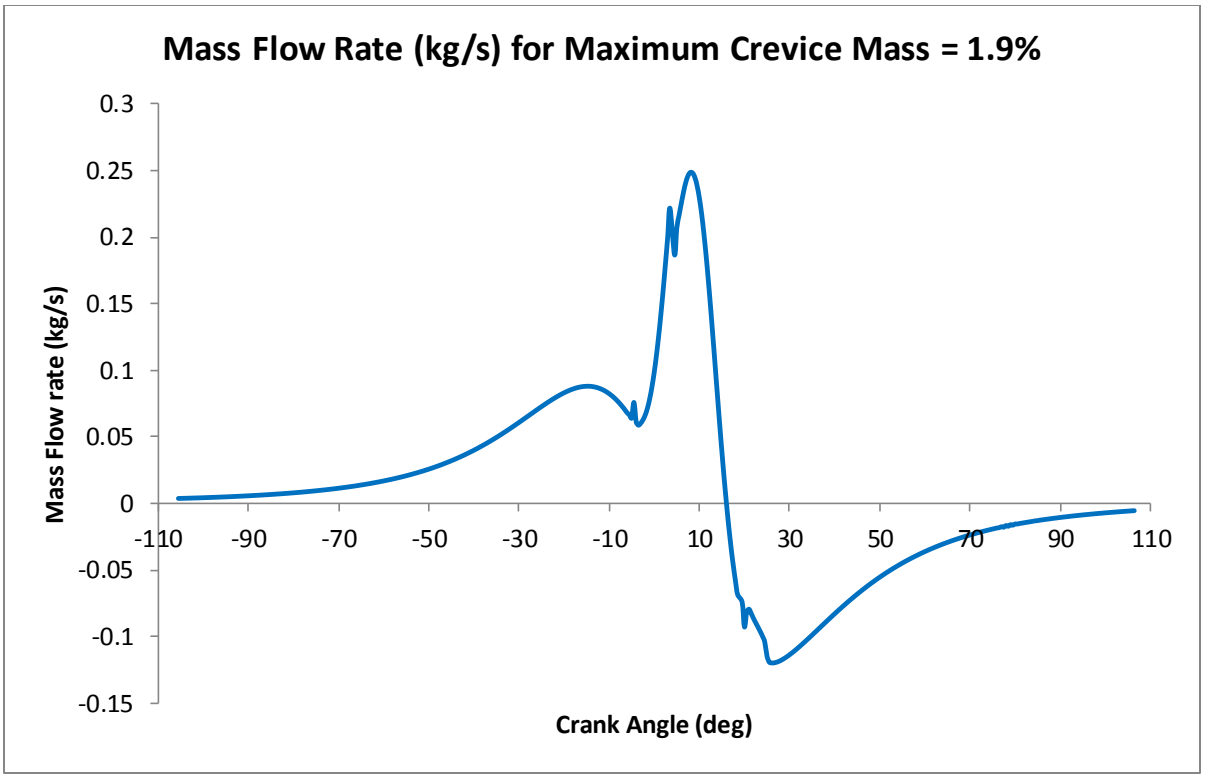

Figure 4.9: Mass flow rate into crevice for maximum crevice mass of 1.9%

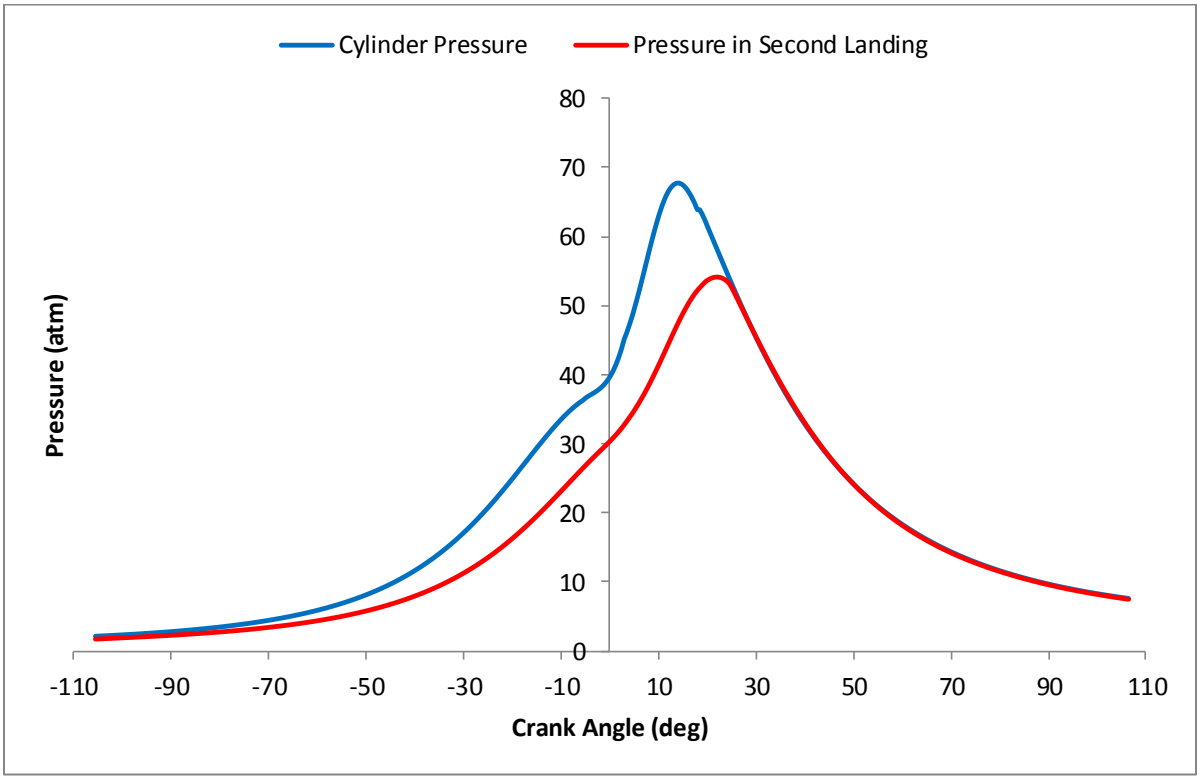

Figure 4.10: Main chamber conditions for crevice mass of 1.9%. Main Chamber Phi = 0.617, Residual Fraction = 0.11

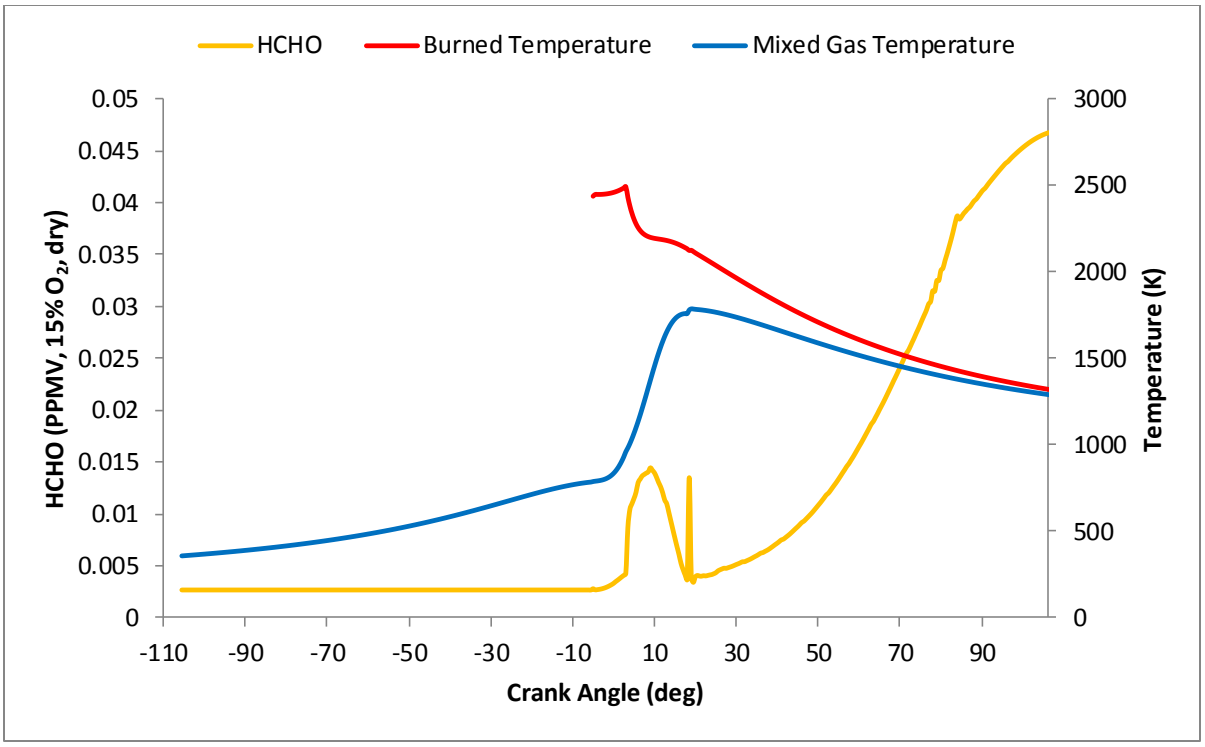

Figure 4.11: Predicted HCHO and temperature for a crevice mass of 1.9% using the 2-Wiebe function model. Main Chamber Phi = 0.617, Residual Fraction = 0.11

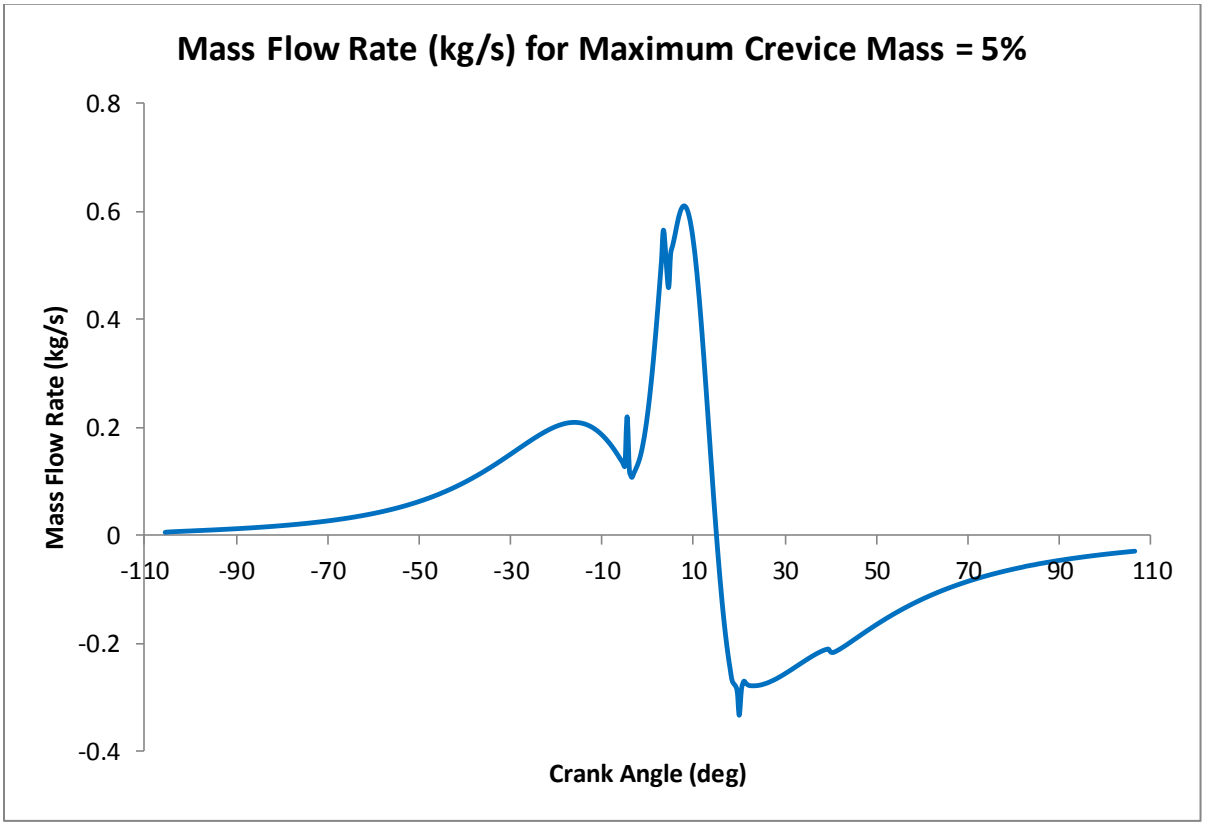

Figure 4.12: Mass flow rate into crevice for maximum crevice mass of 5%

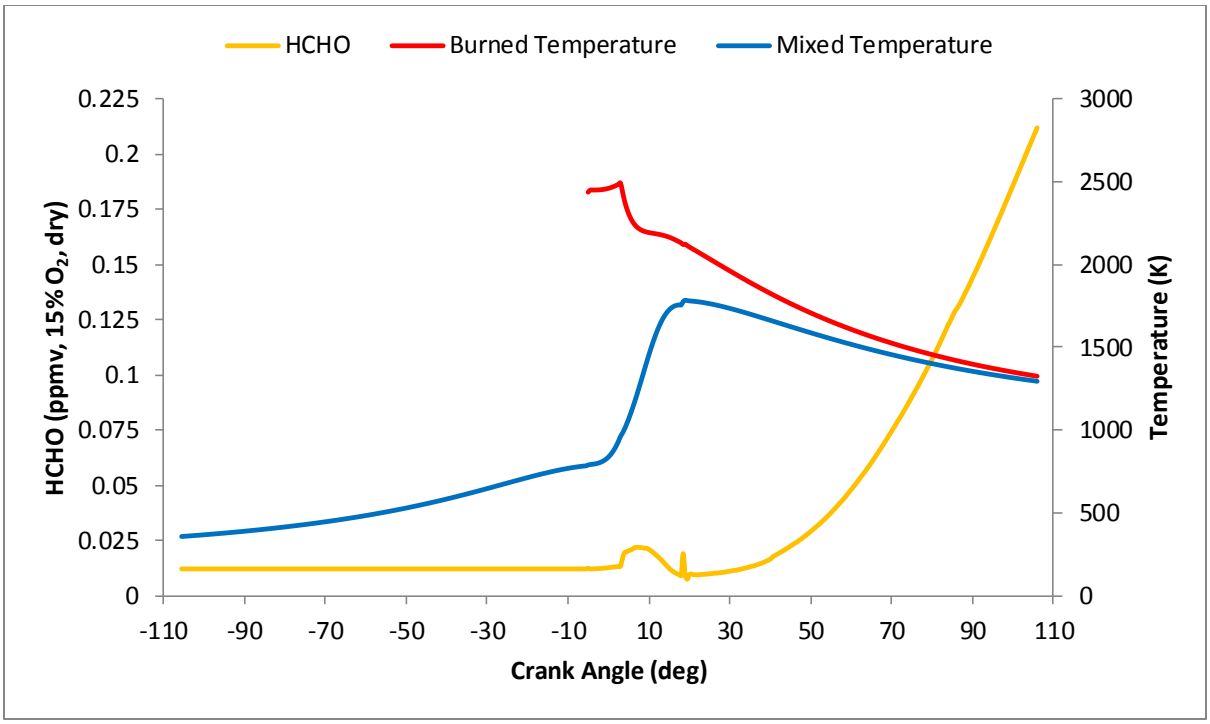

Figure 4.13: Predicted HCHO and temperature for a crevice mass of 5% using the 2-Wiebe function model. Main Chamber Phi = 0.617, Residual Fraction = 0.11

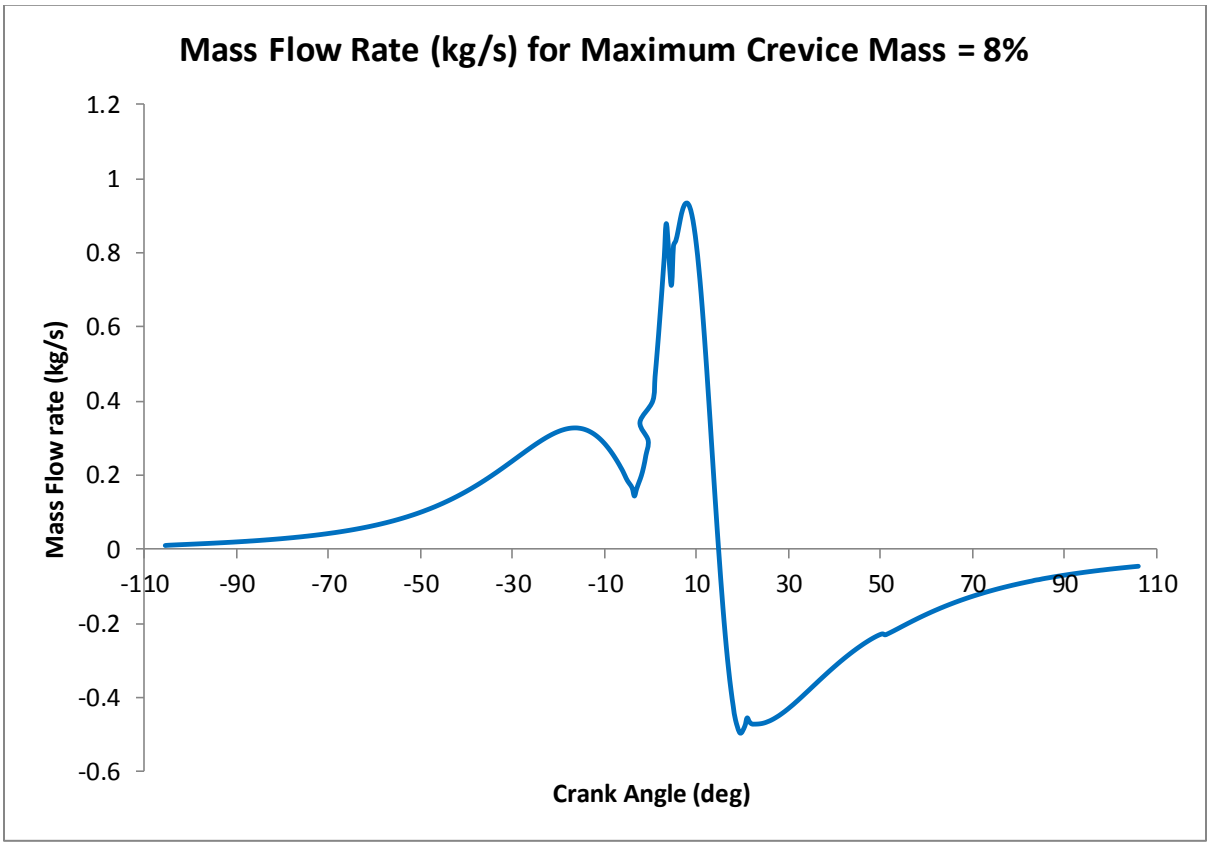

Figure 4.14: Mass flow rate into crevice for maximum crevice mass of 8%

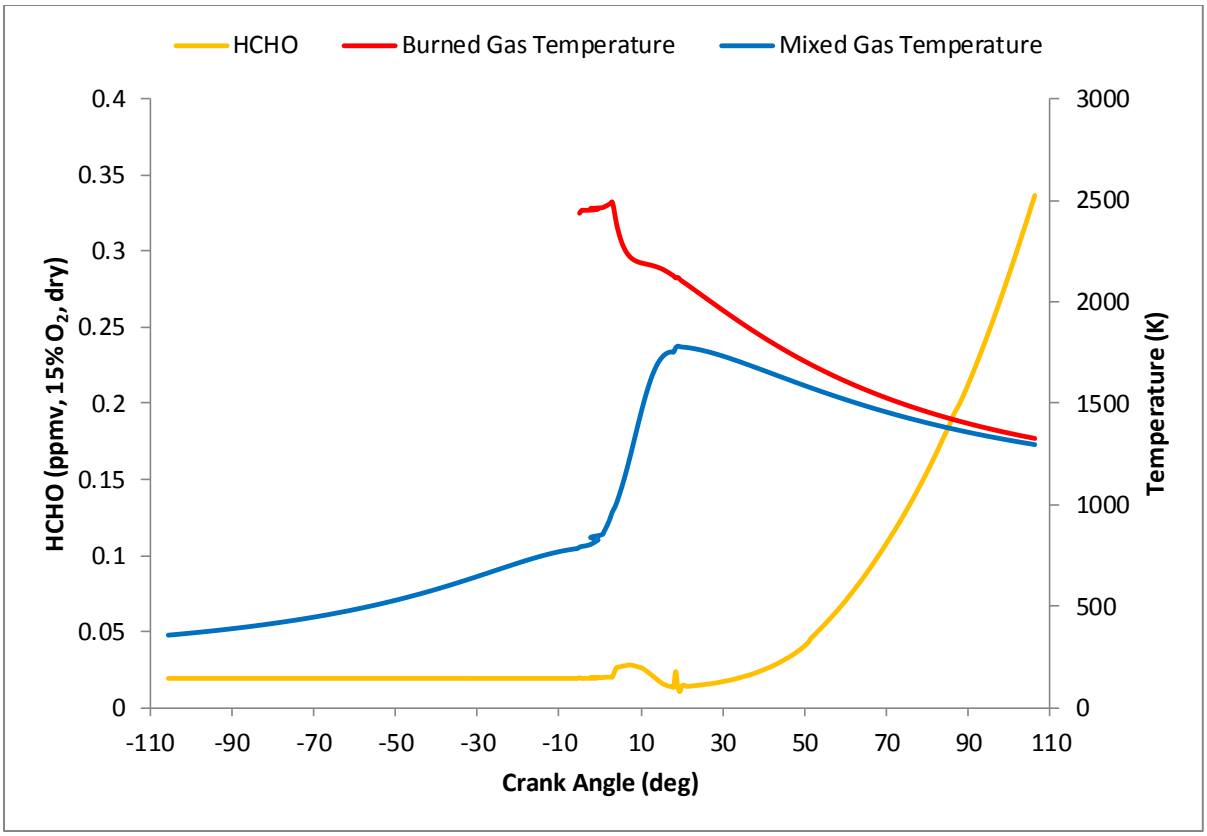

Figure 4.15: Predicted HCHO and temperature for a crevice mass of 8% using the 2-Wiebe function model. Main Chamber Phi = 0.617, Residual Fraction = 0.11

masses. The amount of formaldehyde produced, shown as a function of crank angle in Figure 4.15, is marginally higher than the earlier cases.

The effect of increasing the residual fraction on formaldehyde emission is also studied. Figures 4.16 and 4.17 show formaldehyde concentration as a function of crank angle for crevice masses of 1.9% and 8% of the total cylinder mass. The residual fraction is increased to 0.19 from 0.11 for these cases. The modeling is done using the GRI 3.0 mechanism with a main chamber fuel-air equivalence ratio of 0.617. Increasing the residual fraction has the effect of reducing the burned gas temperature, and increasing the amount of formaldehyde produced. The formaldehyde yield also begins somewhat sooner in the cycle.

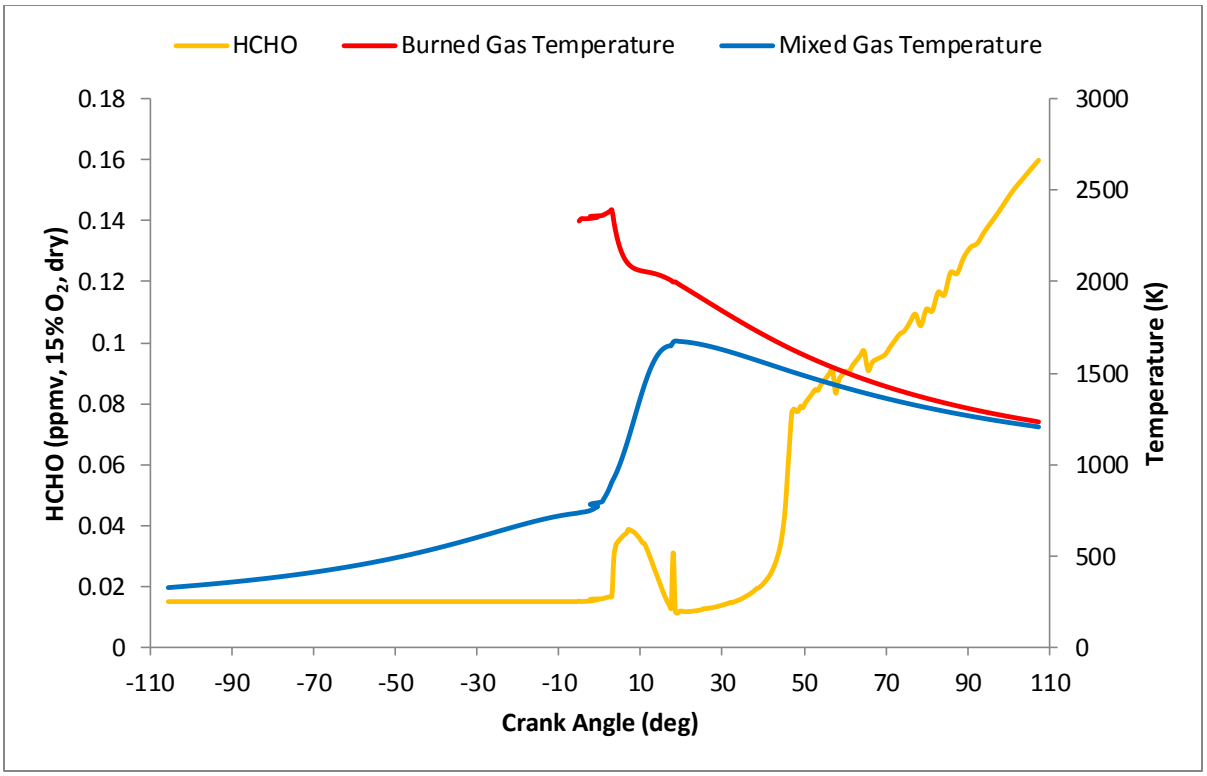

Figure 4.16: Predicted HCHO and temperature for a crevice mass of 1.9% using the 2-Wiebe function model. Main Chamber Phi = 0.617, Residual Fraction = 0.19

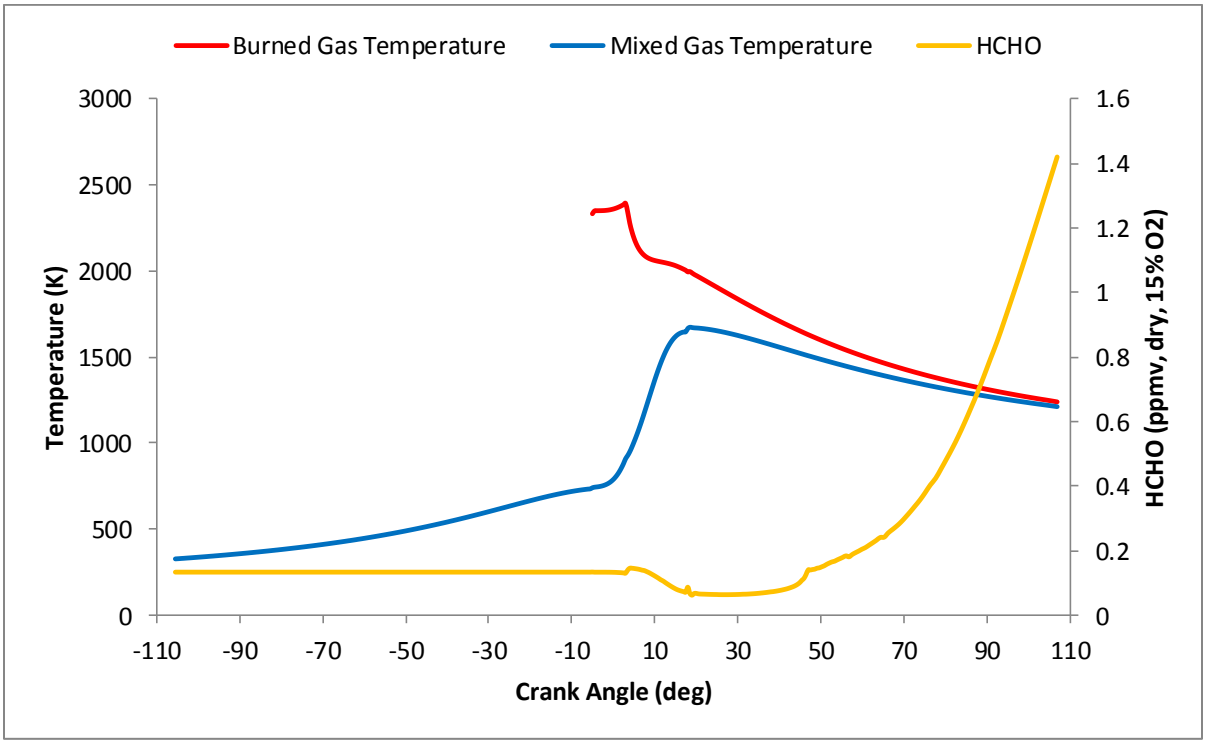

Figure 4.17: Predicted HCHO and temperature for a crevice mass of 8% using the 2-Wiebe function model. Main Chamber Phi = 0.617, Residual Fraction = 0.19

The crevice masses considered in this analysis cover a broad range, since 1.9% of cylinder mass would be a small crevice and 8% of cylinder mass would be a fairly large crevice for an engine. The effect of increasing the residual fraction is also studied. Results obtained indicate that unburned gas trapped in cracks and crevices and later released into the burned gas does not significantly contribute to the formaldehyde emission when compared to the formaldehyde due to incomplete flame propagation. The largest crevice mass modeled (8% of total cylinder mass) yields 0.35 ppmv of formaldehyde, while the smallest crevice mass (1.9%) yields 0.05 ppmv of formaldehyde, both being only a small percentage of the formaldehyde formed due to incomplete propagation of the flame front. This is caused due to the relatively early release of unburned charge from the crevice, which is completely oxidized due to the high temperature in the main chamber of the cylinder. Increasing the residual fraction results in an increase in formaldehyde emission. However, formaldehyde yields remain less than 1.5 ppmv, which is small compared to formaldehyde yields due to incomplete flame propagation.

4.5 Auto-reaction Modeling

Experimental data (Olsen et al., 2001) and the modeling of the previous sections indicates that burning of charge avoided by the flame front late in the cycle at relatively low temperatures contributes significantly to formaldehyde formation. It also indicates that leaner mixtures are more likely to be major sources of formaldehyde. Large bore engines operating at lean conditions have a significant probability of containing fuel-air non-uniformities in the combustion chamber. Large bore engines also operate at low RPM's leading to lower turbulence levels, which enhances non-uniformity in the local fuel-air

ratio. Furthermore, the process of injecting fuel directly into the cylinder can also aid the formation of pockets of non-uniform charge, since the time for fuel-air mixing in these cases is limited. In this chapter, lean pockets of gas bypassed by the main flame front are examined for auto-ignition.

Modeling is accomplished by a chemical reactor model consisting of plug flow reactors at assigned residence time. The chemical kinetic mechanisms used are GRI 3.0 and the mechanism of Hunter, et al. The response of a mixture of methane and air of 0.2 fuel-air equivalence ratio is plotted in Figures 4.18 and 4.19. The initial temperature is 1100 K and the pressure is held constant at 10 atm. Figure 4.18 shows the results of the chemical reactor model run with the Hunter et al. mechanism and Figure 4.19 shows the results with GRI 3.0. It is seen that pre-ignition auto-reaction occurs at about 25 ms for the Hunter mechanism and at about 12 ms for GRI 3.0. The species noted are ethane, HCHO, ethylene, the methyl radical and methanol. The maximum HCHO concentration is noted to be about 1200 ppmv for GRI 3.0 and about 1000 ppmv for the Hunter et al. mechanism. Upon ignition, the species concentrations plotted rapidly decrease, and the temperature increases from the initial 1100 K. In Figures 4.20 and 4.21, the results are plotted for a pressure of 50 atm. Both mechanisms show a decrease in time to auto-ignition; auto-ignition occurs at about 6.5 ms for the Hunter et al. mechanism and about 3.5 ms for the GRI 3.0 mechanism. The HCHO concentration prior to auto-ignition for both mechanisms falls slightly, but is still around 1000 ppmv. Therefore, the main difference between the two is the reduction in time to auto-ignition. Figures 4.22 and 4.23 show the results for a pressure of 10 atm, when the initial temperature is increased to 1150 K. The time to auto-ignition for the Hunter et al. mechanism is about 12 ms, and for

the GRI 3.0 mechanism is about 6 ms. The maximum HCHO concentration for both mechanisms is roughly 1000 ppmv. Figures 4.24 and 4.25 show the results when the pressure is increased to 50 atm. The time to auto-ignition for both mechanisms reduces, but the maximum HCHO concentration remains close to 1000 ppmv.

The two chemical kinetic mechanisms used in this analysis, GRI 3.0 and the Hunter et al. mechanism, do not agree on the time required for the mixture to auto-ignite. The Hunter et al. mechanism predicts an auto-ignition time of almost twice the time predicted by GRI 3.0, for the same conditions. The maximum concentration of HCHO predicted by both mechanisms for the same conditions is in good agreement.

From this chemical reactor modeling, it is observed that reactions leading to auto-ignition form a significant amount of formaldehyde. The time required for a mixture to auto-ignite is found to decrease with increasing pressure. Increasing the initial temperature of the mixture is also found to decrease the time required for the mixture to auto-ignite. The maximum HCHO concentration is found to stay close to 1000 ppmv for the entire range of initial temperatures and pressures modeled. This indicates that an engine on the verge of auto-ignition or experiencing borderline auto-ignition could emit significant amounts of HCHO.

Initial Temperature (K)	Pressure (atm)	Mechanism	Time to Autoignition (ms)	HCHO (ppmv)
1100	10	GRI 3.0	12	1192
1100	10	Hunter, et al.	25	1024
1100	50	GRI 3.0	3.5	1048
1100	50	Hunter, et al.	6.5	927
1150	10	GRI 3.0	6	1083
1150	10	Hunter, et al.	12	982
1150	50	GRI 3.0	1.7	1134
1150	50	Hunter, et al.	3	935

Table 4.1: Results of chemical reactor modeling

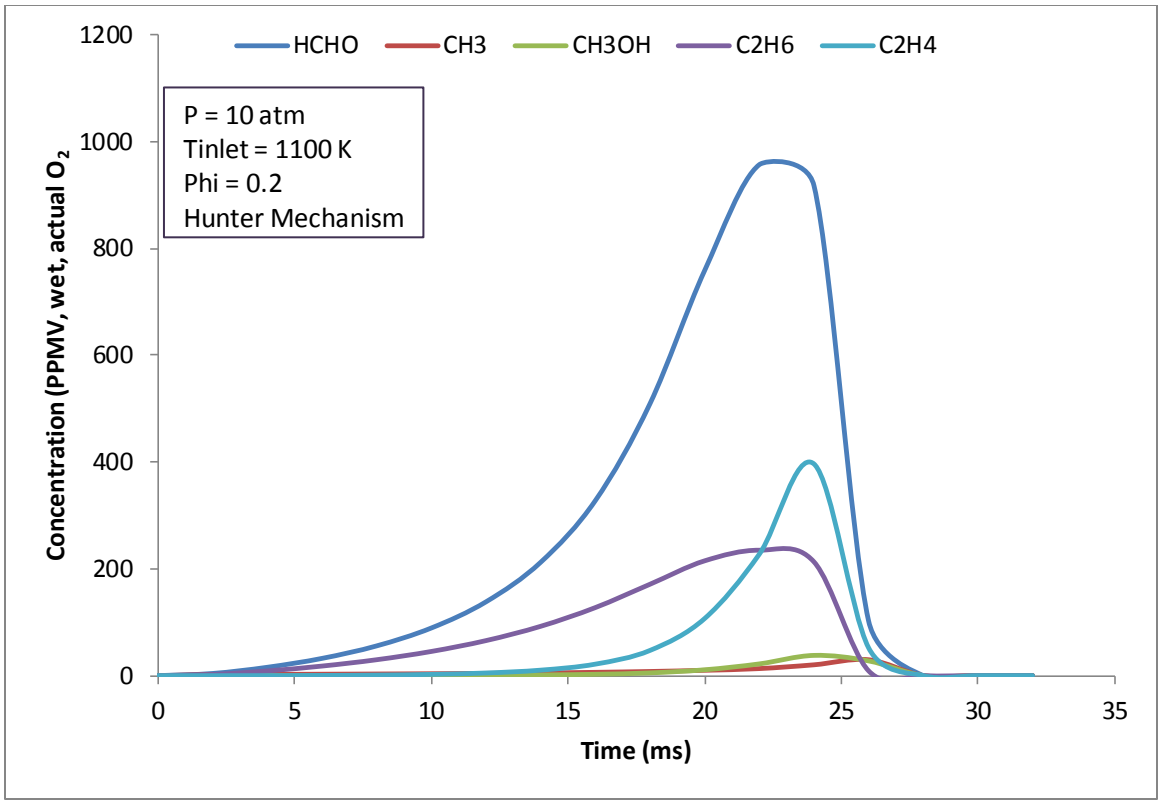

Figure 4.18: Predicted hydrocarbon concentrations using chemical reactor modeling

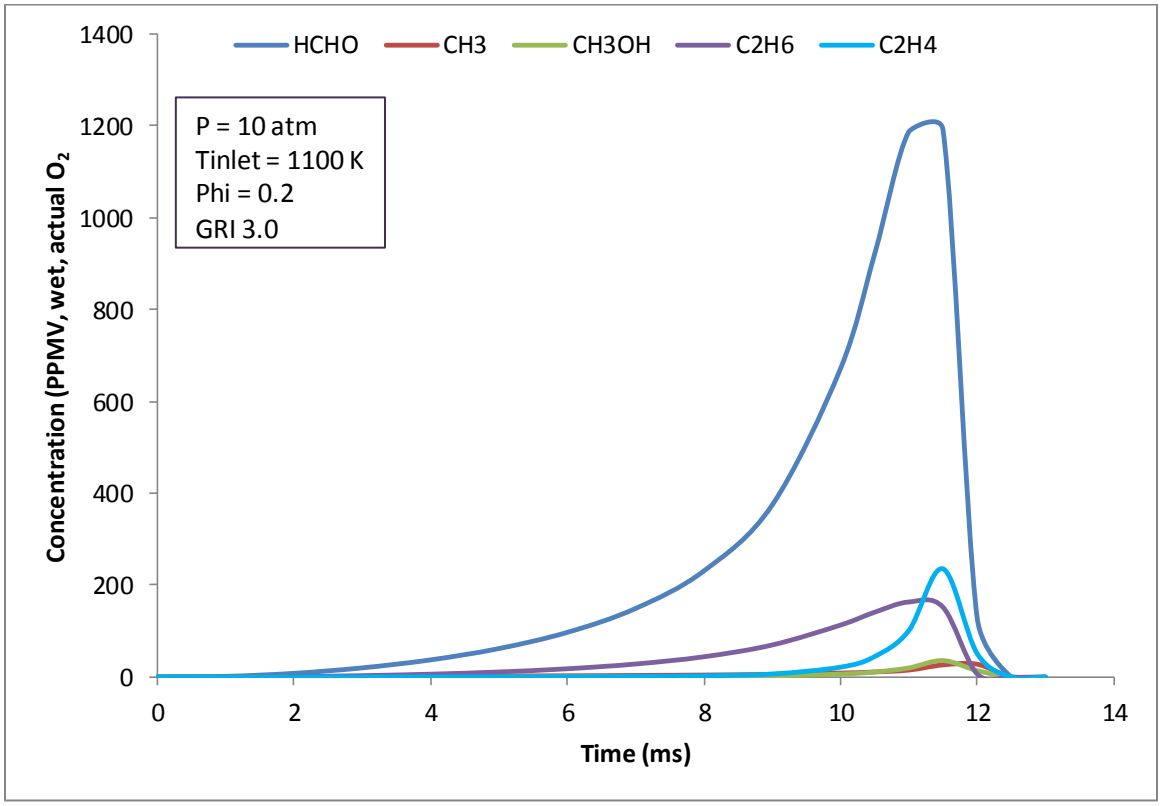

Figure 4.19: Predicted hydrocarbon concentrations using chemical reactor modeling

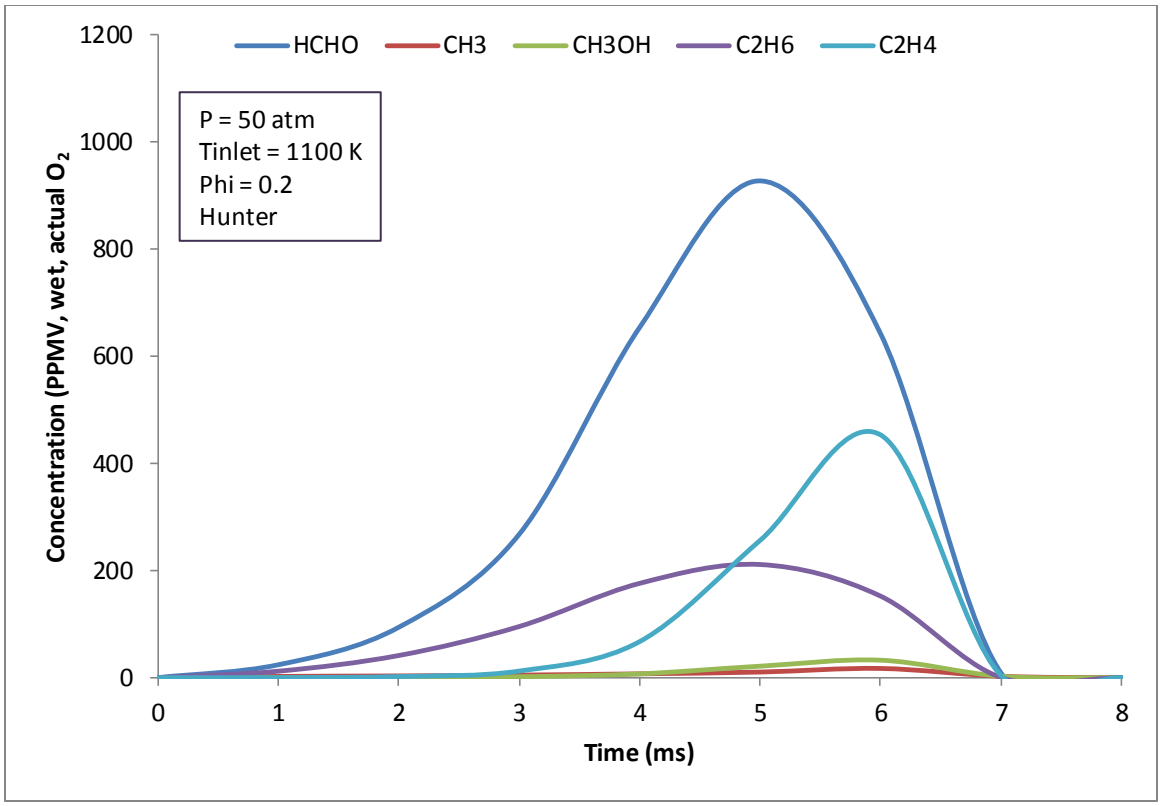

Figure 4.20: Predicted hydrocarbon concentrations using chemical reactor modeling

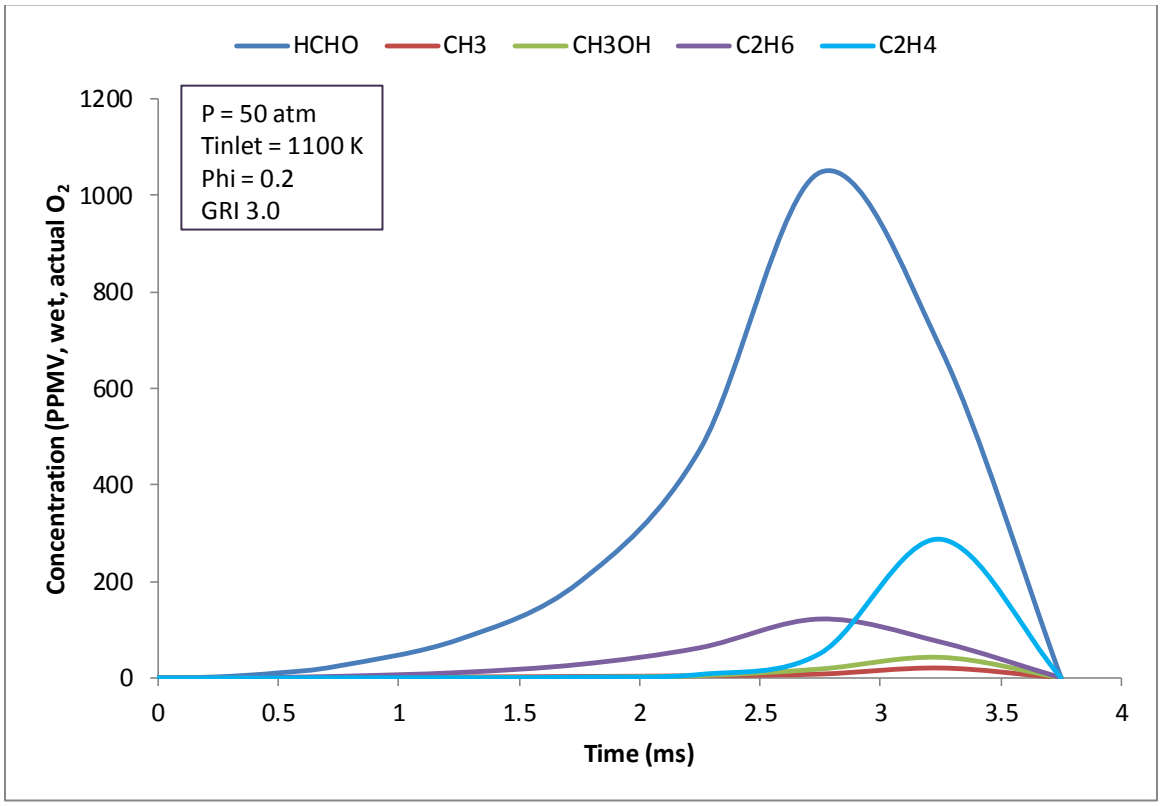

Figure 4.21: Predicted hydrocarbon concentrations using chemical reactor modeling

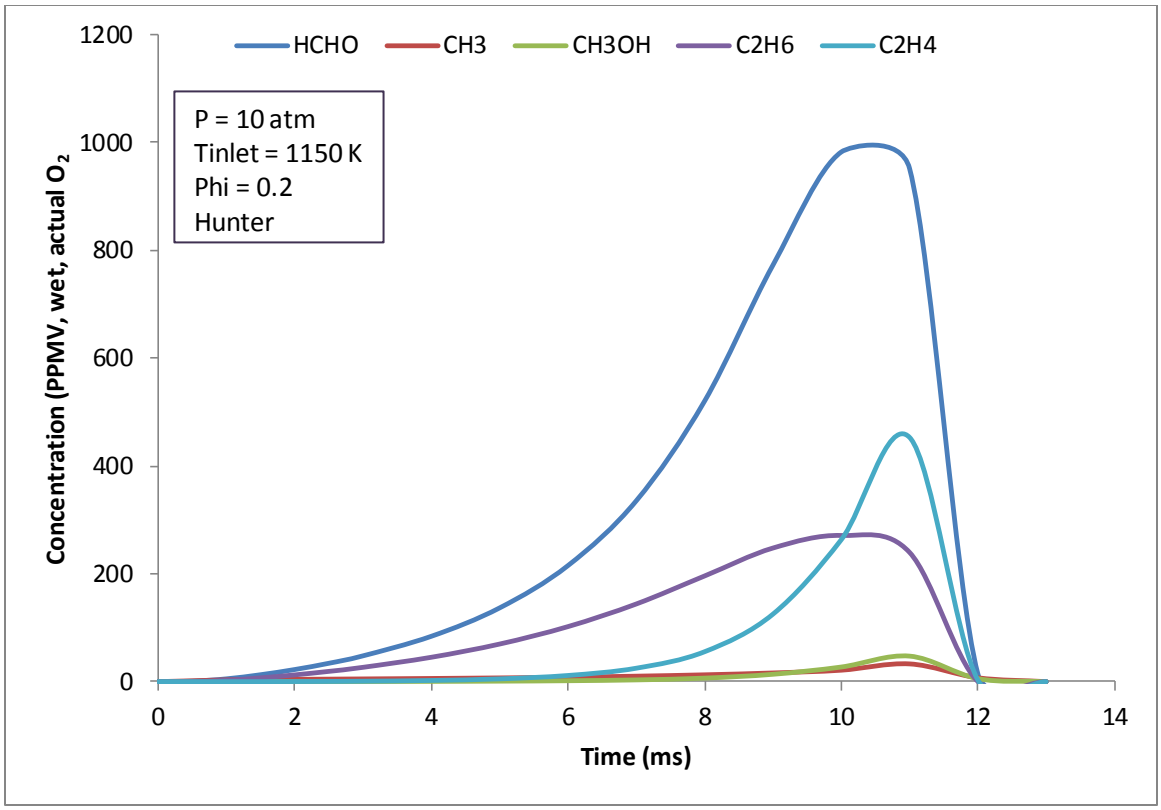

Figure 4.22: Predicted hydrocarbon concentrations using chemical reactor modeling

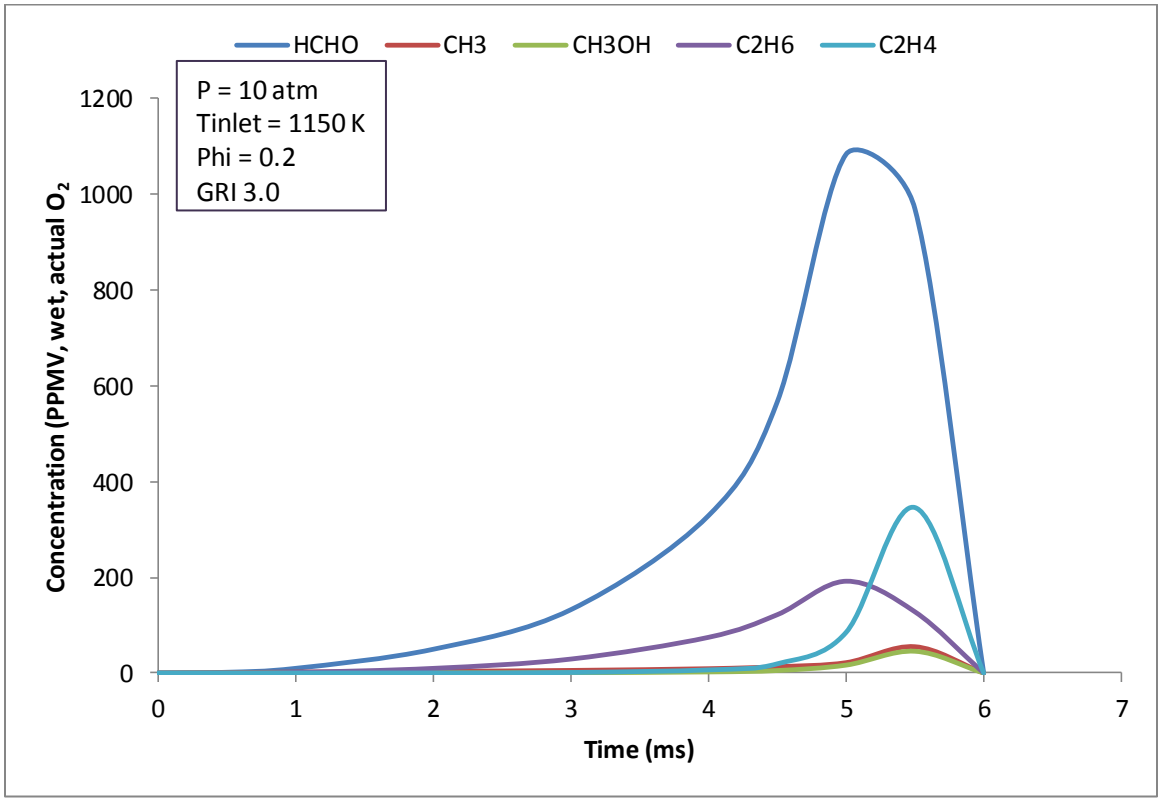

Figure 4.23: Predicted hydrocarbon concentrations using chemical reactor modeling

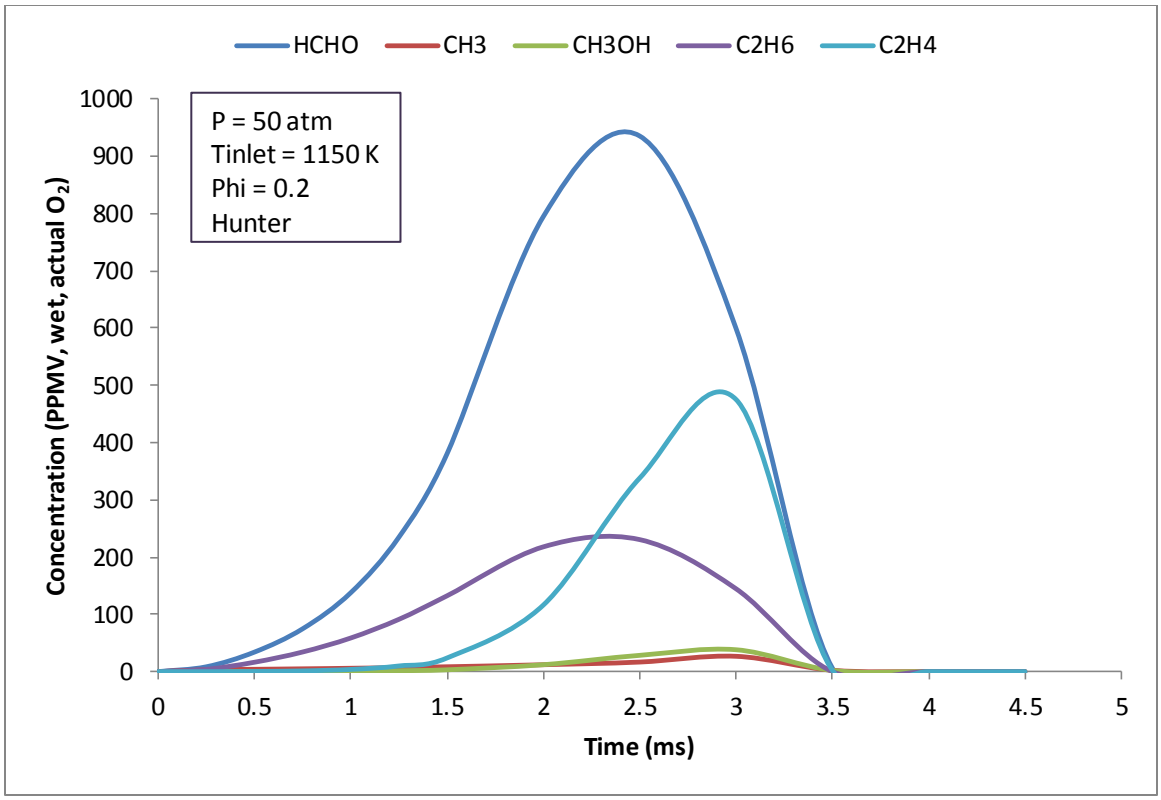

Figure 4.24: Predicted hydrocarbon concentrations using chemical reactor modeling

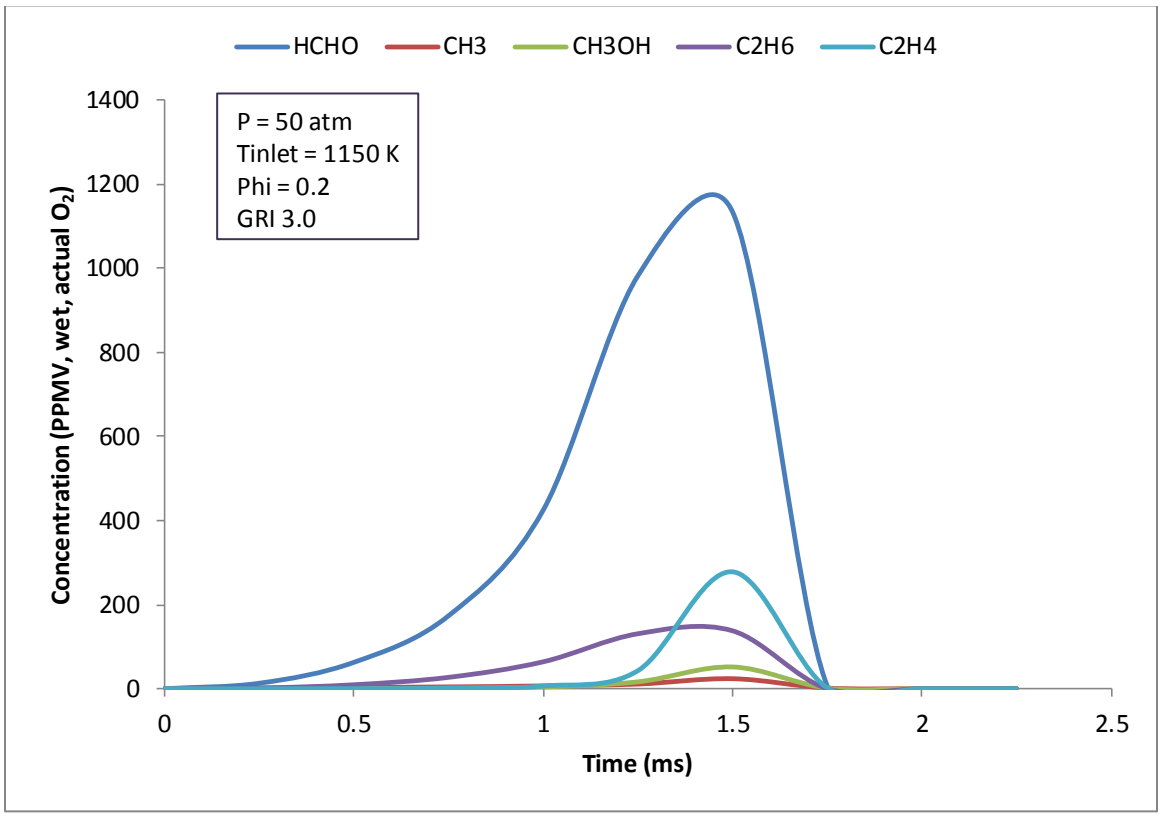

Figure 4.25: Predicted hydrocarbon concentrations using chemical reactor modeling

5.0 NOx Formation Mechanisms in Large Bore Natural Gas Engine

In Chapter 3, NOx predictions were made with the computer program UWSI, using a full chemical kinetic mechanism, GRI 3.0. The models set up matched NOx quite accurately over a range of operating conditions for a particular large bore spark ignition natural gas engine, and were also used to predict formaldehyde, CO and UHC emissions. However, UWSI does not provide us with any information about the mechanisms of formation of oxide of nitrogen in the simulations performed.

In this chapter, the pathways of NOx formation in lean-burn large-bore natural gas engines are examined using chemical reactor modeling, accomplished with the commercial software package CHEMKIN. The chemical reactor modeling provides us with information pertaining to NOx formation within the flame front as well as the post-flame region at various pressures and temperatures, while UWSI can be used to provide information about the overall effectiveness of a particular pathway in forming NOx in a cycle. Both these approaches are used to examine NOx formation at different operating conditions. The results hence obtained are then used in Chapter 6 to develop a simplified NOx prediction model.

5.1 NOx Formation Pathways

Nitric oxide is an important species in combustion due to its contribution to air pollution. Nitric oxide (NO) and nitrogen dioxide (NO_2) are collectively known as oxides of nitrogen (NOx). These two species are interchangeable in the environment and in combustion systems; hence they are treated as a single pollutant, NOx. Equilibrium considerations at flame temperature overwhelmingly favor the formation of NO over

NO_2. In the combustion of fuels that do not contain nitrogen, NO can by formed by four pathways from the nitrogen in air: the Zeldovich mechanism, the N_2O mechanism, the Fenimore or prompt mechanism and the NNH mechanism. Each of these pathways is explained below.

5.1.1 Zeldovich Mechanism

The Zeldovich mechanism is the principal pathway for NOx formation in high temperature combustion, especially at temperatures above 1800 K. It consists of the following reactions:

$$O + N_2 \Leftrightarrow NO + N \quad (5.1)$$

$$N + O_2 \Leftrightarrow NO + O \quad (5.2)$$

$$N + OH \Leftrightarrow NO + H \quad (5.3)$$

An O atom combines with a nitrogen molecule to produce an NO molecule and an N atom. The N atom combines with an oxygen molecule to form another NO molecule and an O atom. The third reaction is another important step for the N atom to oxidize to NO. Together, these three reactions are also known as the extended Zeldovich mechanism.

The Zeldovich mechanism is an important contributor to NOx emissions above 1800K. This mechanism is coupled to combustion chemistry through O_2, O and OH. If significant NOx formation takes place after the fuel has been consumed, it can be assumed that O_2, N_2, O and OH species are in equilibrium, and N atoms are in steady state. Therefore, for a given air fuel ratio, their concentration is primarily a function of temperature, which makes the NOx produced a function primarily of temperature and residence time. Hence,

the Zeldovich mechanism is also referred to as the thermal NOx mechanism. If we assume that the NO concentration remains much lower than its equilibrium value, the reverse Zeldovich rates can be neglected. The first reaction is the rate limiting step, which yields a rather simple rate expression (neglecting reverse reaction rates):

$$\frac{d[NO]}{dt} = 2k_{N1,f}[O]_{eq}[N_2]_{eq}$$

Where $k_{N1,f}$ is the forward rate constant of reaction 5.1, and $[O]_{eq}$ and $[N_2]_{eq}$ are the equilibrium concentrations of O and N_2, respectively.

5.1.2 Nitrous Oxide Mechanism

The nitrous oxide mechanism plays an important role in lean, low temperature combustion processes. Malte and Pratt (1974) proposed the mechanism to explain NOx formed in lean, high-intensity combustors. It is now taken to include the following reactions:

$$O + N_2 + M \Leftrightarrow N_2O + M \quad (5.4)$$

$$O + N_2O \Leftrightarrow N_2 + O_2 \quad (5.5)$$

$$H + N_2O \Leftrightarrow NO + NH \quad (5.6)$$

$$O + N_2O \Leftrightarrow NO + NO \quad (5.7)$$

$$H + N_2O \Leftrightarrow N_2 + OH \quad (5.8)$$

$$OH + N_2O \Leftrightarrow N_2 + HO_2 \quad (5.9)$$

N_2O is formed primarily by reaction 5.4, while NO is formed by reactions 5.6 and 5.7.

5.1.3 Fenimore Prompt Mechanism

The Fenimore mechanism was discovered by Fenimore in 1971 and is linked to the combustion chemistry of hydrocarbons. Hydrocarbon radicals react with nitrogen to form cyano compounds or amines, which are ultimately converted to NO. This NOx formation pathway is initiated by the following reaction

$$CH + N_2 \Leftrightarrow HCN + N \tag{5.10}$$

For fuel-air equivalence ratios lower than 1.2, the following reactions convert HCN to NO:

$$HCN + O \Leftrightarrow NCO + H \tag{5.11}$$

$$NCO + H \Leftrightarrow NH + CO \tag{5.12}$$

$$NH + H \Leftrightarrow N + H_2 \tag{5.13}$$

$$N + OH \Leftrightarrow NO + H \tag{5.14}$$

For equivalence ratio greater than 1.2, the chemistry becomes complex as other reaction pathways open up.

5.1.4 NNH Mechanism

The NNH mechanism was proposed by Bozzelli and Dean (1995). The two key steps in this mechanism are:

$$N_2 + H \Leftrightarrow NNH \tag{5.15}$$

$$NNH + O \Leftrightarrow NO + NH \tag{5.16}$$

This pathway has been shown to be important for hydrogen combustion as well as combustion for fuels with large carbon-to-hydrogen ratios. NNH is mainly formed by reaction 5.15, while NO is produced mainly by reaction 5.16.

5.2 Overall NOx Contribution from Each Pathway

The UWSI code is used to determine the contribution of each pathway to NOx formation in this section. The test cases of 315% theoretical air and 430% theoretical air are considered.

The full NOx mechanism of GRI 3.0 is shown in Table 5.1, reproduced from the dissertation of K. Boyd Fackler (2011). The units are as follows: the pre-exponential factor for each reaction is equal to 10^A (mole/cm^3-s), b is the temperature exponent corresponding to $(T/To)^b$, To is 298 K, and the activation energy, Ea, has units of kcal/mole.

The contribution of each pathway is determined as follows. For the Zeldovich and Prompt mechanisms, the rate-controlling step of each mechanism is the first step, which converts nitrogen to a reactive species, with the rest of the reactions being relatively faster. For the NNH and nitrous oxide mechanisms also, the rate-controlling steps are the reactions that convert nitrogen to a reactive species. Therefore, the disabling of the key initiation reactions of each pathway effectively cripples the entire mechanism. This is much more effective than removing all reactions of a pathway, since all pathways have certain reactions in common. To determine the NOx formed by the Fenimore/Prompt pathway, reaction 23 is commented out. The difference in NOx emission between the total GRI 3.0 mechanism and this edited mechanism gives us the NOx formed due to the

Zeldovich Mechanism										
Reaction	**Reactants**				**Products**			**A**	**b**	**Ea**
1	N	NO		↔	N_2	O		13.431	0	0.355
2	N	O_2		↔	NO	O		9.954	1	6.5
3	N	OH		↔	NO	H		13.526	0	0.385
Nitrous oxide Mechanism										
Reaction	**Reactants**				**Products**			**A**	**b**	**Ea**
4	N_2O	M		↔	N_2	O	M	10.898	0	56.02
5	N_2O	O		↔	N_2	O_2		12.146	0	10.81
6	N_2O	O		↔	NO	NO		13.462	0	23.15
7	N_2O	H		↔	N_2	OH		14.588	0	18.88
8	N_2O	OH		↔	N_2	HO_2		12.301	0	21.06
9	NH	NO		↔	N_2O	H		14.562	-0.45	0
NNH Mechanism										
Reaction	**Reactants**				**Products**			**A**	**b**	**Ea**
10	NNH			↔	N_2	H				
11	NNH	M		↔	N_2	H	M	14.114	-0.1	4.98
12	NNH	O_2		↔	HO_2	N_2		12.699	0	0
13	NNH	O		↔	OH	N_2		13.398	0	0
14	NNH	H		↔	H_2	N_2		13.699	0	0
15	NNH	OH		↔	H_2O	N_2		13.301	0	0
16	NNH	CH_3		↔	CH_4	N_2		13.398	0	0
17	NNH	O		↔	NH	NO		13.845	0	0
18	NH	OH		↔	N	H_2O		9.301	1.2	0
19	NH	O		↔	NO	H		13.602	0	0
20	NH	O_2		↔	NO	OH		6.107	1.5	0.1
21	N	O_2		↔	NO	O		9.954	1	6.5
22	N	OH		↔	NO	H		13.526	0	0.385
Fenimore prompt Mechanism										
Reaction	**Reactants**				**Products**			**A**	**b**	**Ea**
23	CH	N_2		↔	HCN	N		9.494	0.88	20.13
24	HCN	O		↔	NCO	H		4.307	2.64	4.98
25	NCO	O		↔	NO	CO		13.371	0	0
26	NCO	OH		↔	NO	H	CO	12.398	0	0
27	NCO	O_2		↔	NO	CO_2		12.301	0	20
28	HCN	O		↔	NH	CO		3.705	2.64	4.98
29	NCO	H		↔	NH	CO		13.732	0	0
30	NH	OH		↔	N	H_2O		9.301	1.2	0
31	NH	O		↔	NO	H		13.602	0	0
32	NH	O_2		↔	NO	OH		6.107	1.5	0.1
33	N	O_2		↔	NO	O		9.954	1	6.5
34	N	OH		↔	NO	H		13.526	0	0.385

Table 5.1: Full NOx mechanism in GRI 3.0, reproduced from the PhD thesis of Fackler (2011)

Fenimore prompt pathway. Similarly, the NOx formed due to the NNH mechanism is determined by dropping reactions 10 and 11, then subtracting the resulting NOx prediction from the NOx yield predicted by the full mechanism. Reactions 4, 5, 7 and 8 are dropped to determine the NOx contribution from the nitrous oxide pathway, while reaction 1 is dropped to determine the NOx contribution from the Zeldovich pathway. The sum of the contribution of each pathway should add up to the NOx yield predicted by the full mechanism.

Figure 5.1 shows the NOx distribution obtained by the method outlined above for the baseline case of 315% theoretical air and the leanest case of 430% theoretical air. The NOx formed by the NNH and Prompt pathways is negligible in both cases. The NOx distribution for the 430% theoretical air case is about 60% Zeldovich and 38% N_2O NOx, while for the 315% theoretical air case is about 72% Zeldovich and 24% N_2O NOx. Therefore, the contribution of the nitrous oxide mechanism to NOx is greater at lean operating conditions.

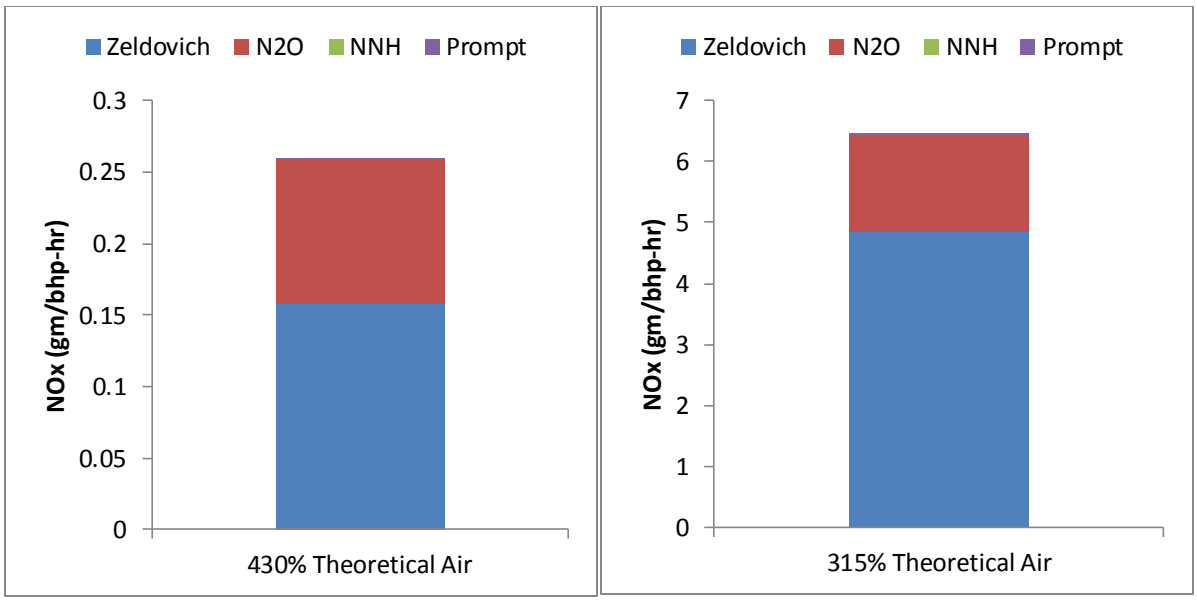

Figure 5.1: NOx distribution of 430% and 315% theoretical air calculated using UWSI

5.3 NOx Formation in the Flame Front and Post Flame Region

Figure 3.1 in Section 3 shows NOx as a function of crank angle. From the figure, it is seen that most of the NOx is formed between spark ignition and 22° ATDC. The cessation of NOx formation after about 25° ATDC can be attributed to the reduction in burned gas temperature. This period of NOx formation can be examined in greater detail using chemical reactor modeling. UWSI treats the flame front as a perfectly stirred reactor sized to incipient blowout condition, followed by plug flow reactors at assigned pressure, temperature and residence time. The mass of charge burned at each crank angle interval is calculated using the Wiebe function. Since UWSI provides us with a burned gas temperature profile and pressure trace for each simulation, the chemical reactor model can be recreated using the commercial software package CHEMKIN, from which NOx formation pathways at different temperatures and pressures can be ascertained.

CHEMKIN is used to study the leanest case of 430% delivered theoretical air, with stratified charge combustion. Spark ignition occurs at -5° crank angle ATDC. Three different cases are set up; the first one follows the charge burnt at -4.5° crank angle ATDC, representative of the first parcel of charge to be ignited. The second case follows the charge burned at 4° ATDC, representative of the charge burned towards the end of the jet-cell. The third case follows the charge burned at 18° ATDC. Each chemical reactor model consists of a perfectly stirred reactor at incipient blowout followed by plug flow reactors at assigned temperature and pressure. This is shown in Figure 5.2. The time step considered for each PFR is the time equivalent to 0.5° engine crank angle. The pressure and temperature for each time step are taken from the UWSI model for the case of stratified charge 430% delivered theoretical air.

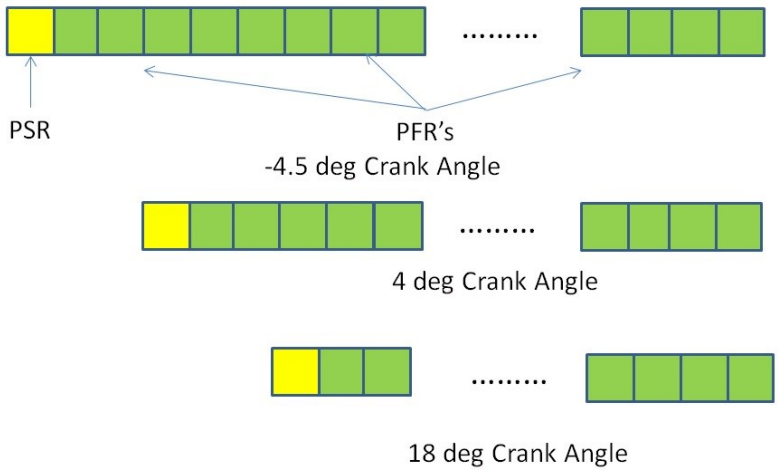

Figure 5.2: Schematic diagram of cases set up using CHEMKIN. Each PFR has a residence time of 0.5° engine crank angle.

The results of the first model, following the charge burned at -4.5° ATDC, are shown in Figures 5.2 to 5.5. The fuel-air equivalence ratio of the charge is 0.65. Figure 5.3 shows the reaction path from N_2 to NO, followed by the absolute rates of reactions that form N_2 and NO in Figure 5.4. Each node in Figure 5.3 represents a species of interest, and each line linking two nodes represents the reactions that convert one species to the other. The numbers on the lines linking two nodes are the overall rate of reaction in moles/(cm^3-sec) for the production of one species from the other. Using the rates of reaction given in Figure 5.4, it is possible to estimate the percentage of NOx produced by each pathway. It is seen that nitrogen is destroyed by first two reactions in Figure 5.4, and mostly regenerated by the next two reactions. The largest contributor to NOx formation is the Zeldovich pathway, followed by the nitrous oxide route and the prompt mechanism. Figure 5.5 shows the reaction path from N2 to NO for the first plug flow reactor, while Figure 5.6 shows the absolute reaction rates of N_2 and NO production. NO is mostly created by the Zeldovich mechanism and the nitrous oxide mechanism, with negligible amounts being contributed by the prompt and NNH mechanisms.

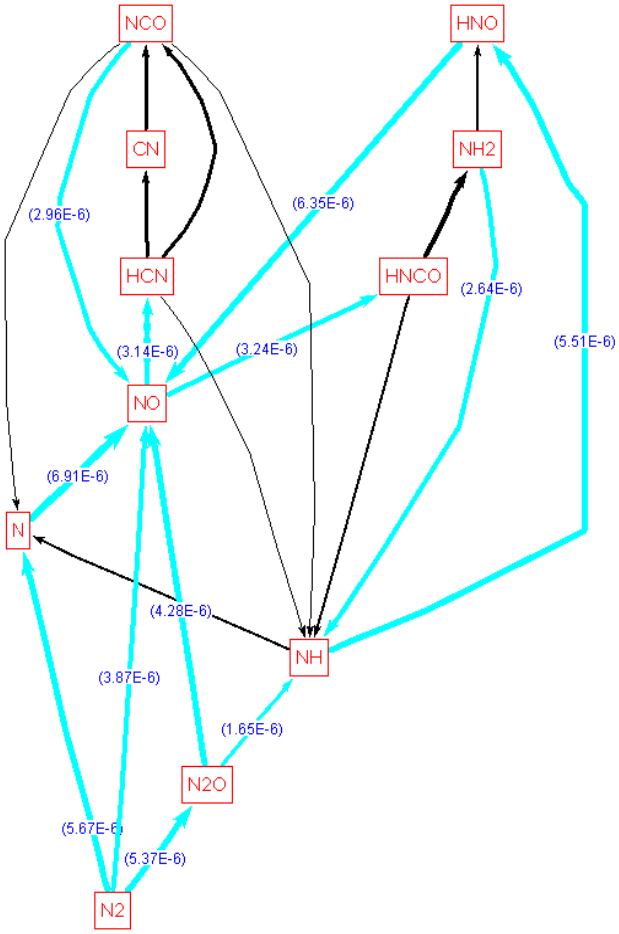

Figure 5.3: Reaction path diagram of the PSR of the first chemical reactor model

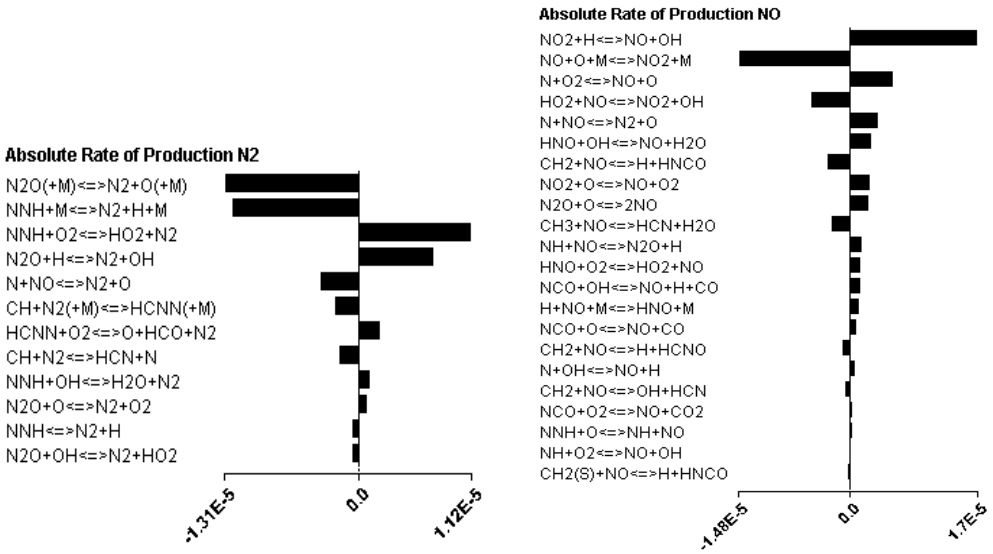

Figure 5.4: Reaction rates of reactions forming N_2 and NO for the PSR of the first chemical reactor model

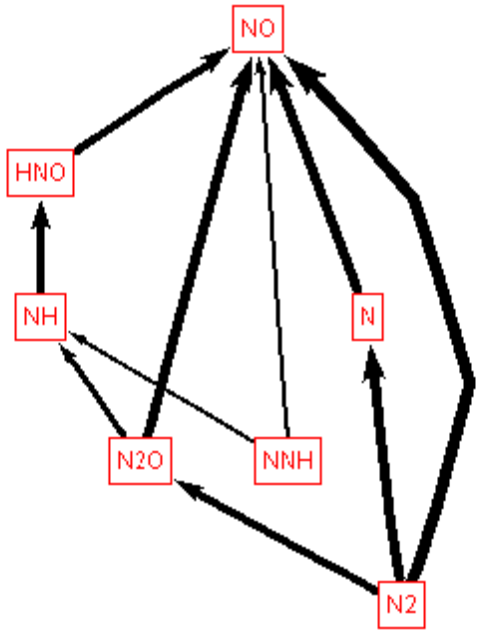

Figure 5.5: Reaction path diagram of the first PFR of the first chemical reactor model

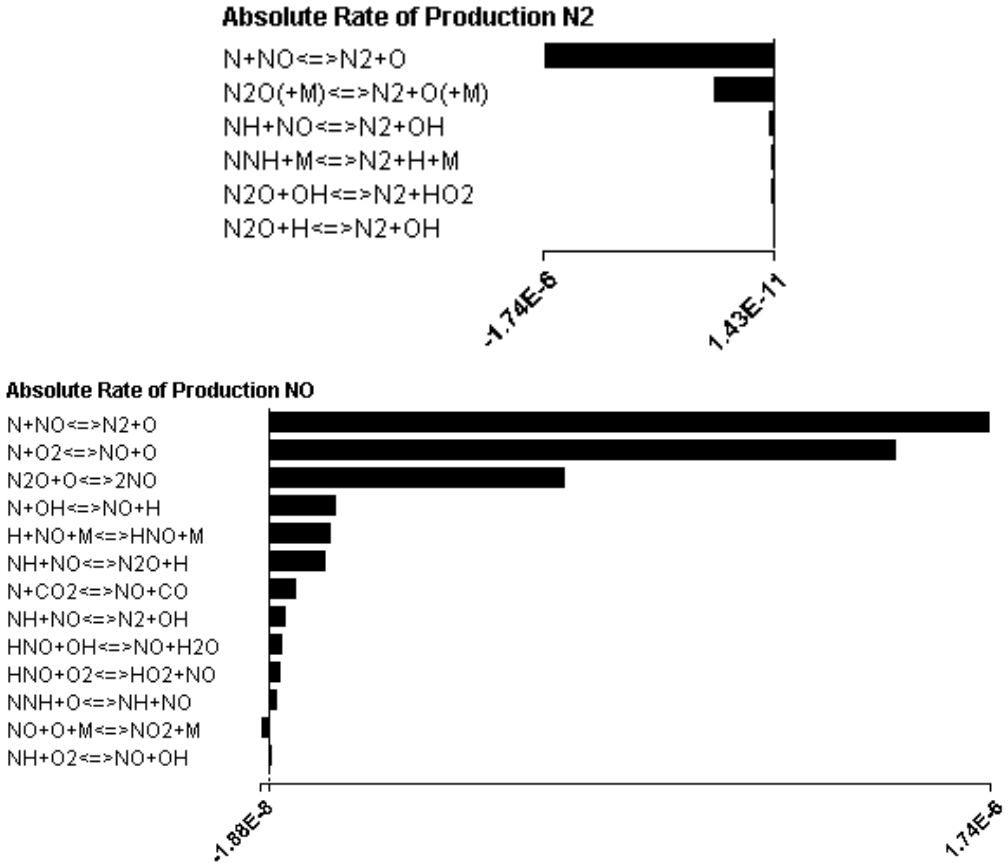

Figure 5.6: Reaction rates of reactions forming N_2 and NO for the first PFR of the first chemical reactor model

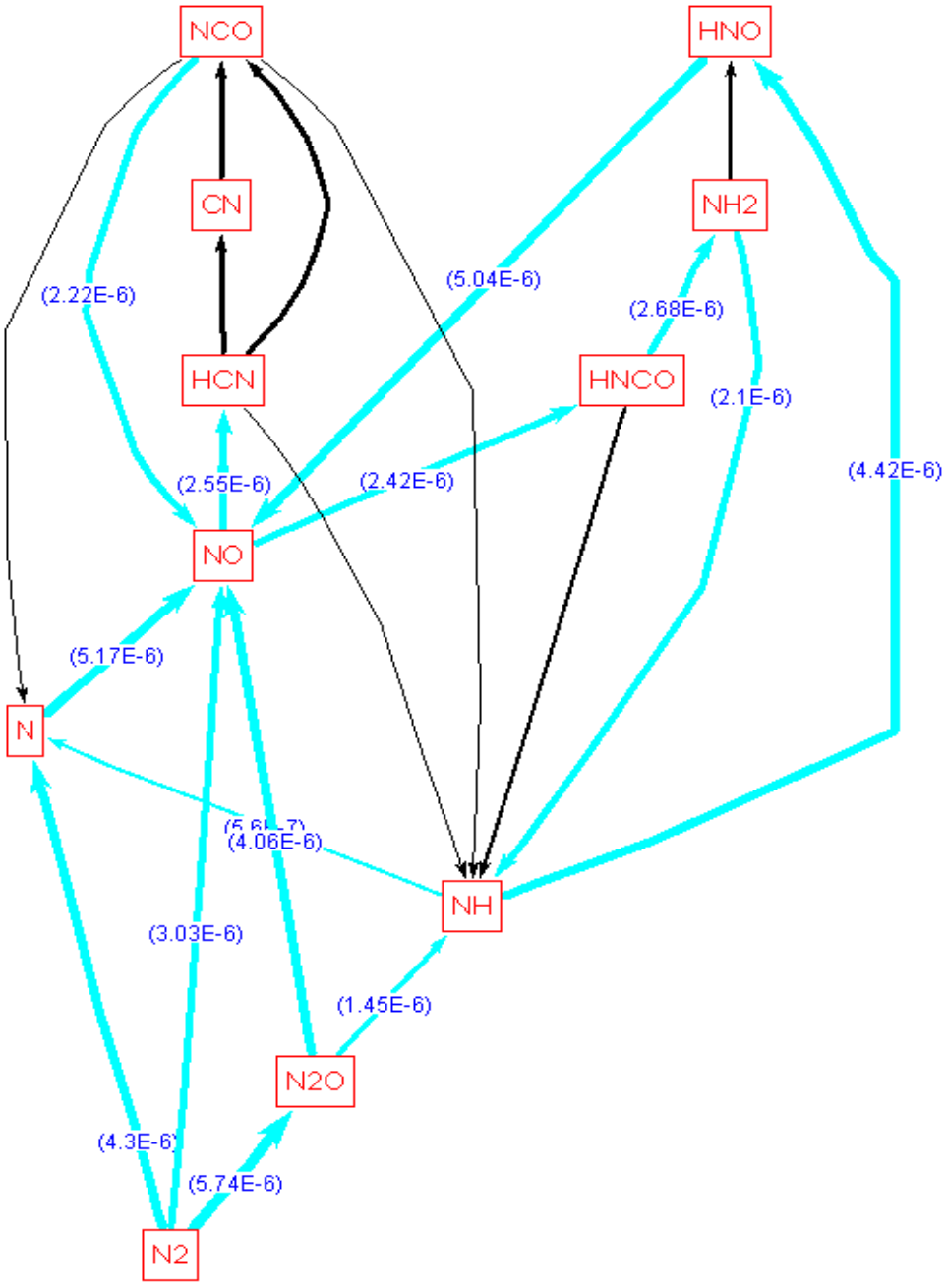

Figure 5.7: Reaction path diagram of the PSR of the second chemical reactor model

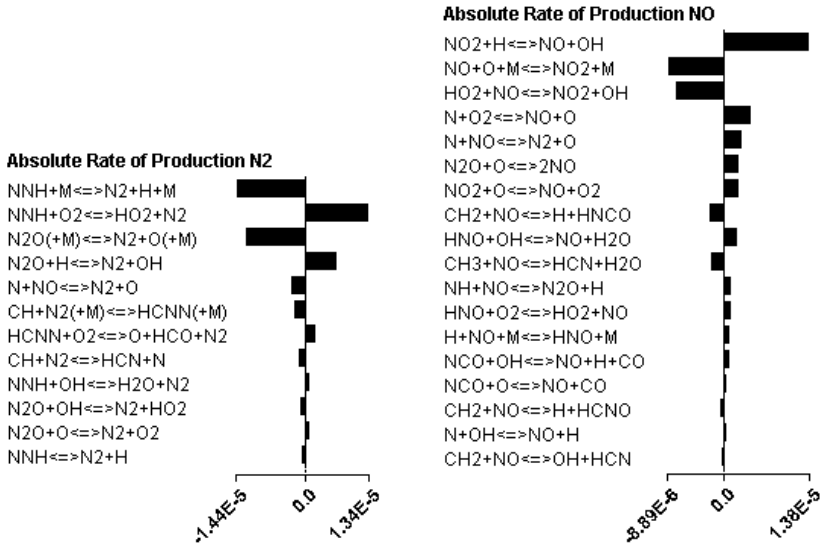

Figure 5.8: Reaction rates of reactions forming N_2 and NO for the PSR of the second chemical reactor model

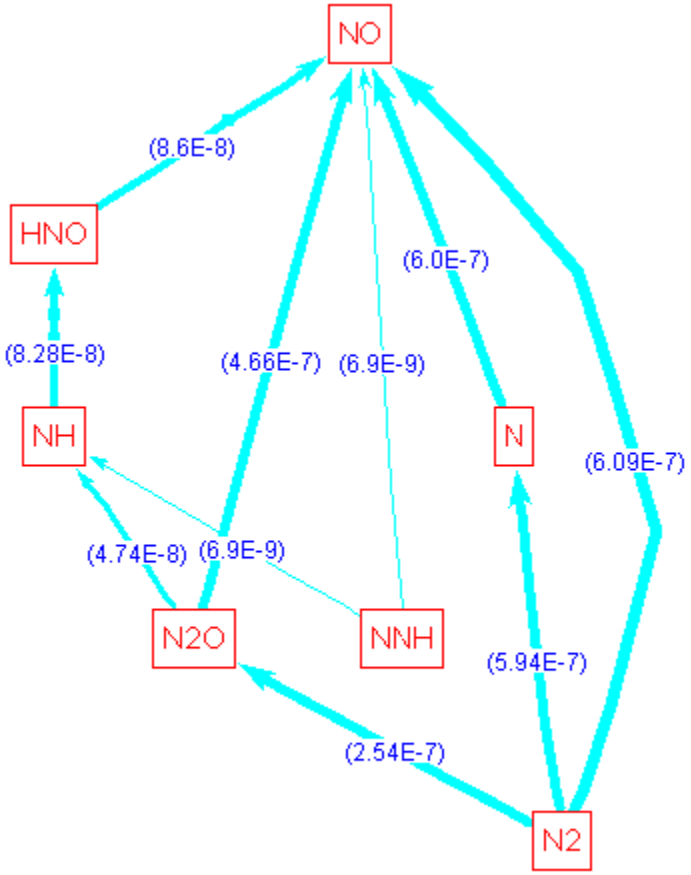

Figure 5.9: Reaction path diagram of the first PFR of the second chemical reactor model

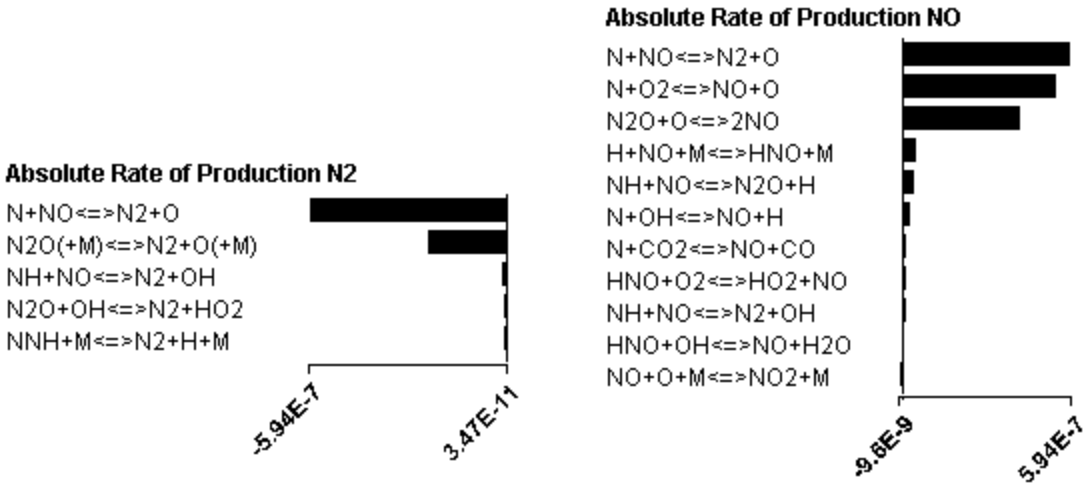

Figure 5.10: Reaction rates of reactions forming N_2 and NO for the first PFR of the second chemical reactor model

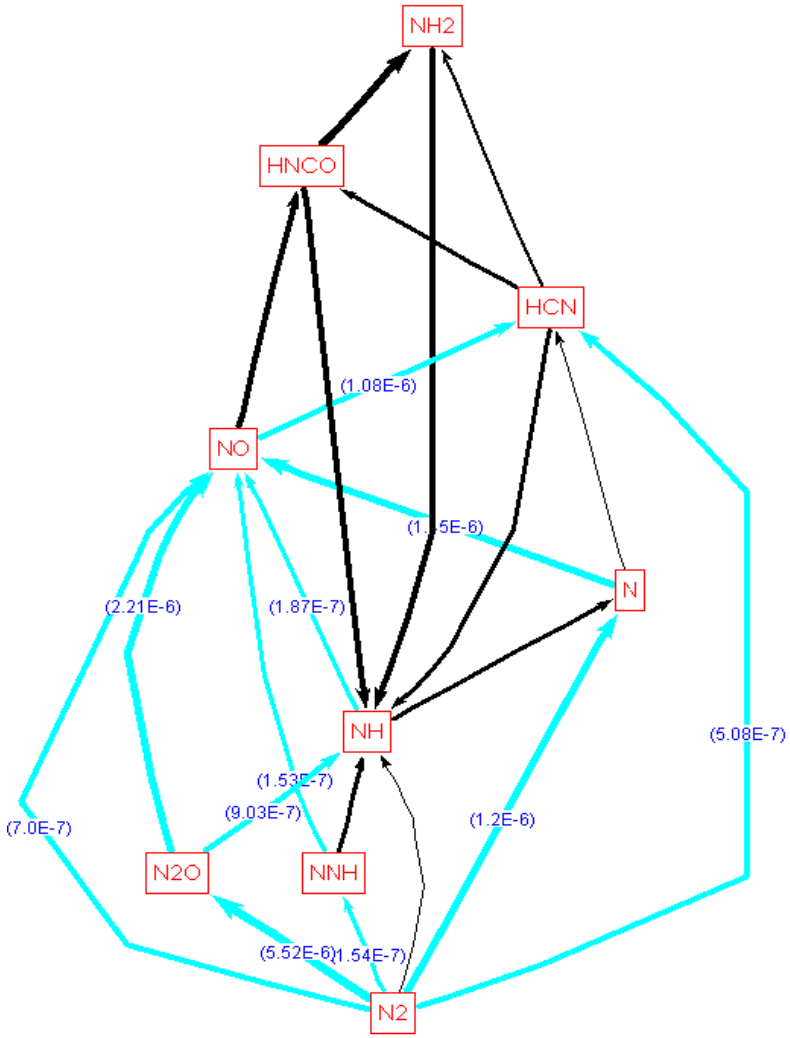

Figure 5.11: Reaction path diagram of the PSR of the third chemical reactor model

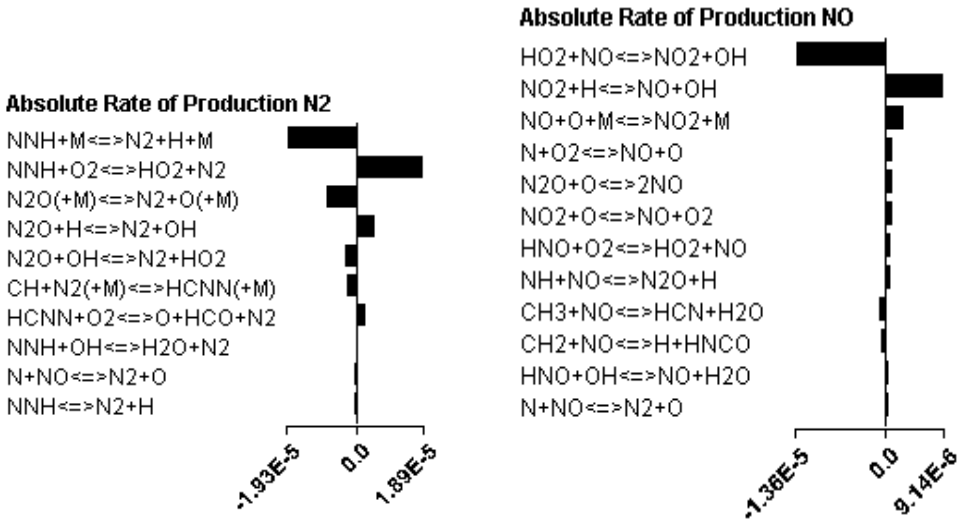

Figure 5.12: Reaction rates of reactions forming N_2 and NO for the PSR of the third chemical reactor model

The results of the second case, following the charge burned at 4° ATDC are shown in Figure 5.7 to 5.10. The reaction path diagram from N_2 to NO for the PSR is shown in Figure 5.7. The fuel-air equivalence ratio of the charge burned is 0.6215. This is different from the phi of the first case since the first case was burned in the jet-cell; the burned phi will lie between the jet-cell phi and the main chamber phi. The results from these figures are quite similar to the results from the previous PSR; the most important contributor is the Zeldovich pathway, followed by the nitrous oxide mechanism and the Prompt mechanism. Figure 5.9 shows the reaction path diagram from N_2 to NO for the first PFR, followed by the absolute reaction rates for NO and N_2 production. As before, the Zeldovich mechanism contributes the maximum amount of NO, followed by the N_2O mechanism and the NNH and Prompt mechanism do not contribute significantly.

Figures 5.11 and 5.12 pertain to the third case. The phi for this case is 0.51. Figure 5.11 shows the reaction pathway from N_2 to NO for the PSR. Due to the low temperature, the Zeldovich and nitrous oxide pathway contribute similar amounts of NOx, with the

prompt mechanism contributing the rest. The percentage of NOx formed by each pathway in the flame front for each case is shown in Figure 5.2. As phi decreases, NOx formed by the Zeldovich pathway decreases while NOx formed by the N_2O pathway increases. NOx formed by the prompt pathway stays approximately the same for all phi's considered. The NNH mechanism does not contribute significantly to NOx formation in the flame front for any phi considered.

Pathway	% NOx formed		
	First case	Second case	Third case
Zeldovich	54.87	48.96	40.67
N2O	30.89	38.34	41.40
NNH	2.15	2.02	3.28
Prompt	10.70	8.82	10.83

Table 5.2: Percentage of NOx formed by each pathway in the PSR and first PFR of each case modeled

Figure 5.13 shows the N_2O concentration from the last chemical reactor model as a function of time. It is seen that the N_2O concentration reaches the equilibrium concentration of nitrous oxide after the first few reactors. Therefore, the NOx formed by the nitrous oxide mechanism can be thought of as formed by a thermal mechanism, since the concentration of nitrous oxide is nearly the equilibrium concentration.

5.4 Effect of Hydrocarbon Radical Attack on NOx Formation

Figure 4.3 shows the NOx yield as a function of crank angle for the baseline engine case, with a stratified charge phi of 0.983, modeled using the prescribed mixing model. The NOx reaches a peak at about 26^o ATDC and some part of it is subsequently destroyed. The reason for the destruction of NOx was found to be the effect of hydrocarbon radical attack on the NO molecule due to the prescribed mixing model. The case considered for

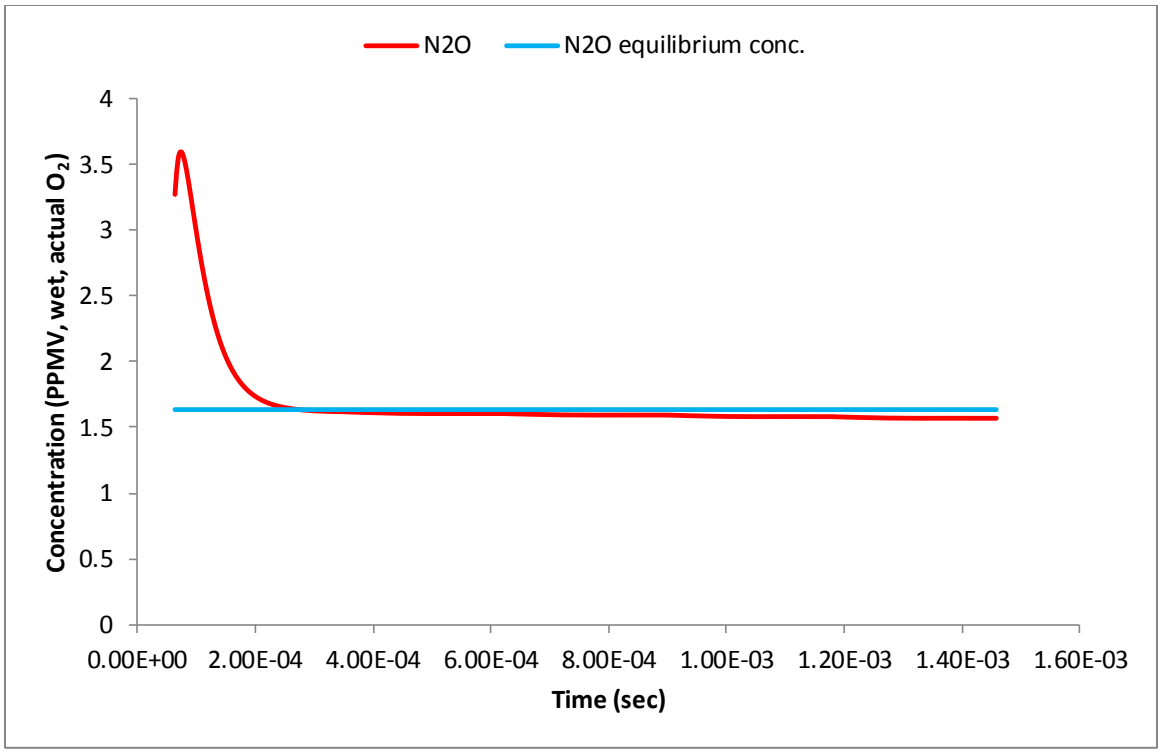

Figure 5.13: Comparison of N_2O concentration in chemical reactor model with equilibrium N_2O concentration

this analysis is the 315% theoretical air, homogeneous charge engine with a spark timing of 6° BTDC and trapped main chamber phi of 0.62. Figure 5.14 shows the NOx yield as a function of crank angle for this case. The destruction of NOx is observed to start at about 33° ATDC. The prescribed mixing model is then replaced with the 2-Wiebe function model, and the resulting NOx trace is plotted in Figure 5.15. No NOx destruction is observed. We draw the conclusion that the PMM is responsible for the destruction of NOx during the latter part of the cycle.

Figure 5.16 shows the effect of disabling all reactions except those which have HC radicals reacting with the NO in the NOx mechanism. No NOx is observed to be destroyed during the latter part of the cycle, which indicates that the reactions of HC

radicals with the NO molecule are responsible for the destruction of NOx. The problem is now examined with a chemical reactor model.

A chemical reactor model consisting of a stirred reactor at assigned temperature and residence time followed by plug flow reactors at assigned temperatures is set up in CHEMKIN. In order to model the PMM, methane-air mixture is introduced into the PFR's at intervals of time equivalent to 0.5^{o} engine crank angle. The assigned temperature profile for the reactors is taken from the UWSI model of this case, starting at 45^{o} crank angle ATDC. NO is introduced into the first PFR until the NO concentration in the PFR is equal to the NO concentration predicted by UWSI. Reactions occurring in the subsequent PFR's are then examined for NO destruction.

Figures 5.17 and 5.18 show the results pertaining to the PFR after NO injection. It is observe that very little NO is created, but the existing NO is destroyed by the attack of CH_2 and CH_3 radicals on it. The NO is reduced to several cyanospecies such as HCNO, HNCO and HCN.

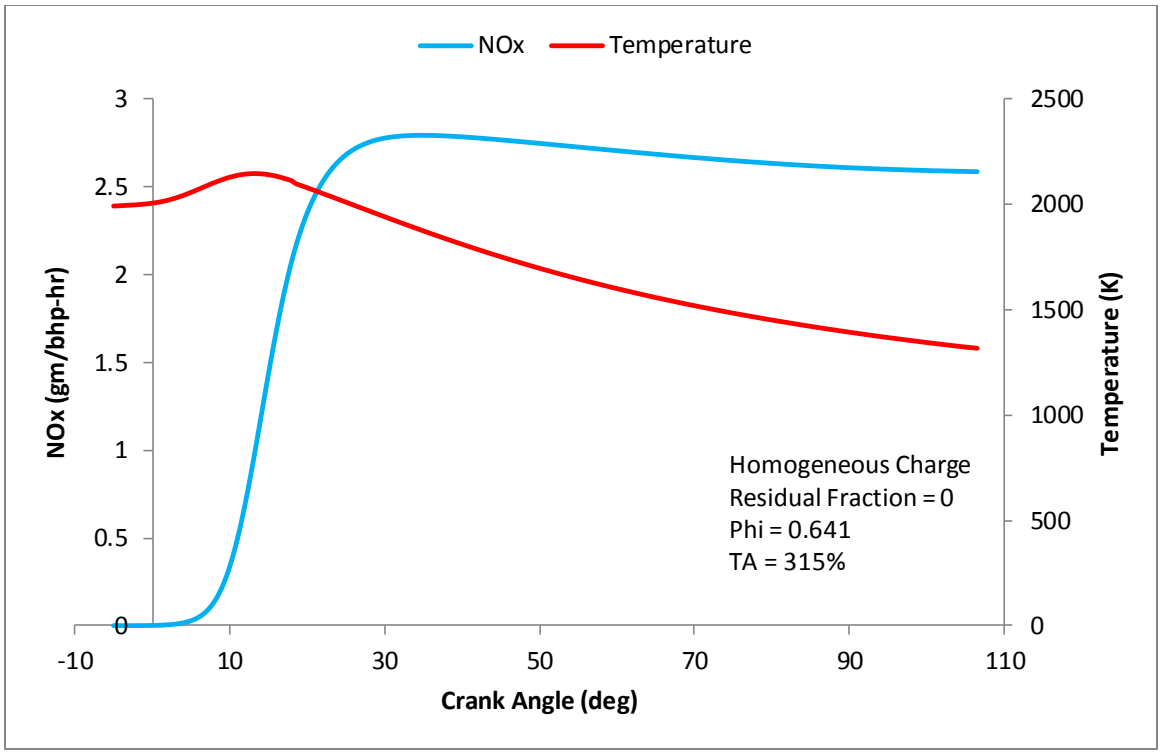

Figure 5.14: NOx as a function of engine crank angle using Prescribed Mixing Model with GRI 3.0

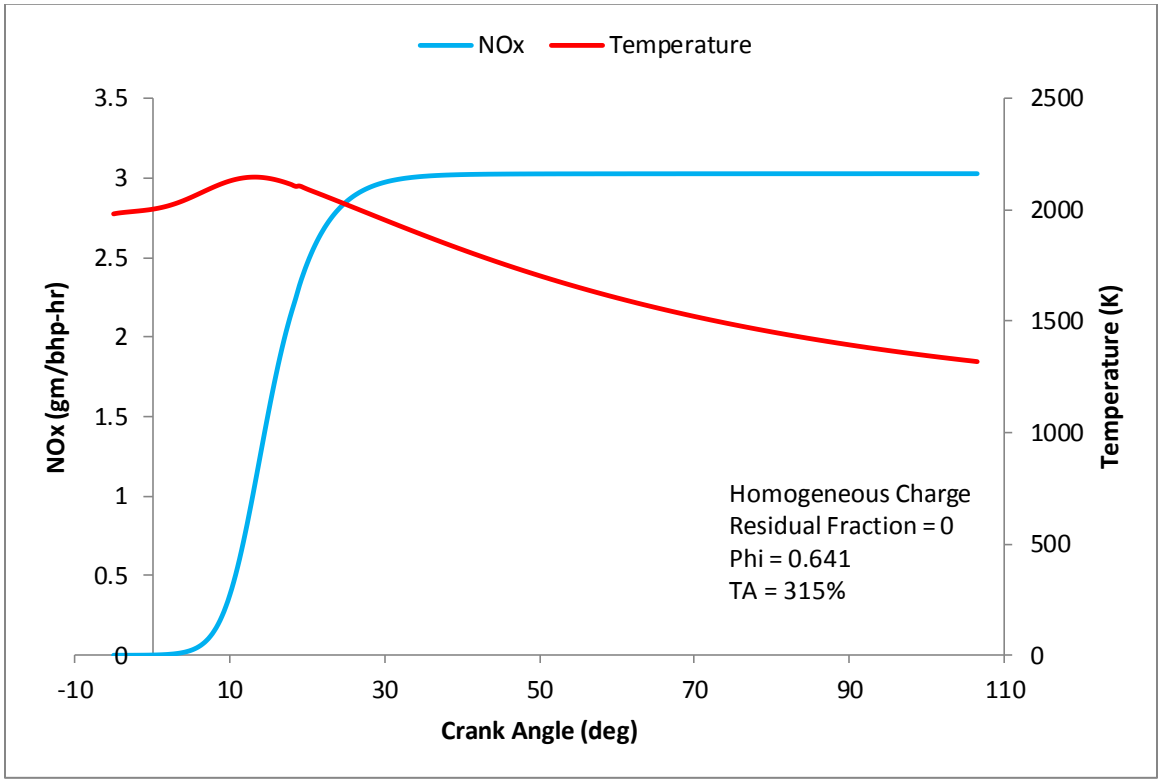

Figure 5.15: NOx as a function of engine crank angle using 2-Wiebe function model with GRI 3.0

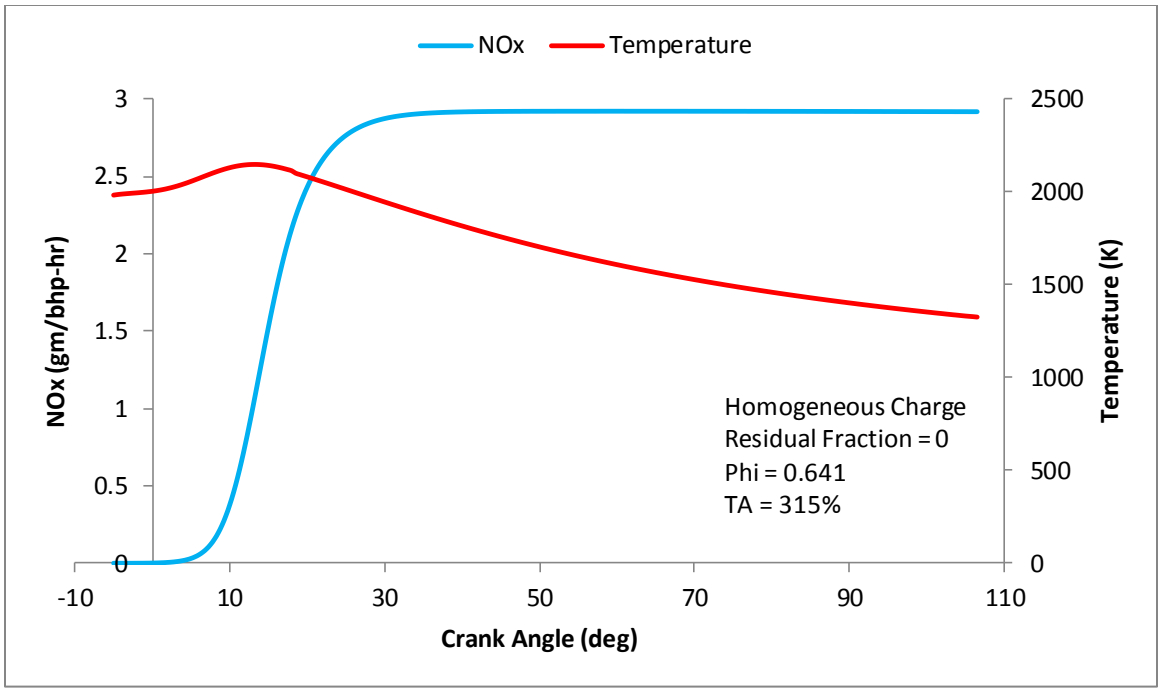

Figure 5.16: NOx as a function of engine crank angle using prescribed mixing model with GRI 3.0, excluding reactions of NO and HC radicals.

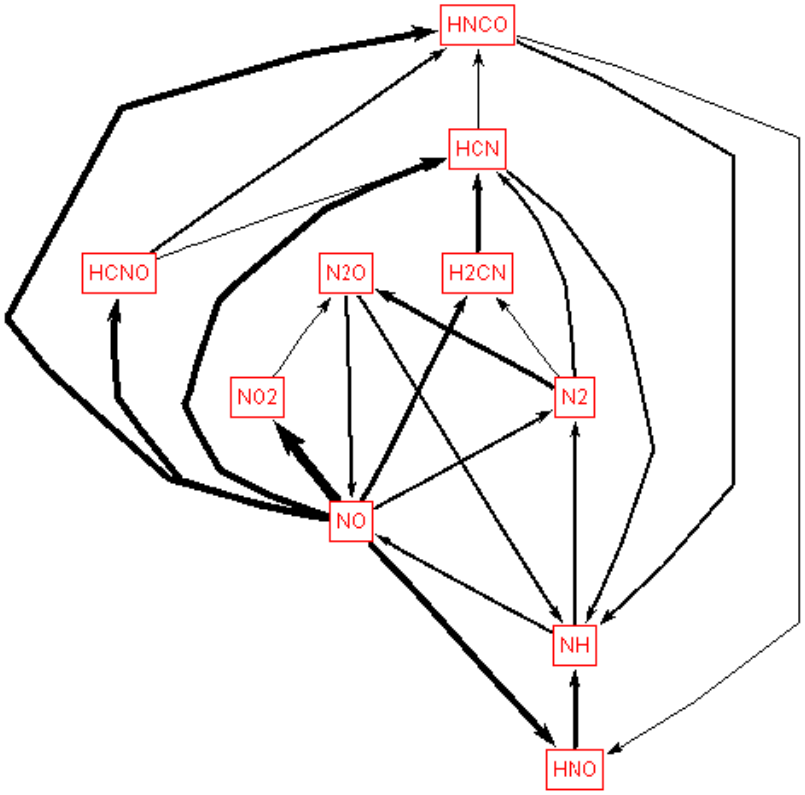

Figure 5.17: Reaction Mechanism of NO destruction due to reaction with hydrocarbon radicals.

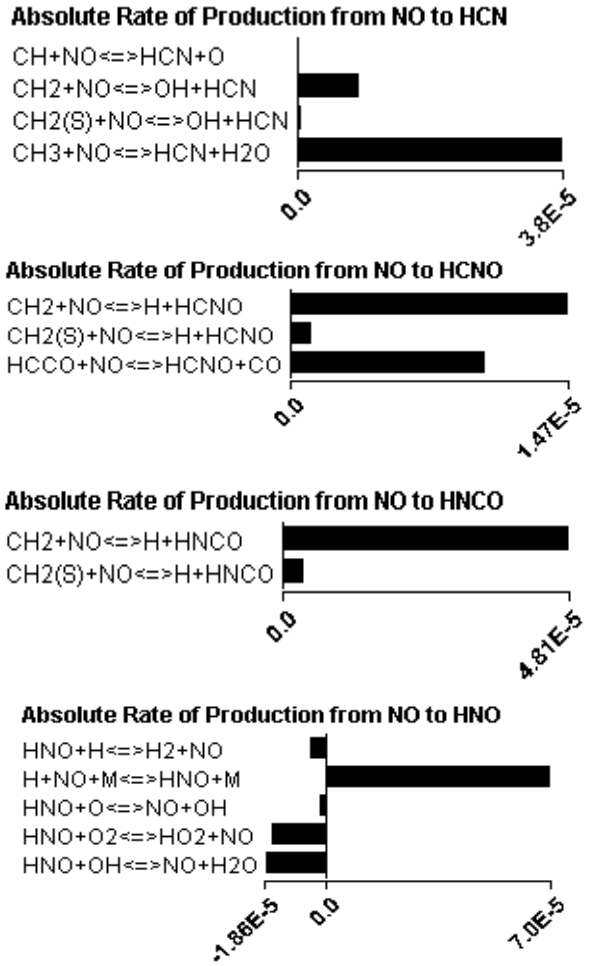

Figure 5.18: Absolute rates of production of cyano species from NO due to hydrocarbon radical attack, units moles/(cm^3-s)

6.0 A Simplified NOx Prediction Model for Lean Operating Conditions

From the modeling of the previous chapter, NOx formation in lean-burn large-bore natural gas engines is found to occur through two major pathways; the Zeldovich mechanism and the nitrous oxide mechanism. It is also found that for the leanest case modeled, the nitrous oxide concentration in the post-flame region approaches the equilibrium concentration at the given pressure and temperature. In this chapter, a simple NOx prediction model based on these assumptions is formulated and its predictions compared against results from the UWSI model.

6.1 Description of the Simplified NOx Prediction Model

Based on results from the previous chapter, the model assumes that NOx is formed only through the Zeldovich and nitrous oxide mechanisms. Furthermore, the method assumes that nitrous oxide is at equilibrium concentrations.

Single pockets of charge are tracked from the time of ignition (or when the flame front reaches it), and the NO produced by it from both the Zeldovich and nitrous oxide mechanisms is calculated. The combustion chamber is divided into 220 such pockets (from spark ignition to opening of the exhaust port), each pocket representing the charge burned in 0.5^{o} of engine crank angle. Each burned pocket does not contain the same amount of mass; the mass fraction and volume fraction burned per 0.5^{o} crank angle are calculated using the Wiebe function, also obtained from UWSI. The resulting data are in the form of NO concentration per crank angle per pocket. From this, the total NO concentration in the combustion chamber at each crank angle is calculated. The reactions considered for the Zeldovich mechanism are:

$$O + N_2 \Leftrightarrow NO + N \quad (6.1)$$

$$N + O_2 \Leftrightarrow NO + O \quad (6.2)$$

$$N + OH \Leftrightarrow NO + H \quad (6.3)$$

The reactions considered for the nitrous oxide mechanism are

$$H + N_2O \Leftrightarrow NO + NH \quad (6.4)$$

$$O + N_2O \Leftrightarrow NO + NO \quad (6.5)$$

These reactions are known to contribute the most to NOx production in the previous chapter. In the N_2O mechanism, it is assumed that all NH formed is converted to NO. N_2O is also assumed to be at equilibrium concentrations. For the NO formed by the Zeldovich mechanism, it is assumed that the N atom is in steady state concentration and negligible NO is destroyed by reverse reaction. Therefore, the rate of formation of NO from the Zeldovich mechanism is found to be

$$\frac{d[NO]_{Zeld}}{dt} = 2k_{N1,f}[N_2]_{eq}[O]_{eq}$$

Where $k_{N1,f}$ is the forward rate constant of reaction 6.1, and $[N_2]_{eq}$ and $[O]_{eq}$ are equilibrium concentrations of nitrogen and the oxygen atom, respectively. This expression is easily integrated to find the NO formed at each crank angle for the first pocket of charge to be burned. The NO formed in each pocket burned per crank angle is similarly calculated and the resulting data are converted into total NO concentration per crank angle as follows

$$[NO]_m = \sum_{\theta=1}^{m} \sum_{i=1}^{\theta} [NO]_i^{\theta} \, v_i$$

Where $[NO]_m$ = NO conc. in cylinder at crank angle count 'm', kmoles/m^3

$[NO]^{\theta}_i$ = NO conc. in pocket 'i' at crank angle count 'θ', kmoles/m^3

v_i = Volume fraction of pocket 'i', (vol of burned pocket/total vol of cylinder)

One crank angle count is 0.5° of crank angle, beginning from ignition and ending at exhaust port opening. The total crank angle count is the same as the number of pockets, since one pocket is burned per crank angle count.

The rate of NO formation from the N_2O mechanism is calculated by

$$\frac{d[NO]_{N2O}}{dt} = 2k_{N4,f}[N2O]_{eq}[H]_{eq} + 2k_{N5,f}[N2O]_{eq}[O]_{eq}$$

Where $k_{N4,f}$ and $k_{N5,f}$ are the forward reaction rates of reactions 6.4 and 6.5 respectively, while $[H]_{eq}$, $[O]_{eq}$ and $[N_2O]_{eq}$ are the equilibrium concentrations of the hydrogen atom, the oxygen atom and nitrous oxide, respectively. The NO concentration per crank angle is found in the same manner as the Zeldovich mechanism. The resulting NO concentration is converted to gm/bhp-hr and plotted vs. crank angle.

This model is then used to predict NOx emission for three cases: the baseline case of 315% theoretical air with stratified charge, 430% theoretical air with stratified charge and 430% theoretical air with homogeneous charge. The latter case is shown purely for demonstration of the simplified model, since a homogeneous charge engine is unlikely to operate at such low fuel-air equivalence ratios.

6.2 Results

Figures 6.1 through 6.4 show the results pertaining to a stratified charge engine running at 430% theoretical air with a spark timing of 5^{o} BTDC. The pre-chamber fuel-air equivalence ratio for this case is 0.65, while the fuel-air equivalence ratio in the main chamber is 0.5. The residual gases were assumed to be the products of complete combustion in each case. Figure 6.1 shows NOx predicted by UWSI as well as the simplified model as a function of crank angle. Also shown is the burned gas temperature. The NOx yield as a function of crank angle predicted by UWSI is matched almost identically by the NOx prediction of the simplified model. The simplified model does not take into account the NOx destroyed during the mixing of unburned charge into burned charge after flame extinction. However, for very lean conditions the amount of NOx destroyed by hydrocarbon radical attack on NO is negligible, which gives us good agreement for both sets of results. Figure 6.2 shows the comparison of the total NOx and NOx due to the nitrous oxide mechanism predicted by UWSI, while Figure 6.3 shows the comparison of the total NOx and NOx due to the nitrous oxide mechanism predicted by the simplified NOx model. The NOx due to the nitrous oxide pathway predicted by simplified NOx model (35% of the total NOx yield) is slightly lower than the prediction of UWSI (38.2% of the total NOx yield), which corresponds to a difference of about .0072 gm/(bhp-hr). Figure 6.4 shows reaction rates of the Zeldovich and nitrous oxide mechanisms as a function of crank angle. The rates of NO formation are a strong function of temperature.

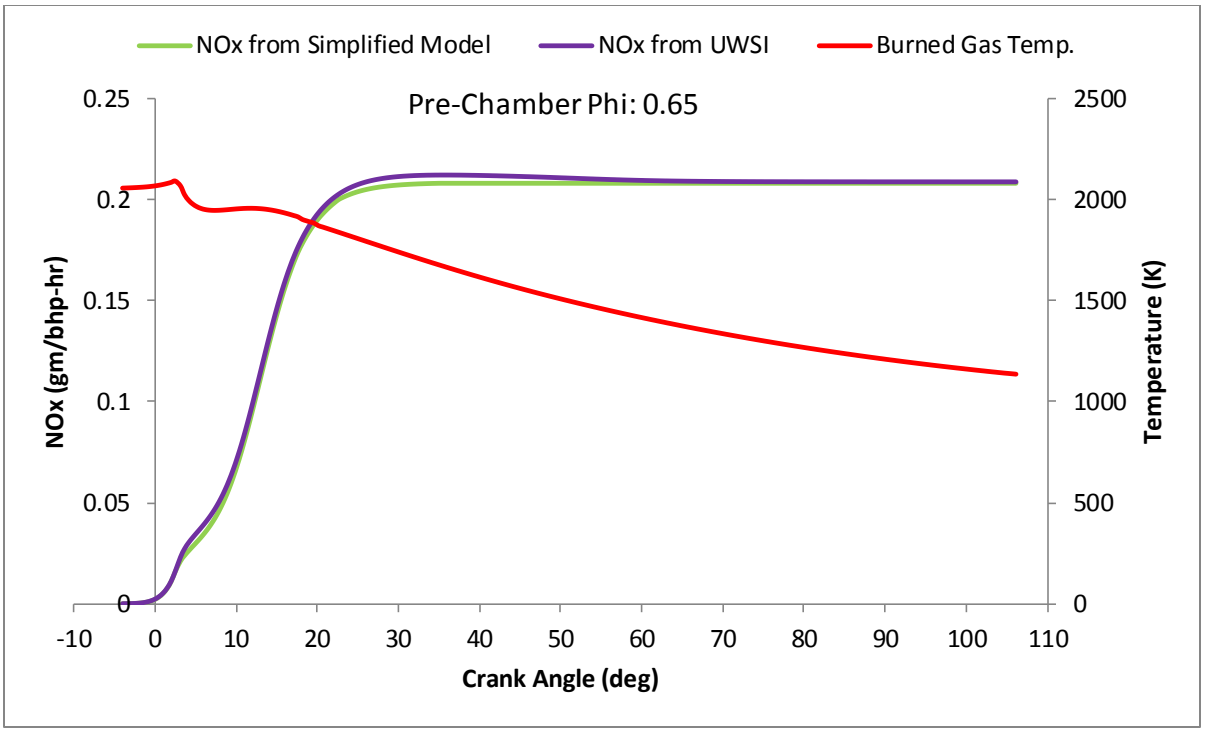

Figure 6.1: Predicted NOx yield from the Simplified Model and UWSI for a Stratified Charge Engine running on 430% Theoretical Air

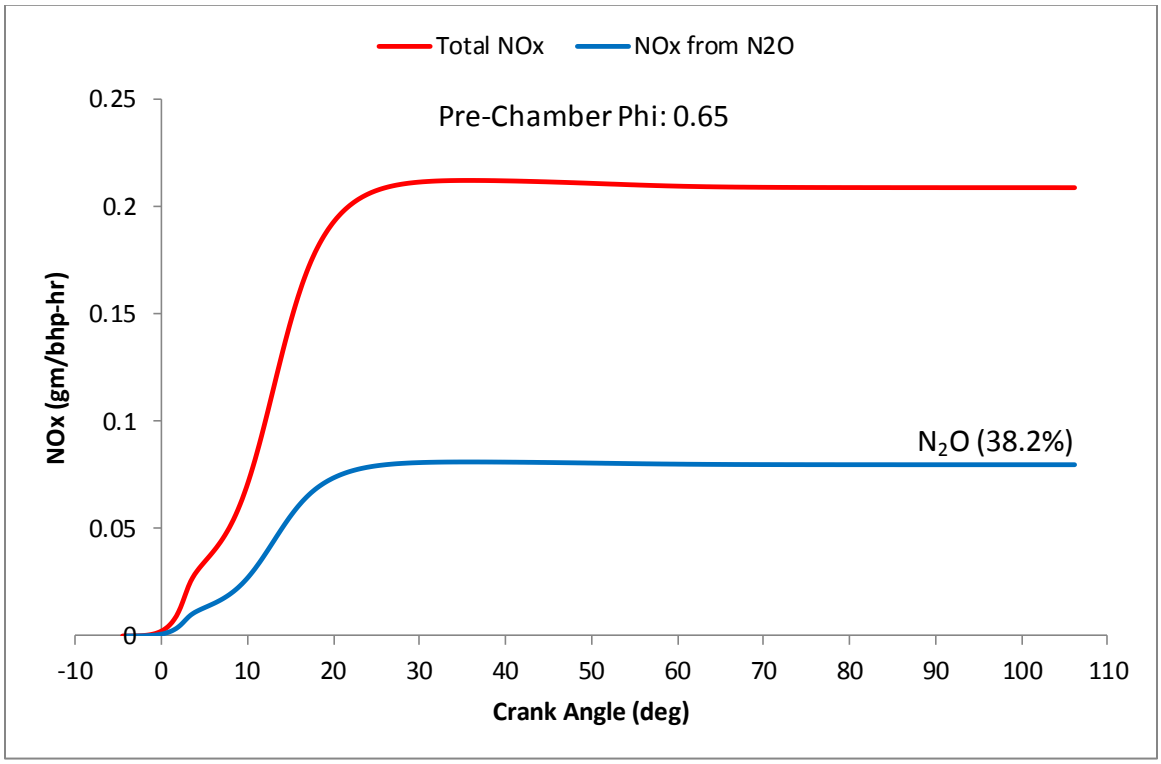

Figure 6.2: Total NOx yield and NOx formed by the Nitrous Oxide Mechanism for a Stratified Charge Engine running on 430% Theoretical Air, predicted by UWSI

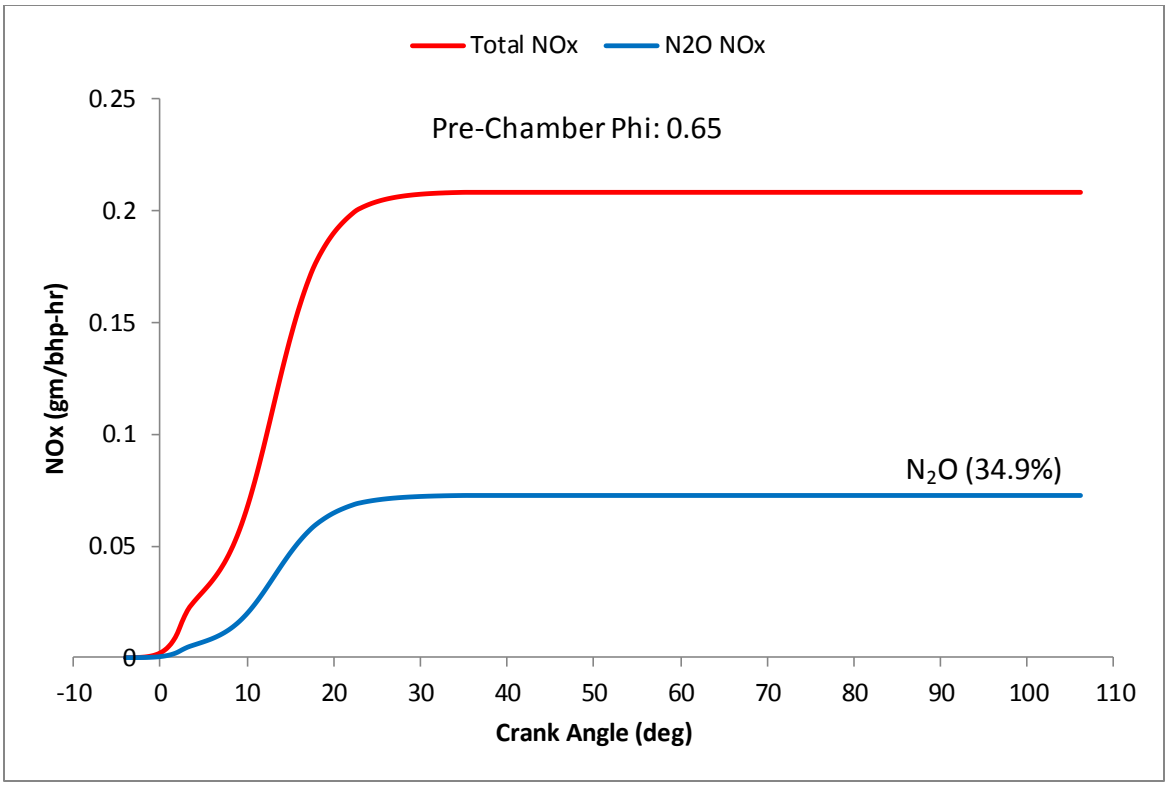

Figure 6.3: Total NOx yield and NOx formed by the Nitrous Oxide Mechanism for a Stratified Charge Engine running on 430% Theoretical Air, predicted by Simplified Model

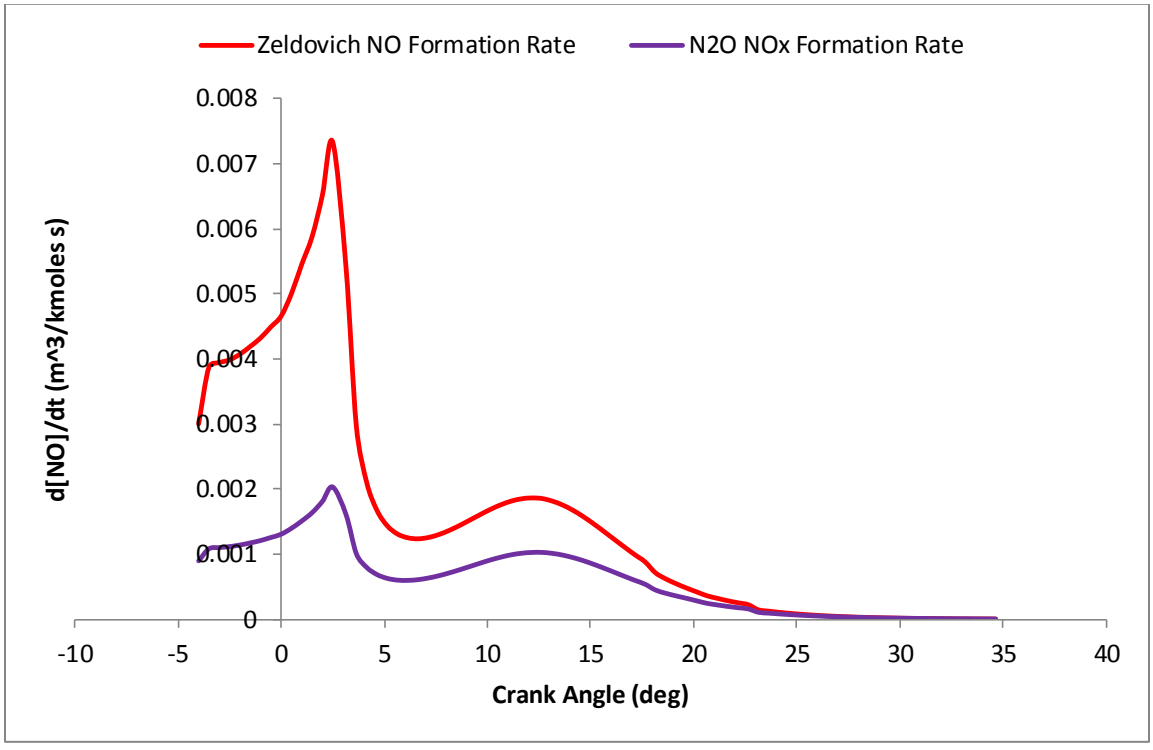

Figure 6.4: NOx formation rates for the Zeldovich and N2O mechanisms for a stratified charge engine running on 430% theoretical air, predicted by simplified model

Both NO formation rates peak near the maximum burned gas temperature, which is achieved in the jet-cell due to a richer fuel air mixture, and are negligibly small below 1800K. This leads to negligible NOx formation after about 25^{o} ATDC.

Figures 6.5 through 6.8 show the results for a homogeneous charge engine running at 430% theoretical air, with a spark timing of 5^{o} BTDC. The main chamber fuel-air equivalence ratio of the engine is 0.51. Figure 6.5 shows the NOx yield as a function of crank angle predicted by both the simplified NOx model and UWSI, along with the burned gas temperature for reference. Due to the absence of a jet-cell, the engine runs cooler than a stratified charge engine, which results in a lower NOx yield than a stratified charge engine with the same overall fuel consumption. The NOx predicted by UWSI is well matched by the NOx prediction of the simplified NOx model; however, some under-prediction by the simplified NOx model is observed. This is because the simplified NOx model does not take into account NOx formed due to super-equilibrium concentrations of nitrous oxide in the first few reactors of the chemical reactor model. Figures 6.6 and 6.7 show the NOx yield due to the nitrous oxide pathway along with the total NOx yield as a function of crank angle for reference, as predicted by UWSI and the simplified NOx model, respectively. The NOx yield due to the nitrous oxide pathway is predicted to be 39% of the total NOx yield by the simplified NOx model, and 42% of the total NOx yield by UWSI. Figure 6.8 shows reaction rates of the Zeldovich and nitrous oxide mechanisms as a function of crank angle. NO formation rates are lower than NO formation rates with a jet-cell, which leads to a lower NOx yield. The maximum NO formation rate still occurs at the maximum burned gas temperature, at about 12.5^{o} ATDC. As before, negligible NO formation is seen below a burned gas temperature of 1800 K.

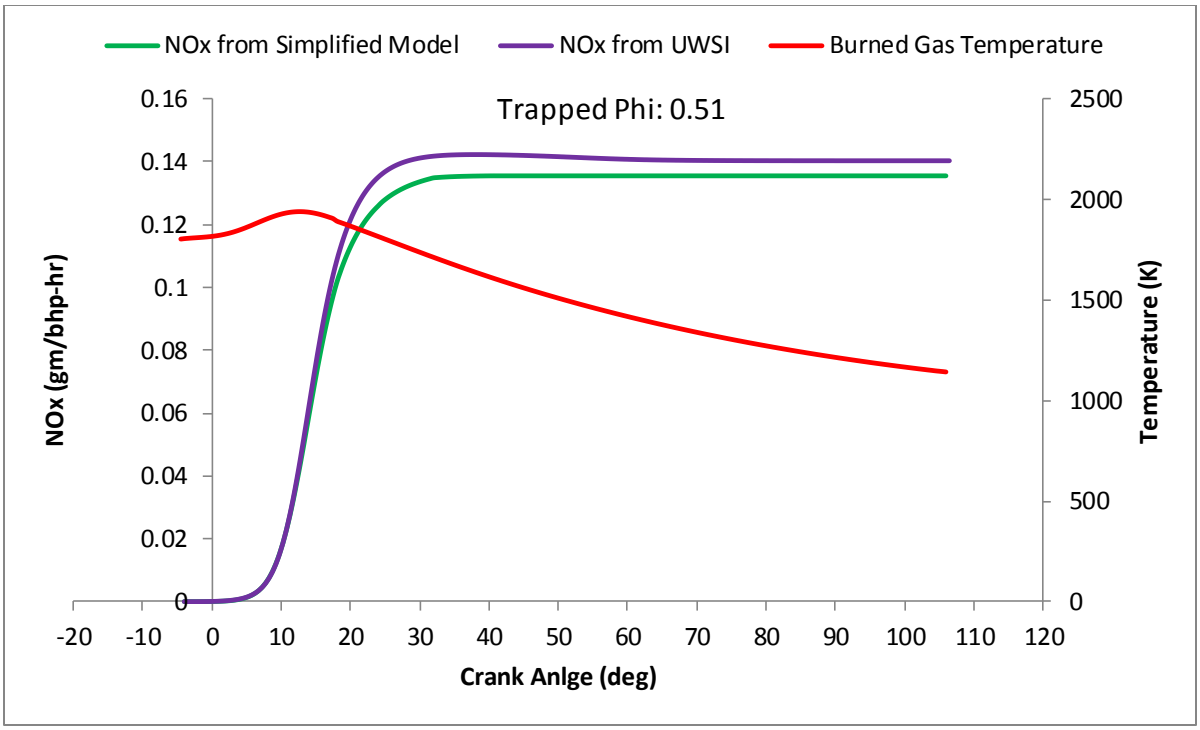

Figure 6.5: Predicted NOx yield from the simplified model and UWSI for a homogeneous charge engine running on 430% theoretical air

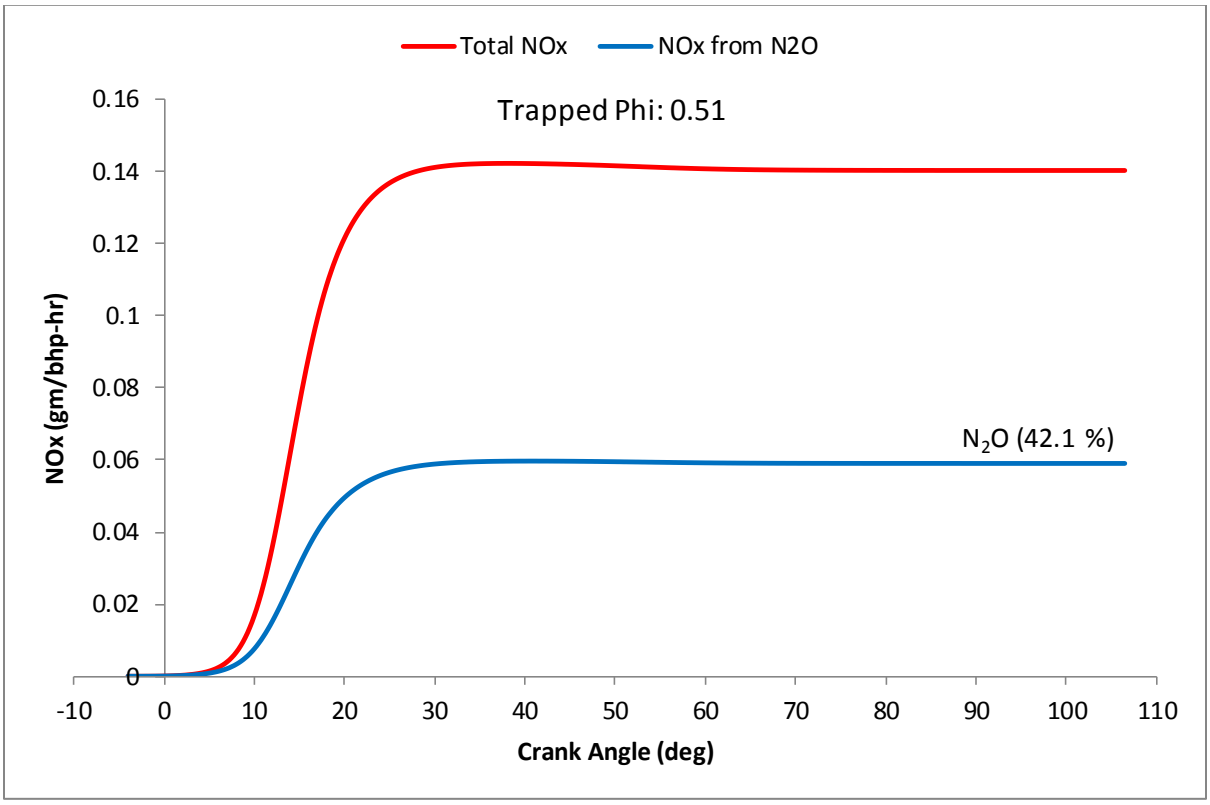

Figure 6.6: Total NOx yield and NOx formed by the nitrous oxide mechanism for a homogeneous charge engine running on 430% theoretical air, predicted by UWSI

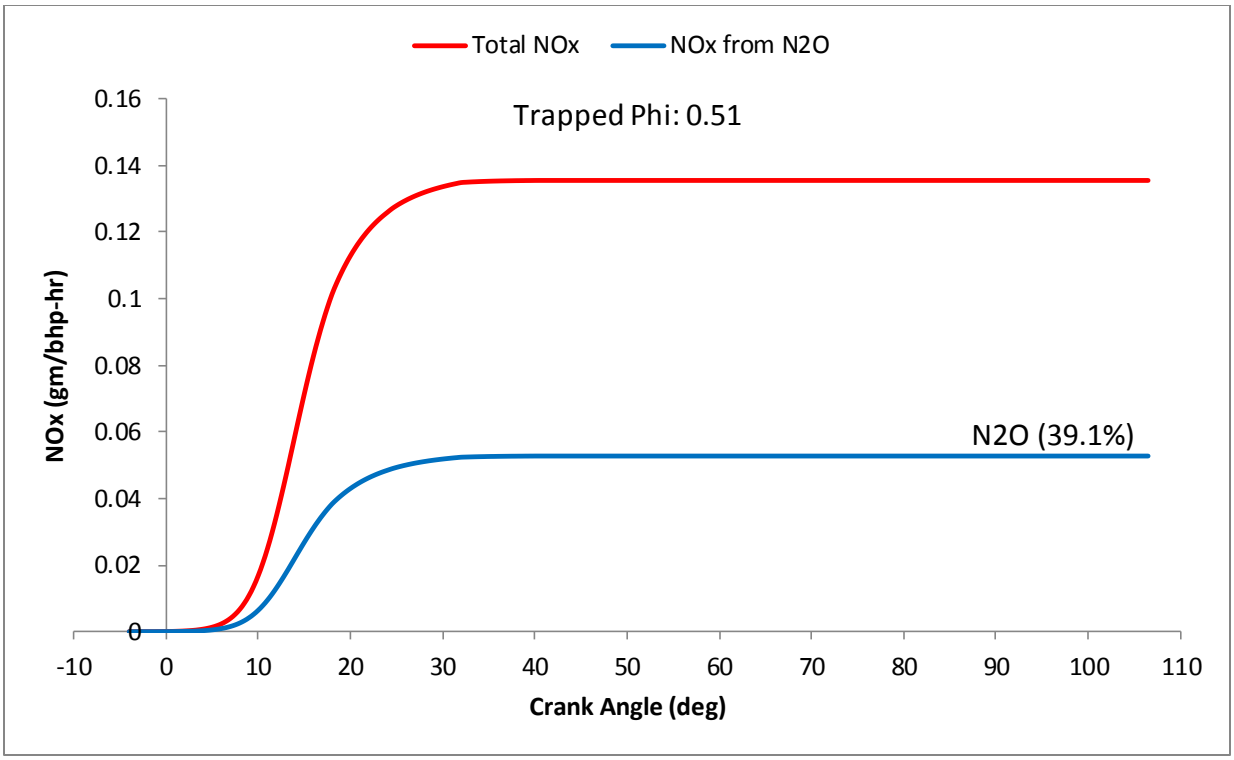

Figure 6.7: Total NOx yield and NOx formed by the nitrous oxide mechanism for a homogeneous charge engine running on 430% theoretical air, predicted by simplified model

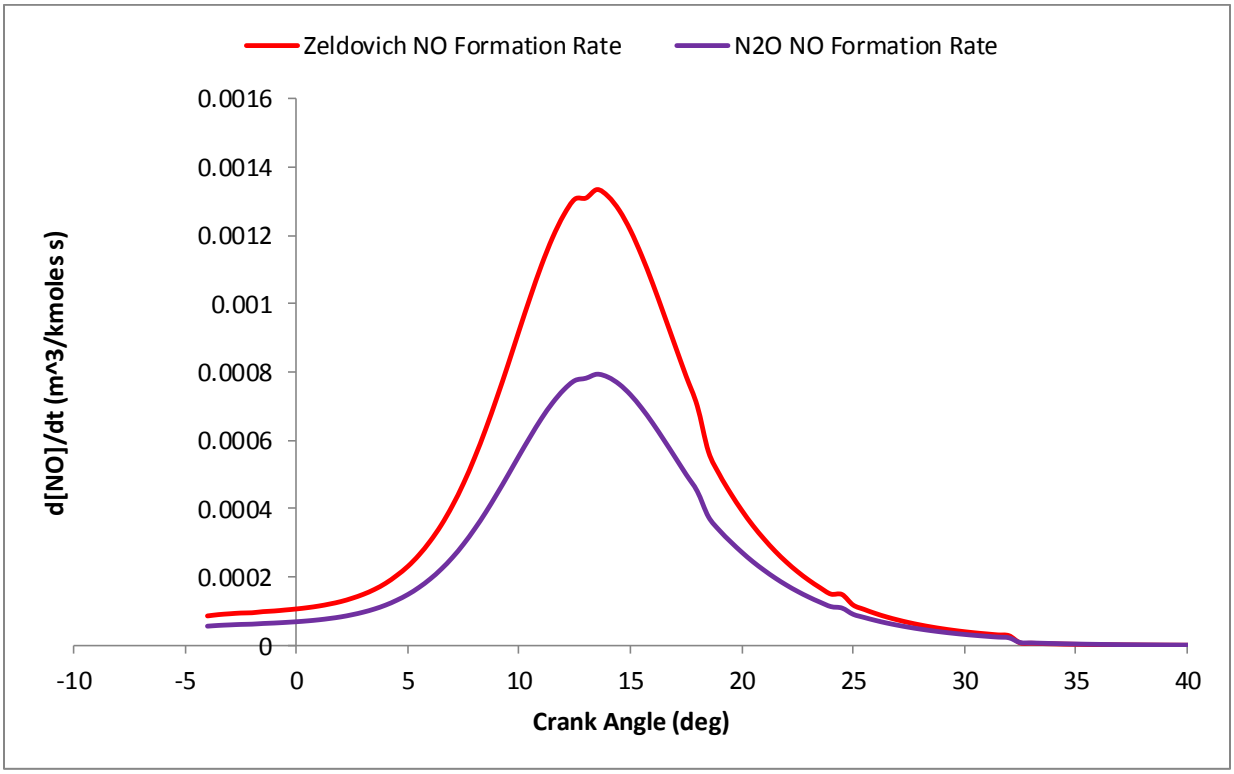

Figure 6.8: NOx formation rates for the Zeldovich and N2O mechanisms for a homogeneous charge engine running on 430% theoretical air, predicted by simplified model

Figures 6.9 through 6.12 pertain to a homogeneous charge engine running at 315% theoretical air, with a spark timing of 6^{o} BTDC. The trapped fuel-air equivalence ratio of the engine is 0.641. The NOx yield as a function of crank angle predicted by UWSI and the simplified NOx model is shown in Figure 6.9. The simplified NOx model under-predicts NOx when compared to the UWSI model. The reason for this is the same as the reason for the under-prediction of NOx in the 430% theoretical air case; however, a greater amount of under-prediction is observed in the richer case. Like the previous cases, the simplified model does not capture NOx destruction due to hydrocarbon radical attack on the NO molecule. Figures 6.10 and 6.11 show the NOx formed by the nitrous oxide pathway along with the total NOx yield as a function of crank angle by the UWSI model and the simplified NOx model, respectively. The NOx formed by the nitrous oxide route as a percentage of the total NOx is approximately the same for both models. Figure 6.12 shows the formation rates of NO by the Zeldovich mechanism and the nitrous oxide mechanism. Trends similar to the homogenous charge engine running on 430% theoretical air are observed. The effect of including the reverse Zeldovich reactions in the calculation of NOx formed by the Zeldovich mechanism is negligible. Due to low NO concentration, there is virtually no NOx destruction, and no noticeable effect of the reverse Zeldovich mechanism is observed.

The three cases considered in this chapter show that it is possible to predict NOx yields accurately at very lean operating conditions by taking into account only two NOx formation mechanisms: the Zeldovich mechanism and the nitrous oxide mechanism. It is seen that the percentage of NOx formed by the nitrous oxide pathway is greater at leaner

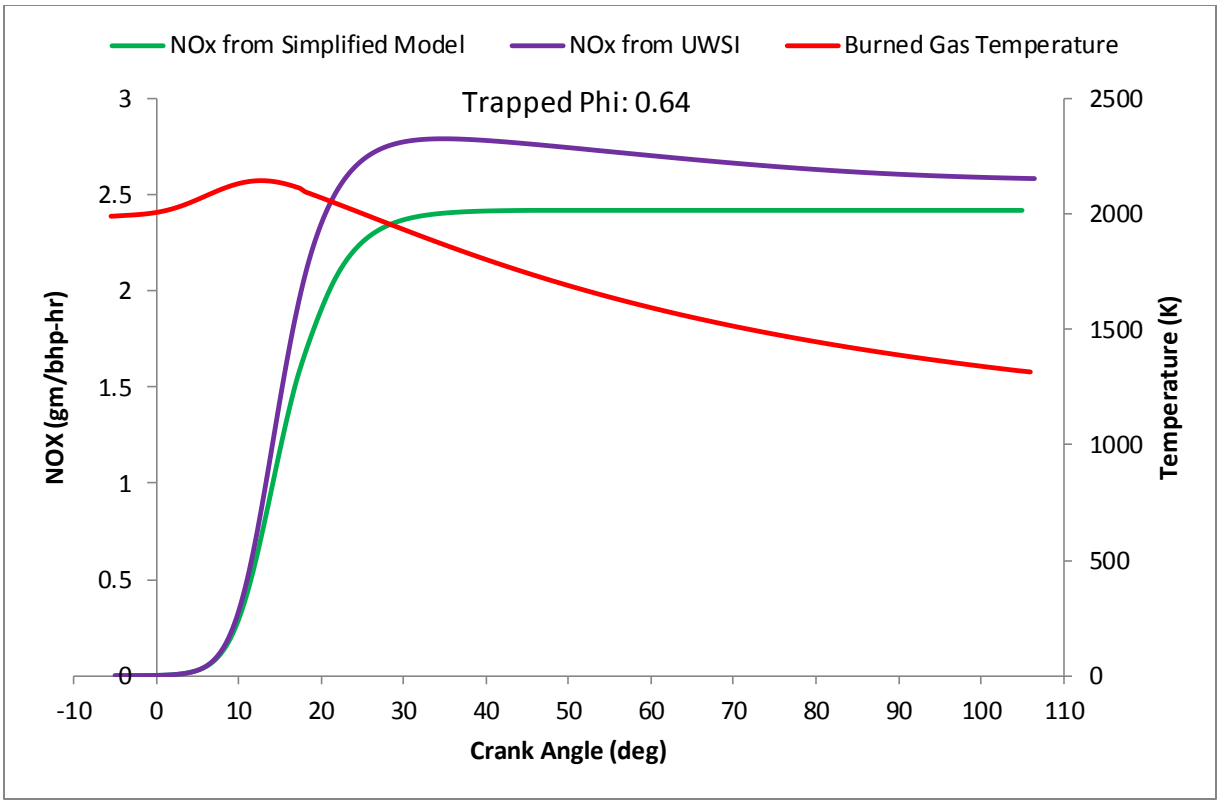

Figure 6.9: Predicted NOx yield from the simplified model and UWSI for a homogeneous charge engine running on 315% theoretical air

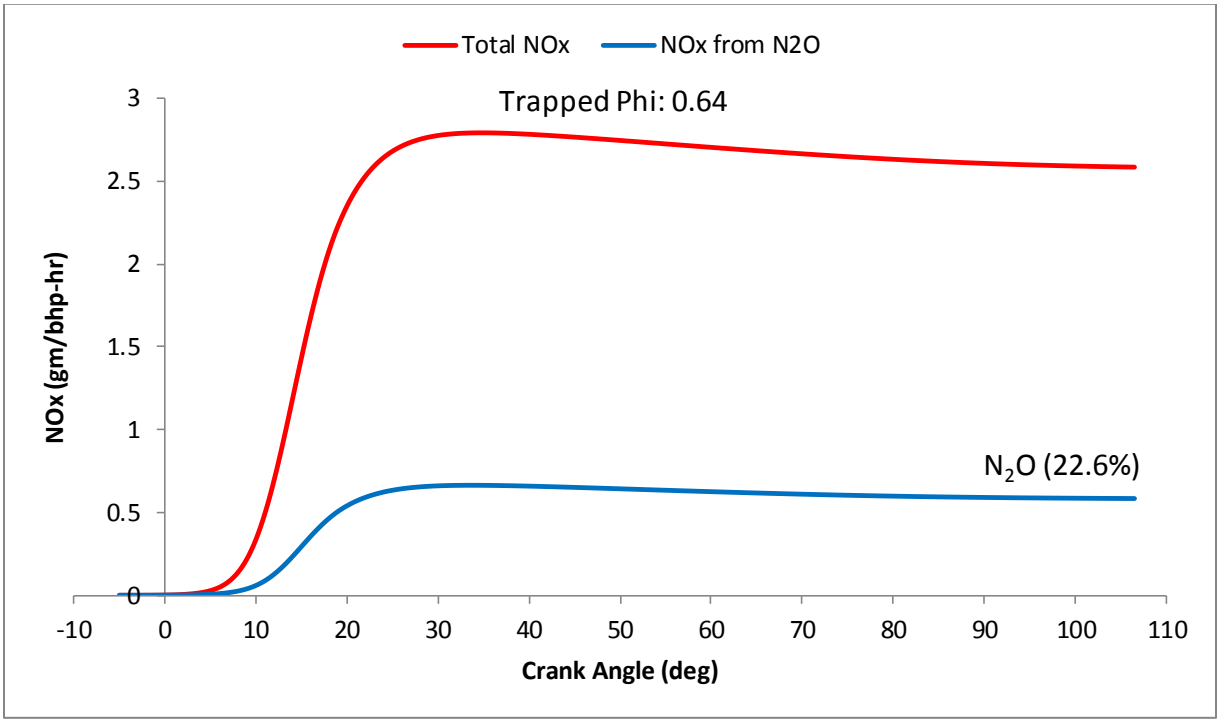

Figure 6.10: Total NOx yield and NOx formed by the nitrous oxide mechanism for a homogeneous charge engine running on 315% theoretical air, predicted by UWSI

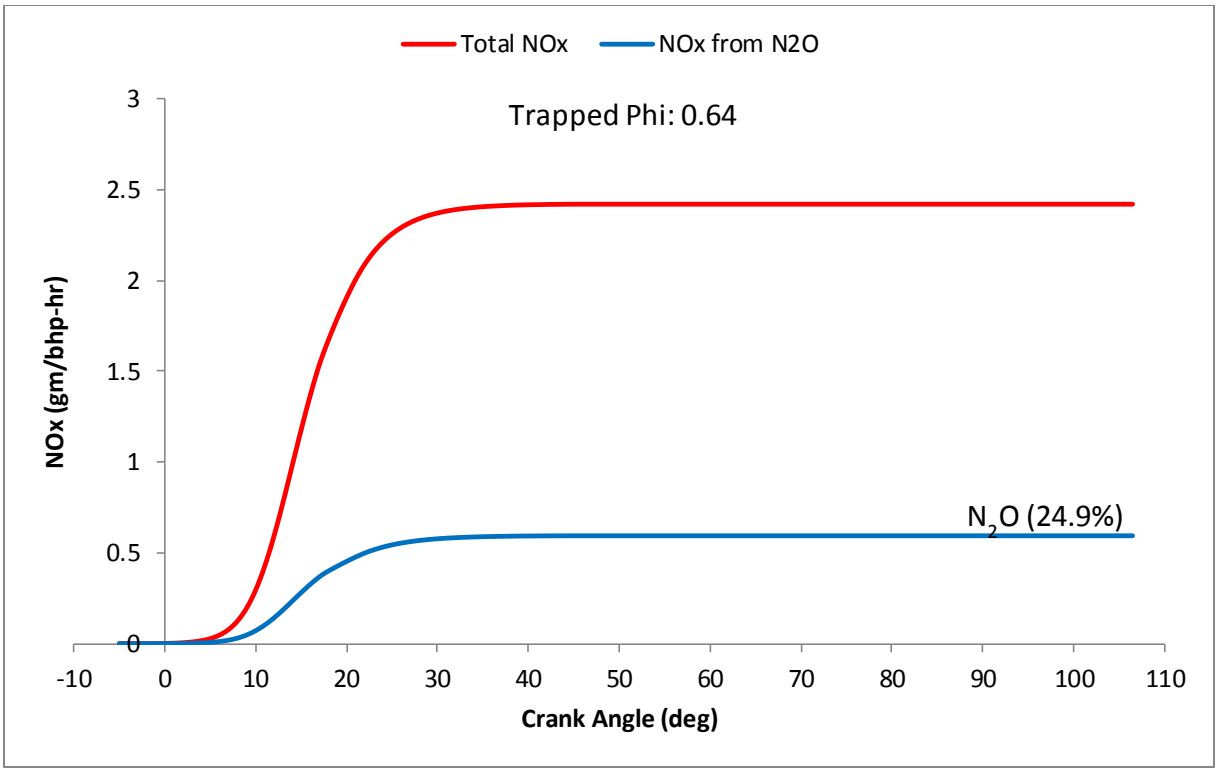

Figure 6.11: Total NOx yield and NOx formed by the nitrous oxide mechanism for a homogeneous charge engine running on 315% theoretical air, predicted by simplified model

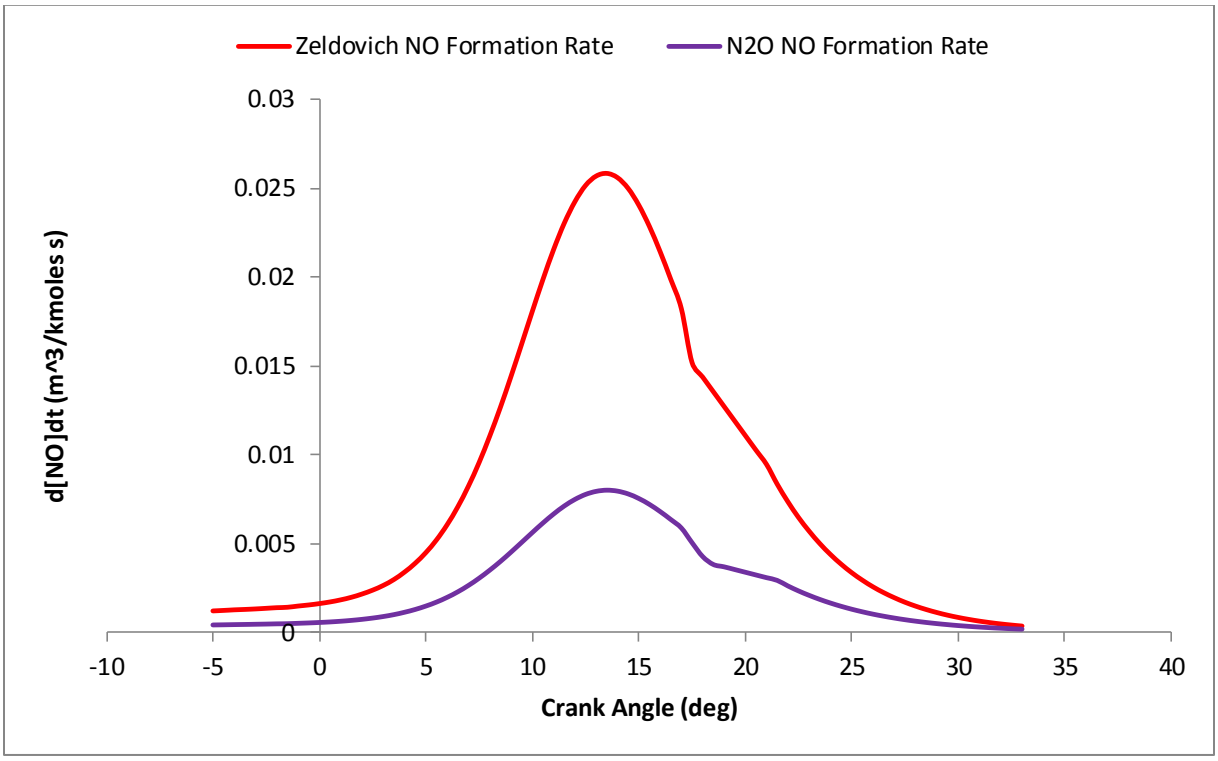

Figure 6.12: NOx formation rates for the Zeldovich and N2O mechanisms for a homogeneous charge engine running on 315% theoretical air, predicted by simplified model

fuel-air equivalence ratios, while the Zeldovich pathway yields greater NOx at relatively higher fuel-air equivalence ratios. This is because a higher phi corresponds to higher temperatures in the cylinder, which favors NOx formation by the Zeldovich mechanism over the nitrous oxide mechanism. It is also observed that the NOx yield predicted by the simplified model differs significantly from the NOx yield predicted by UWSI at relatively richer conditions. This is because the simplified NOx model does not take into account NOx formed due to super-equilibrium concentrations of nitrous oxide in the first few reactors of the chemical reactor model. Also, the assumption of equilibrium concentrations of N_2O, while valid at very lean conditions, may not hold at relatively rich conditions, which results in different predictions from both models.

7.0 Conclusions

NOx and formaldehyde emissions from a large-bore, single-cylinder, lean-burn, stratified charge, natural gas spark ignition engine have been examined using chemical reactor modeling and the UWSI computer program. The model set up using UWSI was calibrated using data from a test case taken from the MS thesis of Clark (1989), which was then used to predict NOx and formaldehyde emissions for several operating conditions. Pathways of formaldehyde emission, such as mixing of unburned charge into burned charge late in the cycle, unburned gas released from cracks and crevices in the cylinder and auto-reaction of lean pockets have also been examined using UWSI. The contribution of NOx pathways was determined using UWSI as well as chemical reactor modeling. Based on results obtained from this chemical reactor modeling, a simplified NOx prediction model has been formulated and predictions for the cases of 315% theoretical air and 430% theoretical air have been made.

Results obtained indicate that the most likely pathway to formaldehyde formation is the incomplete propagation of the flame across the cylinder, when the engine is operating in the partial burn regime. Partial oxidation due to the mixing of unburned charge into burned gas after flame propagation weakens leads to high formaldehyde formation and emission. If these pockets of charge remain unburned, the result is higher UHC emission. Virtually no formaldehyde emitted from the engine is formed in the flame front; all formaldehyde from the flame front is rapidly oxidized due to high temperatures in the post-flame region. Therefore, partial oxidation of unburned charge is critical to the emission of formaldehyde.

Formaldehyde formation due to unburned charge released from cracks and crevices in the engine cylinder has also been explored. These pockets of unburned charge do not contribute significantly to formaldehyde emission, because gas from cracks and crevices in the cylinder is released prior to 70^{o} ATDC crank angle. The temperature in the cylinder during this interval is relatively higher than the window of temperatures required for formaldehyde formation, leading to complete oxidation of the unburned charge. Hence, unburned charge from cracks and crevices in the cylinder does not have a significant impact on formaldehyde emission.

Formaldehyde formation due to the auto-ignition of lean pockets has also been considered. The time required for auto-ignition in all cases considered is less than the residence time of burned gas inside the engine cylinder. Formaldehyde concentration increases in the chemical reactor model, and at auto-reaction, drops rapidly due to the increase in temperature. The maximum concentration of formaldehyde in these cases is on the order of 1000 ppmv and relatively unaffected by pressure. This leads to the conclusion that engines operating close to the ignition limit, towards the leaner end of the partial burn regime can experience significant formaldehyde emission.

NOx formation in these engines is examined using UWSI as well as chemical reactor modeling. At relatively rich operating conditions, the predominant NOx formation pathway is the Zeldovich mechanism, with some contribution from the nitrous oxide mechanism. At very lean conditions, the nitrous oxide pathway contributes significantly to NOx emission. The prompt mechanism contributes to NOx formation in the flame front and the region immediately downstream of the flame. The NNH mechanism does not contribute significantly to NOx emission. At the leanest operating condition, the N_2O

concentration is seen to be close to equilibrium concentrations. Stratified charge combustion, though permitting operation at leaner fuel-air ratios, increases NOx emission due to elevated temperatures in the jet-cell. Some NOx is destroyed due to the reaction of the NO molecule with hydrocarbon radicals from the unburned charge mixed into burned charge towards the end of the cycle.

These results are used to formulate a simplified NOx prediction model. The model assumes that all NOx formation is due to the Zeldovich and nitrous oxide mechanism, with N_2O at equilibrium concentrations. The results of this model are discussed in Chapter 6 of this report. The model predicts NOx emission well at lean operating conditions. At relatively richer conditions, some under-prediction of NOx is observed. This is due to super-equilibrium values of N_2O as well as contributions from other pathways in the flame front and the region immediately downstream of the flame front.

BIBLIOGRAPHY

Danyluk, P.R., Schaub, F.S., "Emission Reduction by Modification in Two Stroke Spark Ignited Gas Engines and by Catalytic Conversion", ASME Paper No. 81-DGP-7, presented at the Energy-Resources Technology Conference, Houston, Texas, 1981.

Denuski, M. "A Computer Model of the Performance and Emissions of Lean Burn Natural Gas Spark Ignition Engines", MSME Thesis, Dept. Of Mechanical Engineering, University of Washington, 1995.

Nicol, D.G., Malte, P.C., "Modeling Formaldehyde and Oxides of Nitrogen in Large-Bore, Lean-Burn, Natural Gas Engines", Report, Dept. of Mechanical Engineering, University of Washington, 1997.

Clark, S.F., "A Computer Model of Nitric Oxide and Carbon Monoxide Formation in a Lean-Burn Gas Fired Spark Ignition Engine", MSME Thesis, Dept. of Mechanical Engineering, University of Washington, 1989.

Wolfrum, J., "Bildung von Stickstoffoxiden bei der Verbrennung", Chemie-Ing.-Techn. 44. Jahrg. 1972, Nr.10, 1972

GRI MECH 3.0, Gregory P. Smith, David M. Golden, Michael Frenklach, Nigel W. Moriarty, Boris Eiteneer, Mikhail Goldenberg, C. Thomas Bowman, Ronald K. Hanson, Soonho Song, William C. Gardiner, Jr., Vitali V. Lissianski, and Zhiwei Qin, http://www.me.berkeley.edu/gri_mech/

Hunter, T.B., Wang, H., Litzinger, T.A., Frenklach, M., "The Oxidation of Methane at Elevated Pressures: Experiments and Modeling", *Combust. Flame* 97:201-224, 1994

Golub, A., and Ghoniem, A., "Modeling NOx Formation in a Small-Bore, Lean Natural Gas, Spark Ignition Engine", SAE Technical Paper Series 1999-01-3480, 1999

Heywood, John B., *Internal Combustion Engine Fundamentals*, Mc-Graw-Hill Inc., New York, 1988.

Turns, Stephen, *An Introduction to Combustion*, Mc-Graw Hill Inc., New York, 2011.

Malte, P.C., and Pratt, D.T.," The Role of Energy-Realeasing Kinetics in NOx Formation: Fuel-lean, Jet-stirred CO-air Combustion.", Combustion Science and Technology, 9:221-231, 1974.

Bozzeli, J. W., and Dean, A. M., "O + NNH: A Possible New Route for NOx Formation in Flames", International Journal of Chemical Kinetics, 27: 1097-1109 (1995)

Fenimore, C.P.," Formation of Nitric Oxide in Premixed Hydrocarbon Flames", In Thirteenth Symposium (International) on Combustion, The Combustion Institute, 1971.

Centers for Disease Control and Prevention, "Formaldehyde: Evidence of Carcinogenicity", Publication Number 81-111, April 1981

De Petris, C., Diana, S., Giglio, V., Golini, S., Police, G., "Numerical Simulation of Combustion in Premixed SI Engines Using Fractal Flame Models", SAE Technical Paper 952383, 1995.

Mitchell, C.E., Olsen, D.B., "Formaldehyde Formation in Large Bore Natural Gas Engines Part 1: Formation Mechanisms", J. Eng. Gas Turbines Power 122(4), pp. 603-610, 1999.

Olsen, D.B., Mitchell, C.E., "Formaldehyde Formation in Large Bore Engines Part 2: Factors Affecting Measured CH_2O", J. Eng. Gas Turbines Power 122(4), pp. 611-616, 1999.

Olsen, D.B., Holden, J. C., Hutcherson, G. C., Willson B. D., "Formaldehyde Characterization Utilizing In-Cylinder Sampling in a Large Bore Natural Gas Engine", J. Eng. Gas Turbines Power 123(3), pp. 669-676, 2000.

Fackler , K.B., Jr., "A Study of Pollutant Formation from the Lean Premixed Combustion of Gaseous Fuel Alternatives to Natural Gas", PhD Thesis, Department of Mechanical Engineering, University of Washington, 2011.

Bauer, M., Wachtmeister, G., "Formation of Formaldehyde in Lean-burn Gas Engines", J MTZ Worldwide, Volume 70, Issue 7-8, pp. 50-57, 2009.

De Wit, J., Karll, B., Nielsen, M., and Kristensen, P., "Emission and Reduction of Organic Flue Gas Components from Lean-Burn Gas Engines", paper presented at the 1998 International Gas Research Conference, San Diego, California, 1998.

Appendix A: UWSI Computer Model

The UWSI computer model is explained in detail in the MS thesis of Denuski (1995). The sub-models added by Nicol and Malte (1997) are described in this section.

The basic operation of UWSI is explained in Chapter 3 of this document. Figure A.1 shows a procedural flow chart for the UWSI code. The code initially reads the provided data file and calculates the state of unburned charge in the cylinder. The state of the gas immediately prior to ignition is calculated via a polytropic process. For each crank angle increment of 0.5^{o}, the following processes are performed:

1. The change in volume during the crank angle increment is computed and from the cylinder geometry, the specific volume of the mixture is calculated.
2. The specific enthalpy and specific volume of all gas elements is calculated assuming frozen composition and variable specific heats, following isentropic expansion or compression to the new cylinder pressure. The new cylinder pressure is calculated using a fully explicit predictor-corrector method.
3. The specific enthalpy and volume of burned gas elements is updated at constant pressure according to a heat transfer model calibrated against measured engine data.
4. Further changes to specific enthalpy and specific volume due to finite-rate chemical reaction are calculated by constant pressure, adiabatic chemical-kinetic batch reaction.
5. The Wiebe function calculates the mass fraction of charge to be ignited in the current crank angle step. If the volume swept by the piston is less than the volume

of the stratified charge, the unburned gas to be ignited has the properties of the charge in the jet-cell. If the volume swept by the piston is greater than the volume of the stratified charge, the unburned charge to be ignited has the properties of the gas in the main chamber. The flame front is modeled as a perfectly stirred reactor sized to blowout conditions, followed by a plug flow reactor for the rest of the time step.

6. The cylinder pressure is determined by applying the ideal gas law to all gas elements. The pressure is calculated according to the formula:

$$P = \sum_{i=1}^{n} \frac{x_i R T_i m_T}{M_i V(\theta)}$$

Where x_i is the mass fraction of each gas element, M_i is its molecular weight, R is the universal gas constant, m_T is the total mass of the charge in the cylinder, T_i is the temperature of each gas element and V is the volume of the cylinder at a given crank angle.

A.1 Cracks and Crevices Sub-Model

The cracks and crevices sub-model was added to the UWSI computer by Nicol and Malte (1997). The model followed has been taken from De Petris, et al. (1995). The features of the model pertinent to the present study are given below.

A phenomenological model is used to account for the crevice-flow. In this model the crevices are modeled with volumes connecting the combustion chamber to the crankcase: immediately below the piston head there is the top land crevice, then there is the first ring, followed by the second crevice. Further on there is a second ring and then, finally,

the crankcase. This arrangement of crevices and rings connecting the combustion chamber to the crankcase is shown in Figure 3.

The crevice-flow sub-model assumes the following:

1) each crevice region has a uniform pressure,
2) flow to and from each region is isentropic,
3) the temperatures of three regions (top land crevice, second crevice, and crankcase) do not change with time and are equal to the average of the cylinder liner and piston temperatures,
4) pressure in the crankcase is constant and does not change during the calculation,
5) chemical composition of the gas in each region is uniform, but changes during the calculation according to the mass flow to and from the three regions.

Since the gas temperature is constant, only one equation needs to be solved to determine the thermodynamic conditions in each region. Assuming perfect gas behavior, the mass flow to and from each region can be calculated using standard isentropic orifice-flow equations. The resulting coupled mass-flow equations are solved explicitly, and the predicted mass and energy flows to and from the combustion chamber are directly incorporated into the main UWSI code. Only unburned charge is assumed to flow into the crevice from the combustion chamber, and the flow from the crevice to the combustion chamber is assumed to mix instantly and uniformly with the previously burnt gas.

The required geometrical properties of the crevice (areas and volumes) and the temperature of the gas inside the crevice are defined by the user. The mixing of the gas exiting from the crevice occurs prior to step 4 of the flow outlined above.

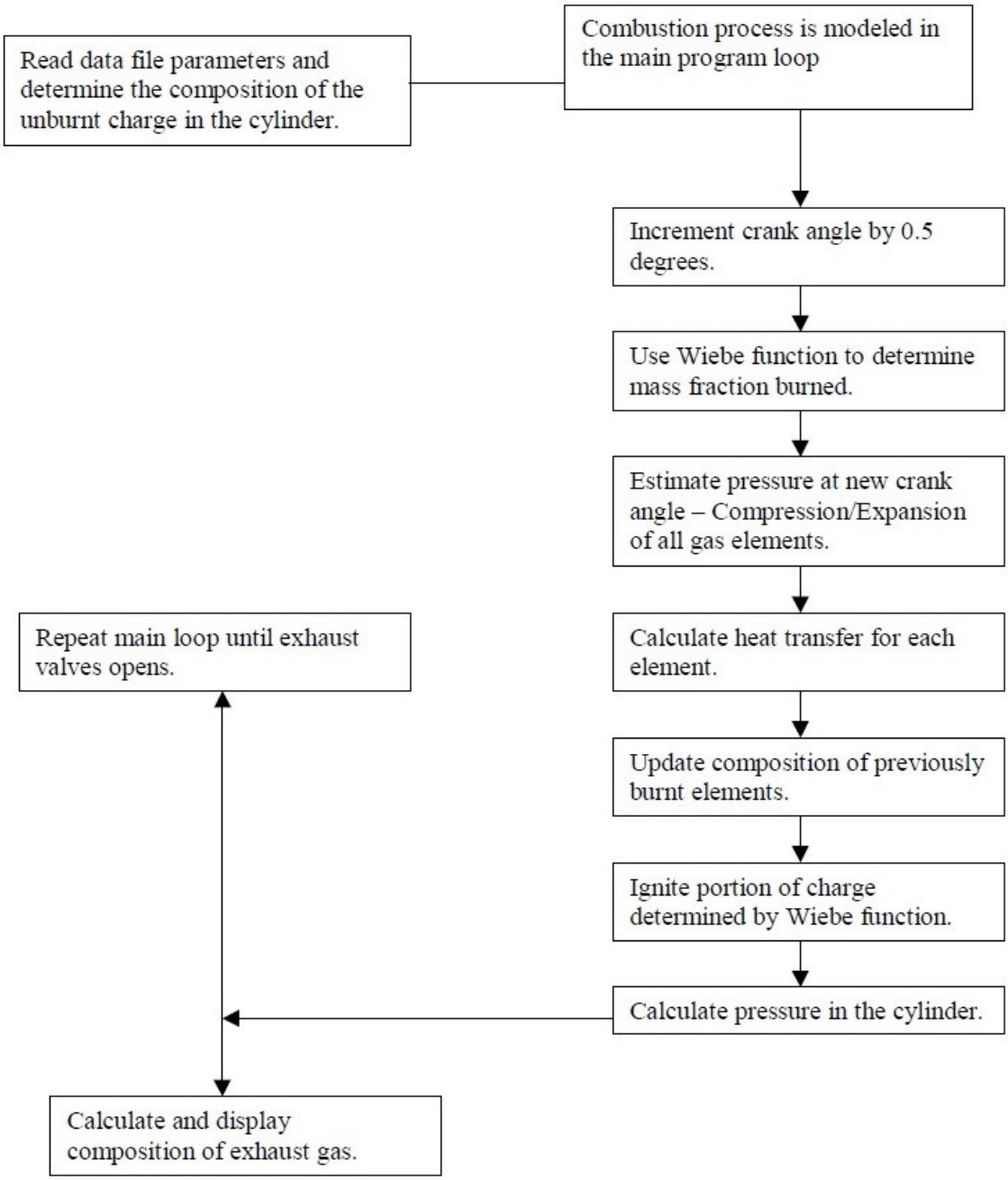

Figure A.1: Flow Chart of the UWSI Computer Code, Nicol & Malte (1997)

Appendix B: Dependence of Auto-ignition on Initial Temperature of Charge

The HCCI sub-model in CHEMKIN was used to check lean pockets for auto-ignition and formaldehyde formation. Premixed charge consisting of methane and air with a fuel-air equivalence ratio of 0.2 is injected into an HCCI engine at atmospheric pressure. The HCCI engine compresses the charge, leading to auto-ignition. The charge is followed from inlet port closure (106^o BTDC) to exhaust port opening (106^o ATDC). The parameter varied from Figure B.1 to Figure B.6 is the initial temperature of the charge, at port closure (106^o BTDC). The residual fraction is 0.1.

In fig B.1, the inlet temperature is 400 K. The charge reaches a peak temperature of about 970 K, and due to this relatively low temperature, only 2.5 ppmv of formaldehyde is formed.

In Figure B.2, the inlet temperature is increased to 450 K. This causes the peak temperature of the charge to reach 1070 K. Formaldehyde is formed starting at the peak temperature, until the temperature reaches about 900 K. The formaldehyde yield is about 250 ppmv.

Figure B.3 shows the result of increasing the inlet temperature to 459 K. This causes an energy release from the charge, as seen by the destruction of methane and an increase in the peak temperature to 1100 K. The formaldehyde reaches a peak concentration of 870 ppmv, after which some of it oxidizes, yielding 830 ppmv formaldehyde at exhaust port opening.

In Figure B.4, the initial temperature is increased to 460.33 K. This causes a greater energy release than the previous case, with the temperature rising to 1060 K after top

dead center, due to the ignition of methane. About half of the formaldehyde formed is oxidized, yielding 510 ppmv at exhaust port opening.

In Figure B.5, the temperature of the inlet charge is increased to 461 K. The charge almost fully auto-ignites, with the methane concentration rapidly falling at ignition. The energy release due to this auto-ignition causes a peak temperature of about 1200 K. Due to full auto-ignition, all of the formaldehyde formed is oxidized, and a low yield of 50 ppmv is obtained.

Finally, in Figure B.6, the inlet temperature is increased to 465 K. In this case, the peak temperature reaches 1500 K, and all formaldehyde formed is rapidly oxidized.

This modeling shows the dependence of formaldehyde formation and emission due to the auto-ignition of a lean pocket on the initial temperature of the lean pocket. Increasing the temperature of the charge by a small amount is enough to ignite the lean pocket and oxidize any formaldehyde formed. Therefore, engines that verge on auto-ignition, or experience borderline auto-ignition are susceptible to greater formaldehyde emission.

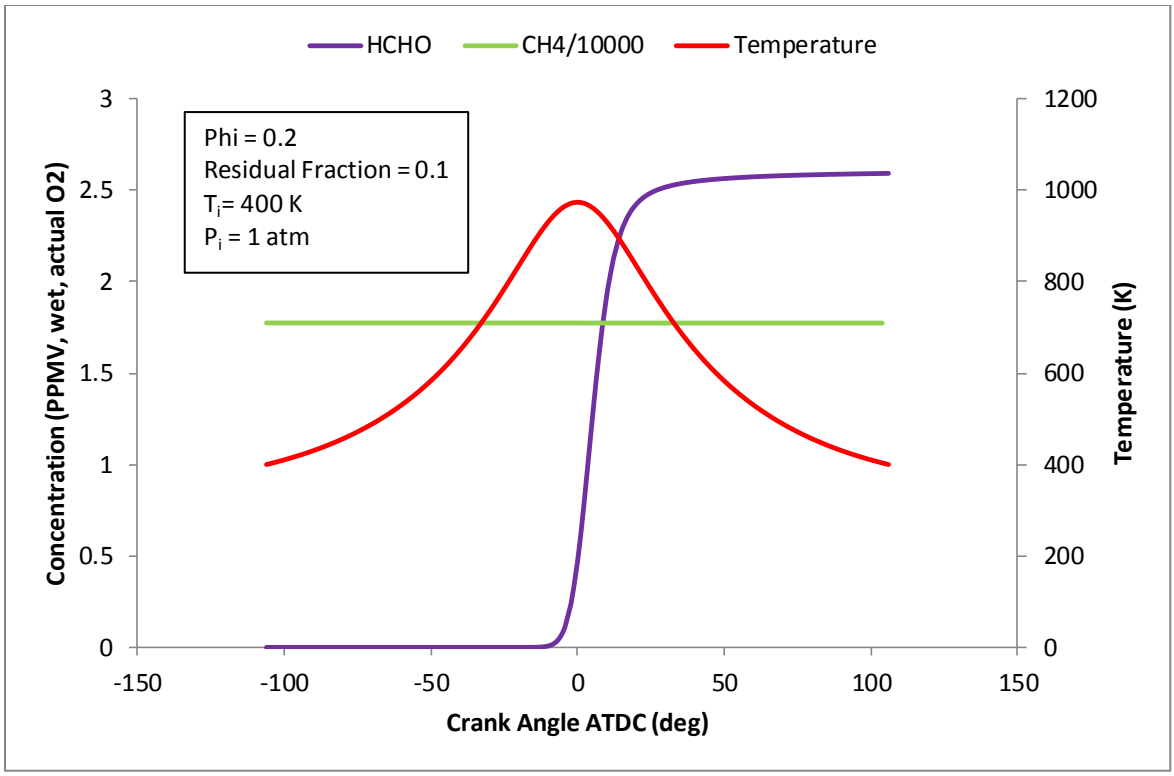

Figure B.1: Predicted Temperature, HCHO and CH4 concentration for auto-ignition of a lean pocket, T_i = 400K, phi = 0.2, residual fraction = 0.1

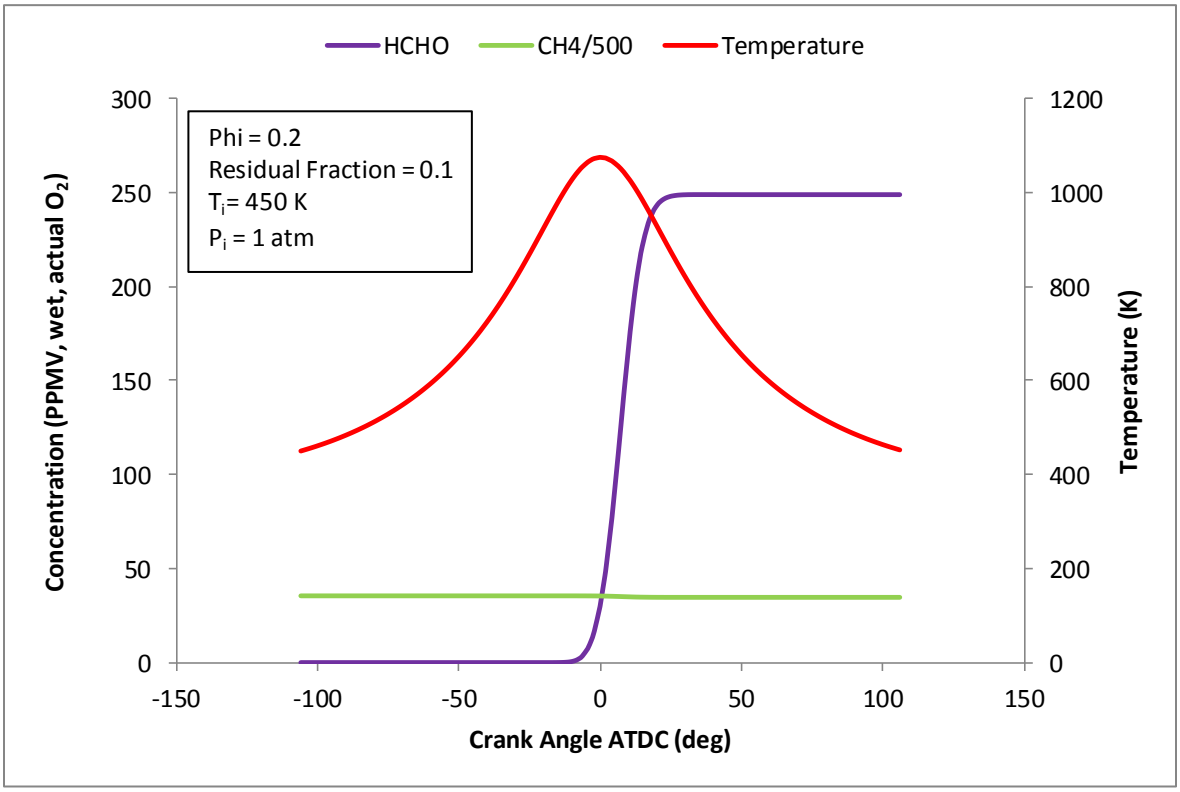

Figure B.2: Predicted Temperature, HCHO and CH4 concentration for auto-ignition of a lean pocket, T_i = 450K, phi = 0.2, residual fraction = 0.1

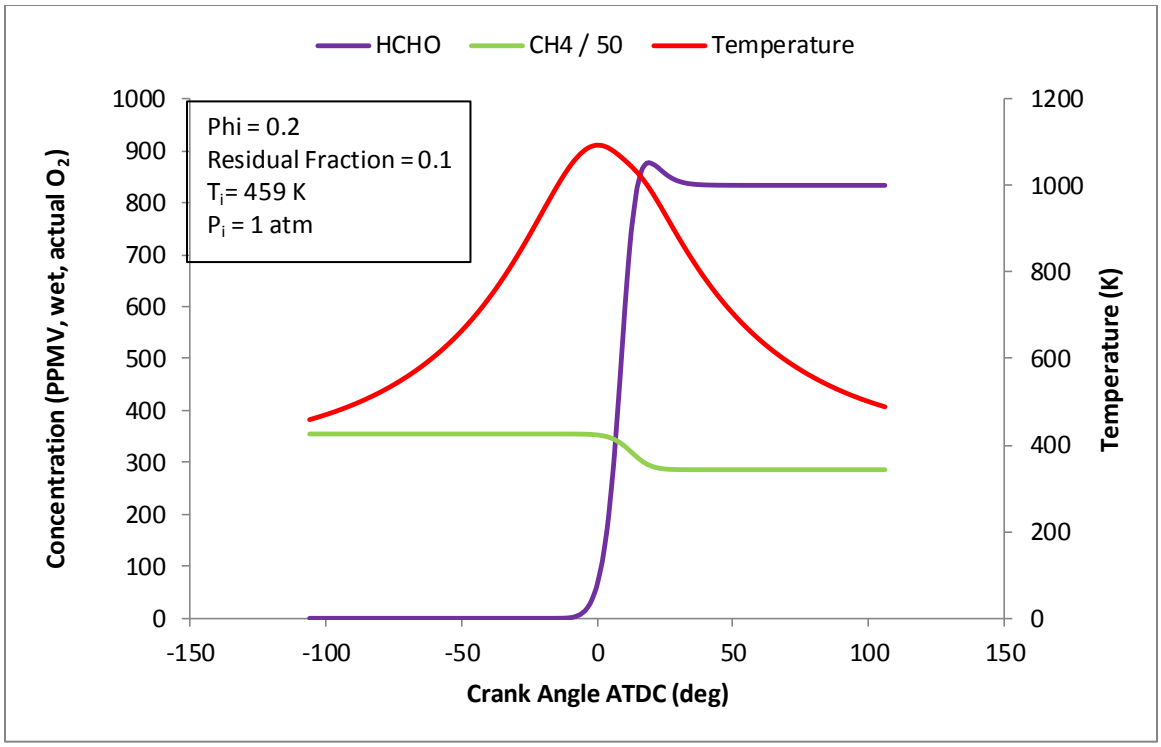

Figure B.3: *Predicted Temperature, HCHO and CH4 concentration for auto-ignition of a lean pocket, T_i = 459K, phi = 0.2, residual fraction = 0.1*

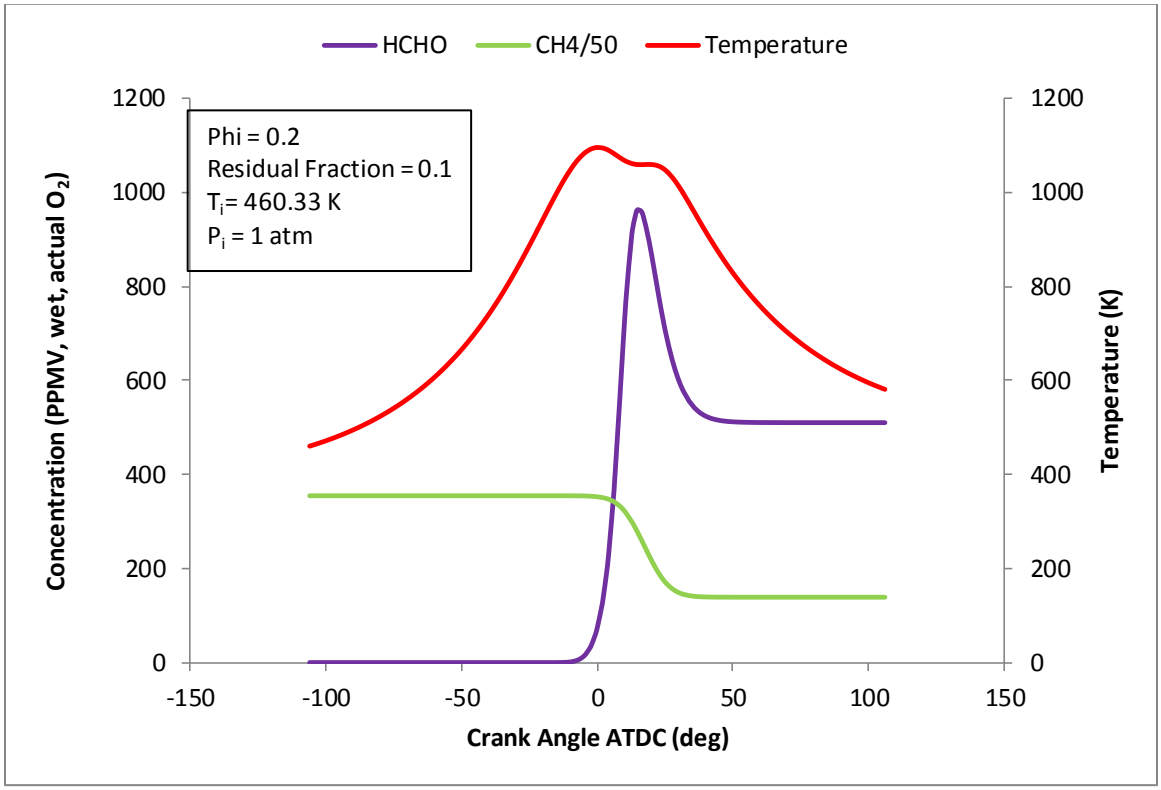

Figure B.4: *Predicted Temperature, HCHO and CH4 concentration for auto-ignition of a lean pocket, T_i = 460.33K, phi = 0.2, residual fraction = 0.1*

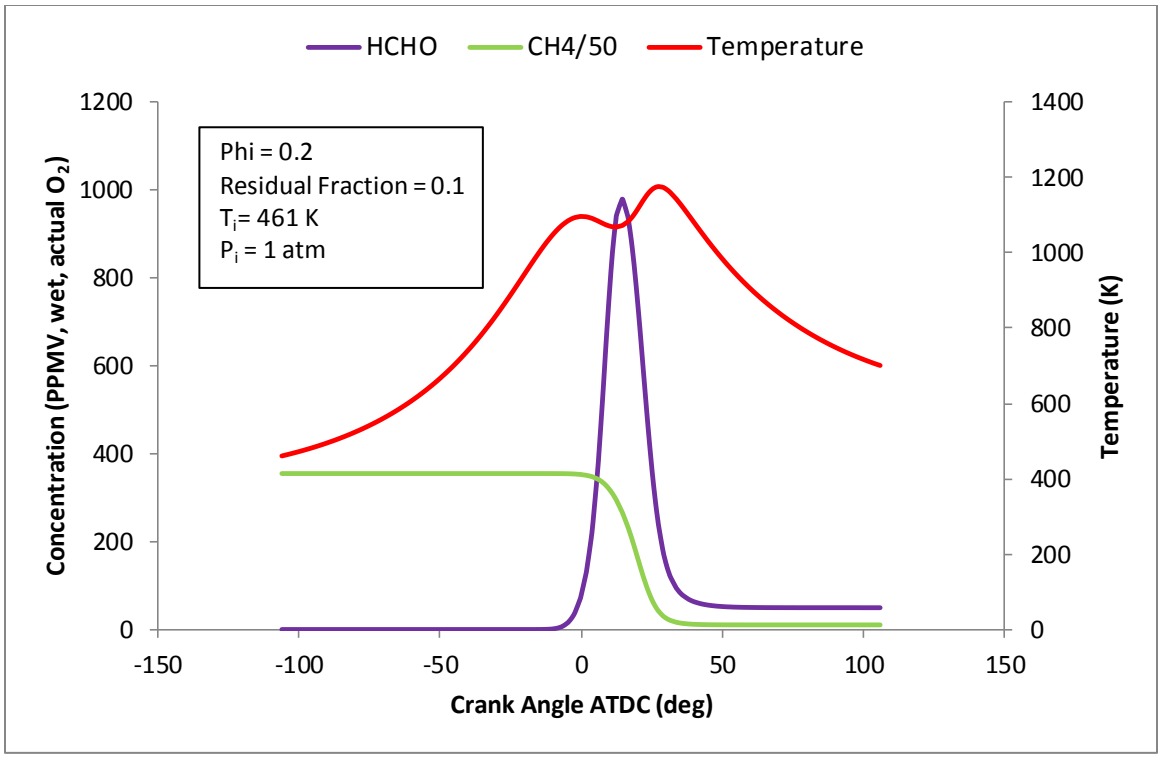

Figure B.5: Predicted Temperature, HCHO and CH4 concentration for auto-ignition of a lean pocket, T_i = 461K, phi = 0.2, residual fraction = 0.1

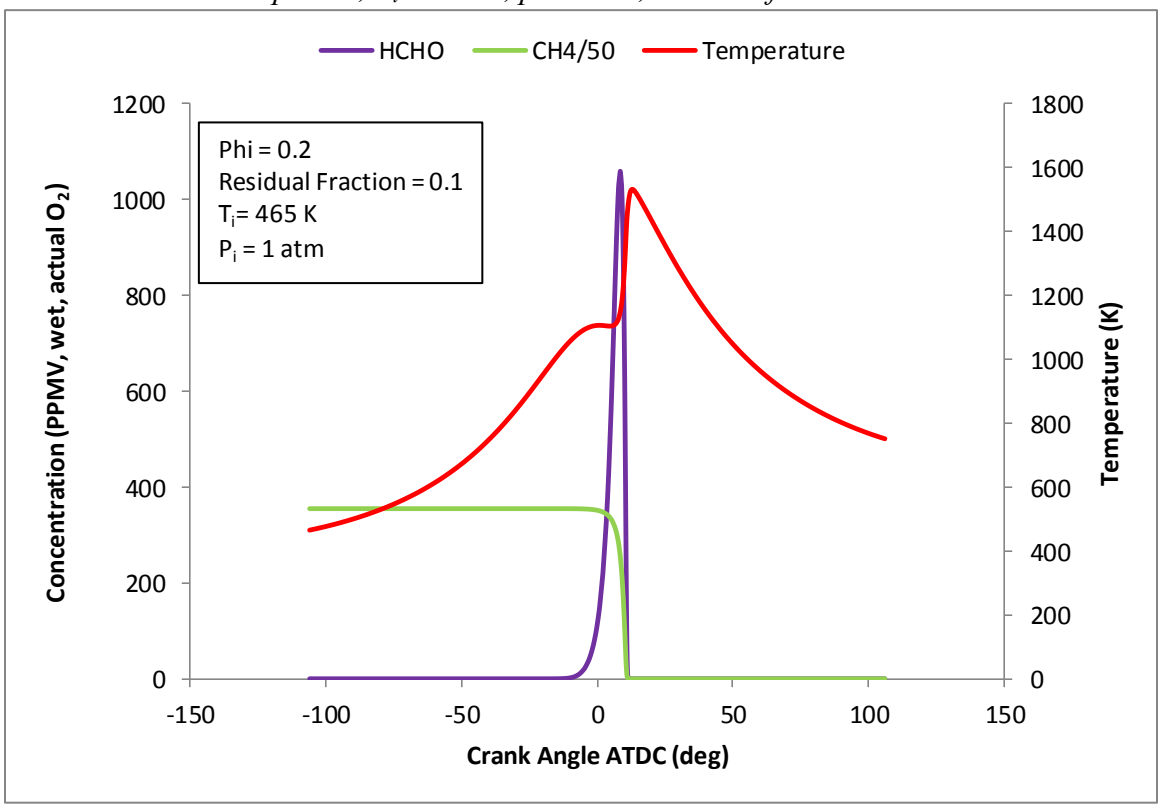

Figure B.6: Predicted Temperature, HCHO and CH4 concentration for auto-ignition of a lean pocket, T_i = 465K, phi = 0.2, residual fraction = 0.1